



**HAL**  
open science

# Oxidative of organic compounds by oxysulfur radicals in the presence of transition metal ions and sulfite

Yanan Yuan

► **To cite this version:**

Yanan Yuan. Oxidative of organic compounds by oxysulfur radicals in the presence of transition metal ions and sulfite. Theoretical and/or physical chemistry. Université Clermont Auvergne [2017-2020]; Université de Wuhan (Chine), 2018. English. NNT : 2018CLFAC052 . tel-02621097

**HAL Id: tel-02621097**

**<https://theses.hal.science/tel-02621097>**

Submitted on 26 May 2020

**HAL** is a multi-disciplinary open access archive for the deposit and dissemination of scientific research documents, whether they are published or not. The documents may come from teaching and research institutions in France or abroad, or from public or private research centers.

L'archive ouverte pluridisciplinaire **HAL**, est destinée au dépôt et à la diffusion de documents scientifiques de niveau recherche, publiés ou non, émanant des établissements d'enseignement et de recherche français ou étrangers, des laboratoires publics ou privés.

UNIVERSITE CLERMONT AUVERGNE

ECOLE DOCTORALE DES SCIENCES FONDAMENTALES

THESE

présentée pour obtenir le grade de

DOCTEUR D'UNIVERSITE

Spécialité : Chimie théorique, physique, analytique

Par  
YUAN Yanan

OXIDATION OF ORGANIC COMPOUNDS BY OXYSULFUR  
RADICALS IN THE PRESENCE OF TRANSITION METAL IONS  
AND SULFITE

Soutenue le « 25/05/2018 », devant la commission d'examen.

Président :

Hui Zhang, PR, Université de Wuhan, Chine

Examineurs :

Feng WU, PR, Université de Wuhan, Chine

Zongping WANG, PR., University of Science and Technology, Wuhan, Chine

Corinne FERRONATO, MCF, Université Claude Bernard Lyon 1, France

Gilles MAILHOT, DR CNRS, Université Clermont Auvergne, France (Directeur de thèse)

Khalil HANNA, PR, Ecole Nationale Supérieure de Chimie de Rennes, France

ED SF n° d'ordre :

**UNIVERSITE CLERMONT AUVERGNE**

**ECOLE DOCTORALE DES SCIENCES**

**FONDAMENTALES**

**THESE**

présentée pour obtenir le grade de

**DOCTEUR D'UNIVERSITE**

*Spécialité : Chimie théorique, physique, analytique*

Par

**YUAN Yanan**

**OXIDATION OF ORGANIC COMPOUNDS BY OXYSULFUR  
RADICALS IN THE PRESENCE OF TRANSITION METAL IONS  
AND SULFITE**

E vue d'une soutenance le « 25/05/2018 », devant la commission d'examen.

Président:

Hui Zhang, PR, Université de Wuhan, Chine

Examineur:

Feng WU, PR, Université de Wuhan, Chine

Zongping WANG, PR., University of Science and Technology, Wuhan, Chine

Corinne FERRONATO, MCF, Université Claude Bernard Lyon 1, France

Gilles MAILHOT, DR CNRS, Université Clermont Auvergne, France

Khalil HANNA, PR, Ecole Nationale Supérieure de Chimie de Rennes, France



# Acknowledgements

I would like to thank gratefully to my supervisors Prof. Marcello BRIGANTE, Prof. Gilles MAILHOT and Prof. Feng WU for giving me the chance to conduct the thesis work. It is my pleasure to work with all of them and I learned a lot of thing from them.

I would also like to thank Engineer Guillaume VOYARD and Prof. Jinjun LI for giving me precious advice and technical supports.

I wish to express my gratitude to Prof. Khalil HANNA (Ecole Nationale Supérieure de Chimie de Rennes, France), Zongping WANG (University of Science and Technology, Chine) and Corinne FERRONATO (Université Claude Bernard Lyon 1, France) for reading and evaluating my thesis. I also wish to thank Prof. Hui ZHANG (Wuhan University) and Prof. Jinjun LI (Wuhan University) for their acceptation to be part of thesis jury.

I also wish to thank all my colleagues in Advanced Oxidation Lab of Wuhan University and Institut de Chimie de Clermont-Ferrand of Université Clermont Auvergne for their kindness help.

Thank for the fund support of China Scholarship Council (CSC) affiliated with the Misistry of Education of P.R. China.

Finally, I would especially like to thank my parents and my husband for always been there with encouragement.



## Structure of the thesis

This thesis is composed of 7 chapters.

**Chapter 1** is an introduction, including background information of organic pollutants in aqueous solution. Advanced oxidation processes (AOPs) based on the Fenton and photo-Fenton processes and sulfate radical activation methods are also introduced.

**Chapter 2** presents a review of recent work related to this study, including: the different methods of advanced oxidation processes such as Fenton, photo-Fenton; and the Advanced oxidation processes based on sulfate radical (SR-AOPs), including PMS-based advanced oxidation processes, PS-based advanced oxidation processes, sulfite-based advanced oxidation processes.

**Chapter 3** is entitled “A simple Cr(VI)-S(IV)-O<sub>2</sub> system for rapid and simultaneous reduction of Cr(VI) and oxidative degradation of organic pollutants”. This chapter deals with simultaneous reduction of Cr(VI) and oxidation of organic contaminants by sulfite ions in the presence of oxygen. A rapid reaction using the azo dye acid orange 7 (AO7, the organic substrate) that is comparable to Cr(VI) reduction is studied in oxidative decolorization at various pH values and Cr(VI)/S(IV) molar ratios. Effect of oxygen and different kinds of radical scavengers used to quench generated radicals are examined. The mechanism of the system and the contribution of reactive oxygen species and reactive sulfur species are preliminarily probed. Furthermore, aniline, phenol, bisphenol A and their substituted analogs are selected to testify the possible application of this system.

**Chapter 4** is entitled “Rapid Oxidation of Paracetamol by Cobalt(II) Catalyzed Sulfite at Alkaline pH”. In this system, promoting the paracetamol degradation in water has been investigated. Paracetamol (PARA), a widely used analgesic and antipyretic drug and an important material for the manufacturing of azo dyes, is chosen as a target contaminant in this work. The effect of pH, initial PARA concentration, Co(II)/S(IV) molar ratio, the presence of oxygen are investigated. Moreover, the activation mechanism and contribution of reactive

oxygen and sulfur species are elucidated by using different kinds of radical scavengers and transient absorption spectroscopy.

**Chapter 5** is entitled “Enhanced oxidation of Aniline using Fe(III)-S(IV) system: Simultaneous enhancement of Fe(III)/Fe(II) cycle and oxysulfur radicals”. In this system, the mechanism of aniline (used as contaminant model compound) oxidation is investigated, with emphasizing the dual role of  $\text{SO}_5^{\bullet-}$  and oxygen. The changes in concentrations of Fe(III) and sulfite, initial pH value of reaction solution are investigated; the second-order rate constant between aniline and  $\text{SO}_4^{\bullet-}/\text{SO}_5^{\bullet-}$  are also measured, then the contribution made by  $\text{SO}_4^{\bullet-}$  and  $\text{SO}_5^{\bullet-}$  are all calculated in this work. Furthermore, the sequential experiment is also conducted to degrade high concentration of aniline providing a simple route for efficient decontamination of organic compounds in industrial waters.

**Chapter 6** is entitled “Enhanced degradation of paracetamol by the Fe(III)-Sulfite system under UV irradiation”. In this system, a detailed discussion on the degradation of paracetamol, which is chosen as an organic substrate, at near-neutral pH and under UV irradiation is reported. The differences between pH 4.0 and 7.0 with or without UV are also checked to find the mechanism for different systems. The effects of initial pH, the Fe(III)/S(IV) molar ratio, oxygen content, buffer are investigated to determine the optimum conditions of the novel photochemical system, and radical scavenger experiment are conducted to determine the predominant oxidant in this system.

Finally, the thesis manuscript ends with **Chapter 7** entitled “General conclusions and perspectives”.

# Summary

|  |     |
|--|-----|
| <b>Acknowledgements</b> .....  | I   |
| <b>Structure of the thesis</b> .....   | III |
| <b>Summary</b> .....   | V   |
| <b>Abstract</b> .....  | 1   |
| <b>Chapter 1 Introduction</b> .....  | 5   |
| 1.1 Background .....   | 6   |
| 1.2 research goals and objective.....  | 8   |
| <b>Chapter 2 Literature review</b> .....   | 14  |
| 2.1 Advanced oxidation process (AOPs).....   | 15  |
| 2.2. Advanced oxidation processes based on sulfate radical (SR-AOPs) .....   | 17  |
| 2.2.1 PMS-based advanced oxidation processes .....   | 17  |
| 2.2.2 PS-based advanced oxidation processes .....  | 21  |
| 2.2.3 Sulfite-based advanced oxidation processes .....   | 26  |
| <b>Chapter 3 A simple Cr(VI)-S(IV)-O<sub>2</sub> system for rapid and simultaneous reduction of Cr(VI) and oxidative degradation of organic pollutants</b> ..... | 38  |
| 3.1 Introduction .....   | 39  |
| 3.2 Material and methods .....   | 40  |
| 3.2.1 Chemicals .....  | 40  |
| 3.2.2 Reaction procedures .....  | 41  |
| 3.2.3 Analysis .....   | 41  |
| 3.3 Results and discussion.....  | 42  |
| 3.3.1 Control experiments .....  | 42  |
| 3.3.2 Effect of pH .....   | 44  |
| 3.3.3 Effect of the Cr(VI)/S(IV) molar ratio .....   | 48  |
| 3.3.4 Effect of oxygen and radical scavengers.....   | 51  |
| 3.3.5 Preliminary study of the mechanism .....   | 53  |
| 3.3.6 Appliance of Cr(VI)–S(IV)–O <sub>2</sub> system for degrading other organic compounds .....  | 54  |
| 3.4 Conclusions .....  | 57  |
| <b>Chapter 4 Rapid oxidation of paracetamol by cobalt(II) catalyzed sulfite at alkaline pH</b> .....   | 61  |
| 4.1 Introduction .....   | 62  |
| 4.2 Materials and methods .....  | 63  |
| 4.2.1 Chemicals .....  | 63  |
| 4.2.2 Degradation experiments.....   | 63  |
| 4.2.3 Chemical analysis.....   | 64  |
| 4.3 Results and discussion.....  | 65  |
| 4.3.1 Control experiments .....  | 65  |
| 4.3.2 Effect of initial pH on paracetamol degradation .....  | 66  |
| 4.3.3 S(IV) and Co(II) effect on the PARA degradation .....  | 69  |
| 4.3.4 Effect of PARA initial concentration on the PARA degradation.....  | 71  |
| 4.3.5 Effect of O <sub>2</sub> .....   | 72  |
| 4.3.6 Radical species involvement .....  | 73  |

|   |            |
|---|------------|
| 4.3.7 Heterogeneous reaction between CoO and $\text{SO}_3^{2-}$ .....   | 76         |
| 4.3.8 Sequential experiments for high concentration PARA.....   | 77         |
| 4.4 Conclusions .....   | 77         |
| <b>Chapter 5 Enhanced oxidation of aniline using Fe(III)-S(IV) system: simultaneous enhancement of Fe(III)/Fe(II) cycle and oxysulfur radicals.....</b> | <b>83</b>  |
| 5.1 Introduction .....  | 84         |
| 5.2 Materials and methods .....   | 85         |
| 5.2.1 Chemicals .....   | 85         |
| 5.2.2 Experimental setup.....   | 85         |
| 5.2.3 Analytical methods .....  | 86         |
| 5.3 Results and discussion.....   | 86         |
| 5.3.1 Effects of Fe(III)/S(IV) ratio and pH .....   | 86         |
| 5.3.2 Determination of the reactivity constants with $\text{SO}_4^{\bullet-}$ and $\text{SO}_5^{\bullet-}$ .....  | 89         |
| 5.3.3 Role of $\text{SO}_4^{\bullet-}$ and $\text{SO}_5^{\bullet-}$ .....   | 92         |
| 5.3.4 Dissolved oxygen implication.....   | 98         |
| 5.3.5 Catalytically cycle investigation .....   | 101        |
| 5.4 Conclusions .....   | 103        |
| <b>Chapter 6 Enhanced degradation of paracetamol by the Fe(III)-sulfite system under UV irradiation .....</b>   | <b>107</b> |
| 6.1 Introduction .....  | 108        |
| 6.2 Material and methods .....  | 109        |
| 6.2.1 Chemicals.....  | 109        |
| 6.2.2 Experimental setup.....   | 109        |
| 6.2.3 Analytical methods .....  | 110        |
| 6.3 Results and discussion.....   | 112        |
| 6.3.1 Control experiments .....   | 112        |
| 6.3.2 Effect of pH on PARA degradation .....  | 113        |
| 6.3.3 Effect of the Fe(III)/S(IV) concentration on PARA degradation .....   | 115        |
| 6.3.4 Effect of oxygen and buffer.....  | 117        |
| 6.3.5 Effect of radical scavengers. ....  | 119        |
| 6.3.6 Effect of transition metal ions-S(IV)- $\text{O}_2^-$ system on PARA degradation .....  | 124        |
| 6.4 Conclusions .....   | 127        |
| <b>Chapter 7 General conclusion and future perspective.....</b>   | <b>131</b> |
| 7.1 General conclusion.....   | 132        |
| 7.2 Perspectives .....  | 133        |
| <b>Publications.....</b>  | <b>135</b> |

# Abstract

In recent years, more and more refractory and toxic organic compounds are detected in wastewater. Many of these organic pollutants are hardly degraded by conventional water treatments. Sulfate radical based advanced oxidation process (SR-AOPs), have emerged as a promising method in the field of oxidative decontamination of polluted water. Past studies focused on this SR-AOPs with peroxydisulfate (PS) or peroxymonosulfate (PMS) as oxidants, especially the systems involving transition metals and oxidants (i.e. Fe(II)/PS system, Ni(II)/PMS system and Co(II)/PMS system), which has been confirmed that  $\text{SO}_4^{\bullet-}$  could have some advantages over  $\text{HO}^{\bullet}$  in the decontamination of wastewater containing organic pollutants. In this dissertation, oxysulfur radicals including sulfite radical  $\text{SO}_3^{\bullet-}$ , sulfate radical  $\text{SO}_4^{\bullet-}$ , peroxymonosulfate radical  $\text{SO}_5^{\bullet-}$  produced by transition metal ions such as Cr(VI), Co(II), Fe(III) activated sulfite are used to degrade organic compounds. The removal efficiency, the oxidation mechanism are examined, and the role of sulfur species are elucidated. The main content and results consist of:

- (1) Cr(VI)-S(IV)- $\text{O}_2$  system containing sulfite ions that rapidly and simultaneously reduces Cr(VI) and oxidize organic pollutants in the presence of oxygen in aqueous solutions is investigated. This Cr(VI)-S(IV)- $\text{O}_2$  system contains the initiator Cr(VI), the reductant S(IV), and the oxidant  $\text{O}_2$ , which produce oxysulfur radicals (mainly  $\text{SO}_4^{\bullet-}$  and  $\text{SO}_5^{\bullet-}$ ) and hydroxyl radicals ( $\text{HO}^{\bullet}$ ). The Cr(VI)/S(IV) molar ratio, pH, and oxygen content play important roles in the entire reaction system. Acidic conditions (pH 3.0) facilitates degradation of organic compounds and reduction of Cr(VI) as well. In addition, experiments of rapid degradation of several kinds of organic pollutants are also conducted. Preliminary results show that the removal rates of the analogs of phenols or aromatic amines in this Cr(VI)-S(IV)- $\text{O}_2$  system have a relationship with the electronic parameters (Hammett constant,  $\sigma$ ) of the substituted groups. Thus, the Cr(VI)-S(IV)- $\text{O}_2$  system, provides an excellent strategy of “waste control by waste” for removing multiple industrial contaminants.
- (2) The efficiency Cobalt (II) (Co(II)) for the activation of sulfite ions following the oxidation of paracetamol used as model contaminants is investigated. Physicochemical parameters

that can impact the paracetamol degradation (pH, initial paracetamol concentration, Co(II)/S(IV) molar ratio, oxygen concentration) and contribution of various radicals are investigated in order to elucidate the chemical mechanism. Main results show that the pH is a key factor controlling the efficiency in the system Co(II)/Sulfite. Higher efficiency is observed for pH between 9.0 and 10.0. Increasing S(IV) concentrations, until 1 mM, slightly promoted the degradation of paracetamol. In fact, an excess of sulfite ions inhibits the reaction through the scavenging of  $\text{SO}_4^{\bullet-}$  and  $\text{SO}_5^{\bullet-}$ . Moreover, degradation efficiency drastically decreases from  $\sim 85\%$  to less than 5% in absence of oxygen.  $\text{SO}_4^{\bullet-}$  is confirmed to be the main oxidant responsible for the paracetamol degradation. For the first time the second order rate constant between  $\text{SO}_4^{\bullet-}$  and paracetamol ( $1.33 \pm 0.79 \times 10^9 \text{ M}^{-1} \text{ s}^{-1}$  (at pH 5) and  $6.14 \pm 0.99 \times 10^8 \text{ M}^{-1} \text{ s}^{-1}$  (at pH 11.0)) is determined. Moreover, radical-scavenging experiments also suggest the possible implication of  $\text{SO}_5^{\bullet-}$ .

- (3) The efficiency of Fe(III)-S(IV) system has been investigated using aniline as pollutant model compound in water. Chemical kinetics, influencing factors, and mechanism of aniline oxidation are examined with emphasizing the contribution of different oxysulfur radicals (mainly  $\text{SO}_4^{\bullet-}$  and  $\text{SO}_5^{\bullet-}$ ). Our results show a significant enhancement of aniline oxidation at pH 4.0 with 1.0 mM of S(IV) and 0.1 mM Fe(III). Moreover, degradation efficiency drastically decreases to 10% in absence of oxygen indicating the relevance of oxygen in this process. Through competition kinetic and radical scavengers experiments we show that  $\text{SO}_5^{\bullet-}$  is responsible for about 60% of the aniline oxidation in the Fe(III)-S(IV) system under our work typical conditions. For the first time we determine the second order rate constants between  $\text{SO}_5^{\bullet-}$  and aniline ( $5.8 \pm 0.6 \times 10^6 \text{ M}^{-1} \text{ s}^{-1}$  (at pH 3) and  $\text{SO}_4^{\bullet-}$  and aniline  $7.7 \pm 0.5 \times 10^9 \text{ M}^{-1} \text{ s}^{-1}$  (at pH 3.0)). Moreover, sequential experiments with addition of sulfite improve the oxidation efficiency.
- (4) The photodegradation of paracetamol (PARA) has been investigated in Fe(III)-S(IV)- $\text{O}_2$  system in the absence and presence of UV irradiation. The results indicate that pH, Fe(III)/S(IV) concentration and oxygen content have an important impact on the disappearance of PARA. To achieve the highest efficiency of PARA degradation, the higher S(IV) concentration should be chosen. Irradiation enhances the PARA degradation through the pH decrease. In fact, the optimal pH range for the degradation of PARA in

Fe(III)-S(IV)-O<sub>2</sub> system is found to be around pH 4.0. Combining the radical scavenger and the ESR experiments, we show that the primary degradation pathway of PARA is the reaction with SO<sub>4</sub><sup>•-</sup>. Experiments are also conducted to examine whether other transition metal ions such as Cr(VI), Co(II) and Cu(II) can react with S(IV) at initial pH of 7.0 under irradiation, and results show that PARA can only be degraded in Cr(VI)-S(IV)-O<sub>2</sub> system with UV irradiation, Co(II) and Cu(II) show no efficiency on PARA degradation under such environment. In conclusion, this work indicate that UV irradiation could be a plausible pathway for PARA degradation by Fe(III)-S(IV)-O<sub>2</sub> system with initial pH around 7.0. This reactivity makes the Fe(III)-S(IV)-O<sub>2</sub>-*hν* system a more powerful system to deal with the wastewater at near-neutral pH values.



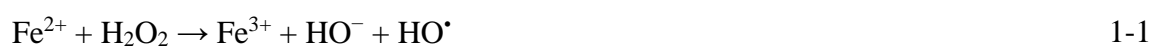
# **Chapter 1 Introduction**

## 1.1 Background

The increase of chemical product use and industries in the recent years has strongly enhanced the presence of refractory, toxic, carcinogenic and mutagenic organic compounds in the aquatic compartment. Organic compounds include dyes, detergents, pharmaceuticals, personal care products, pesticides, carboxylic acids and aromatic compounds [1-7]. The presence of those organic compounds in water poses serious threat to water availability in some regions all over the world [8-9]. The frequent occurrence of pollutants in the aquatic environment as well as in drinking water has raised a concern about their potential impact on environmental and public health. Human exposure to these organic pollutants causes damages to nervous central system, blood system and primary organs like livers, lungs, kidneys etc even at very low concentration [10-11]. Moreover, many organic compounds cannot be eliminated by conventional physical separation methods and biological processes due to their strong stability and toxicity [12]. Therefore, more powerful wastewater treatment methods are required.

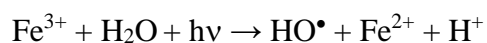
Advanced oxidation processes (AOPs) such as Fenton, photo-Fenton, ozone oxidation, sonolysis and photo-catalytic oxidation have been proved to be effective for degradation of many organic/inorganic compounds from aqueous medium [13-18]. Among the AOPs, those which produce hydroxyl radicals ( $\text{OH}^\bullet$ ) are the most successful, and attracted attention in the field of oxidative decontamination of polluted waters and soils. In fact,  $\text{HO}^\bullet$  has a strong oxidation potential ( $E^0 = 2.8\text{V}$ ), is highly reactive and has a non-selective reactivity [19-20].

Fenton process is based on an electron transfer between hydrogen peroxide ( $\text{H}_2\text{O}_2$ ) and a homogeneous metal catalyst ( $\text{Fe}^{2+}$ ) [21]. In Fenton process, hydrogen peroxide is catalyzed by ferrous ion to produce  $\text{HO}^\bullet$  [22].



The use of Fenton reaction to archive the degradation of several refractory organic compounds such as chlorophenols, chlorobenzene, nitrophenols, has been demonstrated to be an efficient method [23-26]. Furthermore, Fenton process can be improved by using UV radiation and hydrogen peroxide ( $\text{H}_2\text{O}_2$ ), which is so-called photo-Fenton process as shown in eqs 1-2 and 1-3 [27-29];





1-3

Muruganandham et al. [27] investigated the degradation efficiency of Reactive Orange 4 using Fenton and photo-Fenton systems. In their work the disappearance of dye reaches 79.89 % and 95.5% after 40min using Fenton and photo-Fenton processes respectively. In addition, besides photo-Fenton, a combination of electrochemical and Fenton process, namely electro-Fenton process also has been successfully applied in wastewater treatment and achieving a good degradation and mineralization result [30-32].

However, for Fenton system, the disadvantage is related to the high  $\text{Fe}^{2+}$  concentration and the formation of Fe sludge which limit its application [33].

Nowadays, an efficient method for chemical oxidation based on the sulfate radical ( $\text{SO}_4^{\bullet-}$ ) has gained widespread attention (so called Advanced oxidation processes based on sulfate radical (SR-AOPs)) [34-35].  $\text{SO}_4^{\bullet-}$  is a strong oxidant with relatively high standard redox potential ( $E^0 = 2.6 \text{ V vs NHE}$ ) that is closed to the value for hydroxyl radical [36]. In the recent decades, studies have focused on the application of  $\text{SO}_4^{\bullet-}$  for the removal of organic contaminants.  $\text{SO}_4^{\bullet-}$  can react *via* electron transfer, by addition to C-C double bonds and H-abstraction [37,38], thus, it is able to oxidize a large number of pollutants such as dyes, pesticides, antibiotics and aniline in water [39-44].  $\text{SO}_4^{\bullet-}$  can be produced from persulfate (PS) or peroxymonosulfate salts (PMS) by a variety of approaches such as photolysis and thermal activation [45-48]. The addition of transition metals is recognized to be a viable way to achieve PS/PMS activation [49]. Co(II) and Fe(II)/Fe(III) are the most commonly used due to their natural presence in environmental media [50-51].

In the atmospheric liquid phase, Fe(II/III) catalyzes the conversion of S(IV) to S(VI) in the presence of oxygen. Many investigations have extrapolated detailed mechanisms under various conditions, since it is very important for the generation of acid rain [52-57]. On the basis of the mechanism of catalysis by iron, much attention has also been paid to flue gas desulfurization. Except for iron, recently, sulfite ions were also found to react with transition metals such as Ni(II) and Mn(III) to generate  $\text{SO}_4^{\bullet-}$  for water decontamination [57-58]. Furthermore, in order to enhance the efficiency of Fe(II)-S(IV) system, UV-vis irradiation was employed [59].

In my PhD work, transition metal ions such as Cr(VI), Co(II), Fe(III) were chosen to react

with sulfite to promote the organic compounds degradation in aqueous solution. In order to apply the transition metal ions-S(IV) systems at near-neutral pH, UV-vis irradiation was used to test the feasibility. In all those systems, the activation mechanism and contribution of reactive oxygen and sulfur species were elucidated.

## 1.2 research goals and objective

The objective of this work is to study the degradation of model pollutants from water using transition metal ions-S(IV) systems, including Cr(VI)-S(IV)-O<sub>2</sub> system, Co(II)-S(IV)-O<sub>2</sub> system, Fe(III)-S(IV)-O<sub>2</sub> system and Fe(III)-S(IV)-O<sub>2</sub>-*hν* system. The optimum degradation conditions are identified and the activation mechanisms are examined and the role of sulfur species are elucidated. To meet these goals, the following specific objectives for every individual system are defined:

- 1, Experiments are conducted to investigate the parameters on the rapidly and simultaneously reducing Cr(VI) and oxidizing organic pollutants in the presence of oxygen in aqueous solutions in Cr(VI)-S(IV)-O<sub>2</sub> system. The species of oxidants and the contributions of reactive radical species are monitored, then the mechanism of the system can be preliminarily probed.
- 2, Experiments are conducted to investigate the parameters on the paracetamol degradation in alkaline solution in Co(II)-S(IV)-O<sub>2</sub> system. The activation mechanism and contribution of reactive oxygen and sulfur species are elucidated.
- 3, In Fe(III)-S(IV)-O<sub>2</sub> system, experiments are conducted to investigate the parameters on Aniline oxidation. The second-order rate constants between aniline and SO<sub>4</sub><sup>•-</sup>/SO<sub>5</sub><sup>•-</sup> are measured, and the contribution made by SO<sub>4</sub><sup>•-</sup> and SO<sub>5</sub><sup>•-</sup> are calculated. The role of oxygen is emphasized.
- 4, Experiments are conducted to verify the paracetamol degradation in Fe(III)-S(IV)-O<sub>2</sub>-*hν* system at near-neutral pH by UV irradiation. The parameters and oxidant responsible for the organic pollutants degradation are examined.

## References

- [1] Ghuge S P, Saroha A K. Catalytic ozonation for the treatment of synthetic and industrial effluents - Application of mesoporous materials: A review [J]. Journal of Environmental Management, 2018, 211: 83-102.

- [2] Zhang W, Liu W, Zhang J, et al. Characterisation of acute toxicity, genotoxicity and oxidative stress posed by textile effluent on zebrafish[J], 2012, 24(11): 2019-2027.
- [3] Gupta V K, Jain R, Mittal A, et al. Photo-catalytic degradation of toxic dye amaranth on TiO<sub>2</sub>/UV in aqueous suspensions.[J]. Materials Science & Engineering C, 2012, 32(1):12-17.
- [4] Hjelmeland L M. Removal of detergents from membrane proteins [J]. Methods in Enzymology, 1990, 182: 277-282.
- [5] Heberer T. Occurrence, fate, and removal of pharmaceutical residues in the aquatic environment: a review of recent research data [J]. Toxicology Letters, 2002, 131(1-2): 5-11.
- [6] Vymazal J, Březinová T. The use of constructed wetlands for removal of pesticides from agricultural runoff and drainage: a review [J]. Environment International, 2015, 75: 11-20.
- [7] Kulkarni M, Chaudhari A. Microbial remediation of nitro-aromatic compounds: An overview [J]. Journal of Environmental Management, 2007, 85(2): 496-512.
- [8] Rivas J, Gimeno O, Beltrán F. Wastewater recycling: Application of ozone based treatments to secondary effluents [J]. Chemosphere, 2009, 74(6): 854-9.
- [9] BernalMartínez, L. A, BarreraDíaz, C, SolísMorelos, C, et al. Synergy of electrochemical and ozonation processes in industrial wastewater treatment [J]. Chemical Engineering Journal, 2010, 165(1): 71-77.
- [10] Huang Y, Cui C, Zhang D, et al. Heterogeneous catalytic ozonation of dibutyl phthalate in aqueous solution in the presence of iron-loaded activated carbon [J]. Chemosphere, 2015, 119: 295-301.
- [11] Sumpter J P. Xenoendocrine disrupters - environmental impacts [J]. Toxicology Letters, 1998, s 102–103(3): 337-342.
- [12] Pérez M, Torrades F, García-Hortal J A, et al. Removal of organic contaminants in paper pulp treatment effluents by TiO<sub>2</sub>, photocatalyzed oxidation [J]. Journal of Photochemistry & Photobiology A Chemistry, 1997, 109(3): 281-286.
- [13] Puspita P, Roddick F, Porter N. Efficiency of sequential ozone and UV-based treatments for the treatment of secondary effluent [J]. Chemical Engineering Journal, 2015, 268(4): 337-347.
- [14] Pérez M, Torrades F, García-Hortal J A, et al. Removal of organic contaminants in paper pulp treatment effluents under Fenton and photo-Fenton conditions [J]. Applied Catalysis B Environmental, 2002, 36(1): 63-74.

- [15] Huang Y, Cui C, Zhang D, et al. Heterogeneous catalytic ozonation of dibutyl phthalate in aqueous solution in the presence of iron-loaded activated carbon [J]. *Chemosphere*, 2015, 119: 295-301.
- [16] Calza P, Sakkas V A, Medana C, et al. Chemometric assessment and investigation of mechanism involved in photo-Fenton and TiO<sub>2</sub>, photocatalytic degradation of the artificial sweetener sucralose in aqueous media [J]. *Applied Catalysis B Environmental*, 2013, 129(2): 71-79.
- [17] Segura Y, Molina R, Martínez F, et al. Integrated heterogeneous sono-photo Fenton processes for the degradation of phenolic aqueous solutions [J]. *Ultrasonics Sonochemistry*, 2009, 16(3): 417.
- [18] Amat A M, Arques A, López F, et al. Solar photo-catalysis to remove paper mill wastewater pollutants [J]. *Solar Energy*, 2005, 79(4): 393-401.
- [19] Legrini O, Oliveros E, Braun A M. Photochemical processes for water treatment [J]. *Chemical Reviews*, 1993, 93(2): 671-698.
- [20] Prousek J. Advanced Oxidation Processes for Water Treatment. Photochemical Processes [J]. *Chemicke Listy*, 1996, 90(5):307-315.
- [21] Safarzadehamiri A, Bolton J R, Cater S R. The Use of Iron in Advanced Oxidation Processes[J]. *Journal of Advanced Oxidation Technologies*, 2017, 1(1):18-26.
- [22] Ting W P, Lu M C, Huang Y H. The reactor design and comparison of Fenton, electro-Fenton and photoelectro-Fenton processes for mineralization of benzene sulfonic acid (BSA) [J]. *Journal of Hazardous Materials*, 2008, 156(1-3): 421-429.
- [23] Barbeni M, Minero C, Borgarello E P E, et al. Chemical degradation of chlorophenols with Fenton's reagent (Fe<sup>2+</sup> + H<sub>2</sub>O<sub>2</sub>) [J]. *Chemosphere*, 1987, 16(10): 2225-2237.
- [24] Potter F J, Roth J A. Oxidation of Chlorinated Phenols Using Fenton's Reagent [J]. *Hazardous Waste & Hazardous Materials*, 1993, 10(2).
- [25] Sedlak D L, Andren A W. Oxidation of chlorobenzene with Fenton's reagent [J]. *Environmental Science & Technology*, 1991, 25(4).
- [26] Kuo W G. Decolorizing dye wastewater with Fenton's reagent [J]. *Water Research*, 1992, 26(7): 881-886.
- [27] Muruganandham M, Swaminathan M. Decolourisation of Reactive Orange 4 by Fenton and photo-Fenton oxidation technology [J]. *Dyes & Pigments*, 2004, 63(3): 315-321.

- [28] McGinnis B D, Adams V D, Middlebrooks E J. Degradation of ethylene glycol in photo Fenton systems [J]. *Water Research*, 2000, 34(8): 2346-2354.
- [29] Trovó A G, Nogueira R F P, Agüera A, et al. Degradation of the antibiotic amoxicillin by photo-Fenton process - Chemical and toxicological assessment [J]. *Water Research*, 2011, 45(3): 1394-1402.
- [30] Babuponnusami A, Muthukumar K. Advanced oxidation of phenol: A comparison between Fenton, electro-Fenton, sono-electro-Fenton and photo-electro-Fenton processes [J]. *Chemical Engineering Journal*, 2012, 183(4): 1-9.
- [31] Salazar R, Ureta-Zañartu M S. Mineralization of Triadimefon Fungicide in Water by Electro-Fenton and Photo Electro-Fenton [J]. *Water Air & Soil Pollution*, 2012, 223(7): 4199-4207.
- [32] Huang Y H, Su H T, Lin L W. Removal of citrate and hypophosphite binary components using Fenton, photo-Fenton and electro-Fenton processes [J]. 2009, 21(1):35-42.
- [33] Nidheesh P V, Gandhimathi R. Trends in electro-Fenton process for water and wastewater treatment: An overview [J]. *Desalination*, 2012, 299(4): 1-15.
- [34] Dionysiou D D. Degradation of Organic Contaminants in Water with Sulfate Radicals Generated by the Conjunction of Peroxymonosulfate with Cobalt [J]. *Environmental Science & Technology*, 2003, 37(20): 4790-4794.
- [35] Anipsitakis G P, Dionysiou D D. Radical generation by the interaction of transition metals with common oxidants [J]. *Environmental Science & Technology*, 2004, 38(13): 3705-3711.
- [36] Neta P, Huie R E, Ross A B. Rate Constants for Reactions of Proxy Radicals in Fluid Solutions [J]. *Journal of Physical & Chemical Reference Data*, 1990, 19(2): 413-513.
- [37] Lutze H V, Bircher S, Rapp I, et al. Degradation of chlorotriazine pesticides by sulfate radicals and the influence of organic matter [J]. *Environmental Science & Technology*, 2015, 49(3): 1673-1677.
- [38] Ren Y, Lin L, Ma J, et al. Sulfate radicals induced from peroxymonosulfate by magnetic ferrosphenel  $MFe_2O_4$ , (M=Co, Cu, Mn, and Zn) as heterogeneous catalysts in the water [J]. *Applied Catalysis B Environmental*, 2015, 165: 572-578.

- [39] Fang G D, Dionysiou D D, Wang Y, et al. Sulfate radical-based degradation of polychlorinated biphenyls: effects of chloride ion and reaction kinetics [J]. *Journal of Hazardous Materials*, 2012, 227-228(43): 394-401.
- [40] Rastogi A, Al-Abed S R, Dionysiou D D. Sulfate radical-based ferrous–peroxymonosulfate oxidative system for PCBs degradation in aqueous and sediment systems [J]. *Applied Catalysis B Environmental*, 2009, 85(3): 171-179.
- [41] Ji Y, Ferronato C, Salvador A, et al. Degradation of ciprofloxacin and sulfamethoxazole by ferrous-activated persulfate: implications for remediation of groundwater contaminated by antibiotics [J]. *Science of the Total Environment*, 2014, 472(10): 800-808.
- [42] Yang S, Yang X, Shao X, et al. Activated carbon catalyzed persulfate oxidation of Azo dye acid orange 7 at ambient temperature [J]. *Journal of Hazardous Materials*, 2011, 186(1):659-663
- [43] Anipsitakis G P, Dionysiou D D, Gonzalez M A. Cobalt-mediated activation of peroxymonosulfate and sulfate radical attack on phenolic compounds. Implications of chloride ions [J]. *Environmental Science & Technology*, 2006, 40(3): 1000-1007.
- [44] Lin Y T, Liang C, Chen J H. Feasibility study of ultraviolet activated persulfate oxidation of phenol [J]. *Chemosphere*, 2011, 82(8): 1168-1172.
- [45] Zhao D, Liao X, Yan X, et al. Effect and mechanism of persulfate activated by different methods for PAHs removal in soil [J]. *Journal of Hazardous Materials*, 2013, 254: 228-234.
- [46] Antoniou M G, Cruz A D L, Dionysiou D D. Degradation of microcystin-LR using sulfate radicals generated through photolysis, thermolysis and  $e^-$ , transfer mechanisms [J]. *Applied Catalysis B Environmental*, 2010, 96(3): 290-298.
- [47] Wu J, Zhang H, Qiu J. Degradation of Acid Orange 7 in aqueous solution by a novel electro/ $Fe^{2+}$ /peroxydisulfate process [J]. *Journal of Hazardous Materials*, 2012, 215-216(4):138-145.
- [48] Antoniou M G, Cruz A D L, Dionysiou D D. Degradation of microcystin-LR using sulfate radicals generated through photolysis, thermolysis and  $e^-$ , transfer mechanisms [J]. *Applied Catalysis B Environmental*, 2010, 96(3): 290-298.
- [49] Nfodzo P, Choi H. Triclosan decomposition by sulfate radicals: Effects of oxidant and metal doses [J]. *Chemical Engineering Journal*, 2015, 174(2):629-634.

- [50] Liang C, Liang C P, Chen C C. pH dependence of persulfate activation by EDTA/Fe(III) for degradation of trichloroethylene.[J]. *Journal of Contaminant Hydrology*, 2009, 106(3):173-182.
- [51] Do S H, Jo J H, Jo Y H, et al. Application of a peroxymonosulfate/cobalt (PMS/ Co(II)) system to treat diesel-contaminated soil [J]. *Chemosphere*, 2009, 77(8): 1127-1131.
- [52] Berglund J, Elding L I. Manganese-catalysed autoxidation of dissolved sulfur dioxide in the atmospheric aqueous phase [J]. *Atmospheric Environment*, 1995(12): 1379–1391.
- [53] Hoffmann M R, Jacob D J. Kinetics and Mechanisms of the Catalytic Oxidation of Dissolved Sulfur Dioxide in Aqueous Solution: An Application to Nighttime Fog Water Chemistry [J]. 1984.
- [54] Brandt C, Eldik R V. Kinetics and mechanism of the iron(III)-catalyzed autoxidation of sulfur(IV) oxides in aqueous solution. The influence of pH, medium and aging [J]. *Transition Metal Chemistry*, 1998, 23(6): 667-675.
- [55] Kraft J, Eldik R V. ChemInform Abstract: Kinetics and Mechanism of the Iron(III)-Catalyzed Autoxidation of Sulfur(IV) Oxides in Aqueous Solution. Part 1. Formation of Transient Iron(III)-Sulfur(IV) Complexes [J]. *Cheminform*, 1989, 20(40): 2306-2312.
- [56] Zuo Y, Zhan J, Wu T. Effects of Monochromatic UV-Visible Light and Sunlight on Fe(III)-Catalyzed Oxidation of Dissolved Sulfur Dioxide [J]. *Journal of Atmospheric Chemistry*, 2005, 50(2): 195-210.
- [57] Sun B, Guan X, Fang J, et al. Activation of Manganese Oxidants with Bisulfite for Enhanced Oxidation of Organic Contaminants: The Involvement of Mn(III) [J]. *Environmental Science & Technology*, 2015, 49(20): 12414-21.
- [58] Carvalho, Alipázaga L B, Moreno M V, et al. Further studies on the synergistic effect of Ni(II) and Co(II) ions on the sulfite induced autoxidation of Cu(II) penta and hexaglycine complexes [J]. *Journal of the Brazilian Chemical Society*, 2007, 18(18): 1247-1253.
- [59] Zhang L, Chen L, Xiao M, et al. Enhanced Decolorization of Orange II Solutions by the Fe(II)–Sulfite System under Xenon Lamp Irradiation [J]. *Industrial & Engineering Chemistry Research*, 2013, 52(30): 10089-10094.

## **Chapter 2 Literature review**

## 2.1 Advanced oxidation process (AOPs)

Advanced oxidation processes (AOPs) appear as one of the most promising methods for the treatment of soils and waters contaminated by organic compounds [1]. AOPs employ high oxidation-potential sources to produce the primary oxidant species, hydroxyl radical (HO•), an unselective and powerful oxidizing species. HO• reacts with organic compounds with a second order rate constant in the range of  $10^8$ – $10^{10}$  M<sup>-1</sup> s<sup>-1</sup>, yielding to CO<sub>2</sub>, H<sub>2</sub>O and, eventually, inorganic ions as final products [2-5]. The advantage of AOPs over all chemical and biological processes is that the AOPs is totally “environmental-friendly” as they neither transfer pollutants from one phase to the other (as in chemical precipitation and adsorption) nor produces massive amounts of hazardous sludge [6-8]. Due to these characteristics, numerous works have been done to investigate the applications of AOPs to treat different types of contaminated waters. Among the various AOPs proposed in the literature, ultraviolet photolysis (UV), UV/H<sub>2</sub>O<sub>2</sub>, Fenton, photo-Fenton process, photocatalysis are the most common and efficient oxidation technologies which have been applied successfully in wastewater treatment. The mechanism of these methodologies along with equations is presented as follows:

### (1) Photolysis/ ozonolysis

O<sub>3</sub> is widely used in water treatment as disinfectant and oxidant. The decomposition of aqueous ozone in water is initiated by its reaction with hydroxide ion (eqs 2-1), and this reaction leads to the production of free radicals that propagate the decomposition process by chain of radical reactions and produce hydroxyl radical. The purpose of introducing UV radiation in the ozonation process is to enhance the ozone decomposition, yielding more free radicals for reaching a higher oxidation rate 2-2) [9]:



### (2) UV/H<sub>2</sub>O<sub>2</sub> process

When a solution containing H<sub>2</sub>O<sub>2</sub> is irradiated under UV light, the breaking of O-O bond can occur leading to the generation of HO•, eqs. 2-3 [10-13].



When compared the system  $\text{H}_2\text{O}_2$  and  $\text{H}_2\text{O}_2/\text{UV}$ , it was found that UV increased the percentage of degradation to a large extent [14-15].

### (3) Fenton process

The generally accepted mechanism of the Fenton process proposes that  $\text{HO}^\bullet$  are produced in accordance with eqs 2-4 [16-20]; while the catalyst is regenerated through eqs 2-5, or from the reaction of  $\text{Fe}^{3+}$  with intermediate organic radicals (eqs (2-6)–(2-7)) [21-22], as ferrous ions are consumed more rapidly than they are regenerated, hence high concentration of  $\text{Fe}^{2+}$  is required in Fenton process [23].



### (4) Photo-Fenton

Photo-Fenton means when using UV-vis light irradiation, the photolysis of  $\text{Fe}^{3+}$  aqua-complexes ( $\text{Fe}(\text{OH})^{2+}$ ) allows to improve the  $\text{Fe}^{2+}$  generation and the occurrence of Fenton reactions in the presence of  $\text{H}_2\text{O}_2$  (eqs.2-8)[24].



### (5) Photocatalysis

Photocatalysis, which makes use of the semiconductor metal oxide such as  $\text{TiO}_2$ ,  $\text{ZnO}$ ,  $\text{CdS}$  and  $\text{NiO}$  as catalyst is an extensively studied field of AOPs [25-27]. Among them,  $\text{TiO}_2$  in the anatase form is proved to be the most appropriate one due to its characteristics such as high photoactivity, chemical inertness, non-toxic, low cost and easy to obtain [28]. The initiating procedure of the photocatalytic reaction is the absorption of the radiation with the formation of holes ( $h^+$ ) in valence band and electrons ( $e^-$ ) in conduction band in femtosecond timescale (eqs 2-9)



In water, oxidation reactions can take place to form reactive HO• (eqs. 2-10 and 2-11) [29]. During the photocatalytic process, some other reactive radicals like superoxide radical anion (O<sub>2</sub><sup>•-</sup>) are also formed (eqs. 2-12) [30]. According to Eqs. (2-13)–(2-15)), O<sub>2</sub><sup>•-</sup> can lead to the production of HO• [31].



Different oxidation technologies of AOPs are powerful in wastewater treatment of organic pollutants. However, there are still some disadvantages which limit its application, the worst one belongs to the narrow pH range limitation (pH 2.5-3.5) more particularly for AOPs using iron species. In fact, iron ions are precipitated at higher pH values. Another AOPs called advanced oxidation processes based on sulfate radical (SR-AOPs) is a Fenton- like system, which can generate sulfate radical (SO<sub>4</sub><sup>•-</sup>) to achieve the organic compounds degradation. SO<sub>4</sub><sup>•-</sup> can be effectively produced from persulfate (PS) or peroxymonosulfate salts (PMS) by a variety of approaches such as photolysis, radiation, thermal activation and so on.

## 2.2. Advanced oxidation processes based on sulfate radical (SR-AOPs)

### 2.2.1 PMS-based advanced oxidation processes

Potassium peroxymonosulfate (KHSO<sub>5</sub>, KHSO<sub>4</sub>, K<sub>2</sub>SO<sub>4</sub>, PMS, the structure shown in Figure 2-1) commercially available as oxone (HSO<sub>5</sub><sup>-</sup>, PMS), is a widely used as oxidizer in a variety of industrial and consumer applications; specifically, it is sold as a non-chlorine shock-oxidizer for swimming pools and spas. Peroxymonosulfate alone, similarly to hydrogen peroxide [32-33], is not as an efficacious disinfectant as active chlorine compounds. If activated using a catalyzer or photochemically, the generated radicals are very energetic and effective oxidizing agents and it may be used as disinfecting agents. PMS in water solutions is

relatively stable in a way that only 5% of active oxygen dropped in 3 days [37]. Moreover, PMS is stable at pH less than 6 and at pH = 12. Minimum stability of PMS is observed at pH of 9 in which concentrations of  $\text{HSO}_5^-$  and  $\text{SO}_5^{2-}$  are equal ( $\text{pK}_a = 9.4$ ) [37-39].

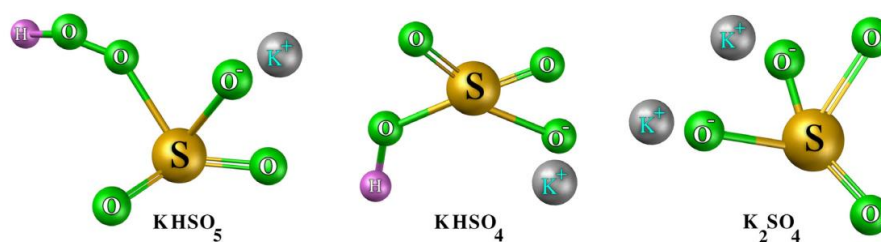


**Figure. 2-1.** The molecular structures of oxone salt

Although PMS is thermodynamically a strong oxidant, its direct reaction with the majority of the pollutants is too slow so that activation is required. From many previous studies, PMS was found to have great potential in water treatment activated by transition metals, especially cobalt, or can be coupled with UV radiation to form  $\text{SO}_4^{\bullet-}$  [40-41].

*(1) PMS activated by transition metal ions in homogeneous systems*

Transition metals have been extremely used to produce free radicals for the degradation of organic compounds. Early in 1956, Ball and Edwards reported the decomposition of peroxymonosulfate by transition metal ions, cobalt ions, for the first time [42]. Decades after, Anipsitakis, Dionysiou and other researchers employed cobalt ion to activate PMS to generate sulfate radical for the organic contaminants degradation [34, 43-46], the general reaction is shown as follows (eqs 2-16)[34]:



The study reported by Anipsitakis and Dionysiou compares the cobalt/peroxymonosulfate (Co/PMS) process with the traditional Fenton process in the dark, over the pH range 2.0 to 9.0 with and without phosphate and carbonate buffers. 2,4-dichlorophenol, atrazine, and naphthalene are used as model contaminants. The results show that Co/PMS process is more efficient than the Fenton process for the degradation of 2,4-dichlorophenol and atrazine. Furthermore, when the experiments are conducted at high pH values, the efficiency of the Fenton process decreases, but the reactivity of the Co/PMS system is sustained at high pH values. For the degradation of naphthalene, Fenton process demonstrates higher degradation

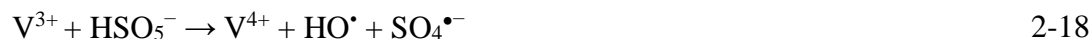
efficiencies at acidic pH, and Co/PMS system is showed more efficient at neutral or even higher pH values. For the effect of mineralization, as total organic carbon removed, also Co/PMS system is proven to be more efficient than the Fenton system [34].

Expect for Co(II), several other kinds of transition metal ions such as Ag(I), Ce(III), Fe(II), Fe(III), Mn(II), Ni(II), Ru(III), and V(III) have been also tested for the activation of PMS. The generated oxidants in those system were also identified as sulfate ( $\text{SO}_4^{\bullet-}$ ), peroxymonosulfate ( $\text{SO}_5^{\bullet-}$ ), and hydroxyl radicals ( $\text{HO}^{\bullet}$ ) [35]. The transition metal ions, Co(II) and Ru(III) are demonstrated to be the best metal catalysts for the activation of PMS. PMS activation efficiency by transition metal ions for 2,4-dichlorophenol degradation is found to be :Ni(II) < Fe(III) < Mn(II) < V(III) < Ce(III) < Fe(II) < Ru(III) < Co(II), Ag(I). PMS activated by different metal ions can generate different radical species:

For Co(II), Ru(III) and Fe(II), sulfate radicals ( $\text{SO}_4^{\bullet-}$ ) are generated via eqs 2-16:



For V(III)/PMS system, sulfate radicals as well as hydroxyl radicals (at a lesser extent) are generated according to eqs 2-17 and 2-18:



As for vanadium, the situation is much more complicated than other metal ions. The interaction of Ce(III) with PMS leads to the formation of a metal-sulfate radicals complex, and the rate-determining step of the Ce(III)/KHSO<sub>5</sub> interaction is suggested to be eqs 2-19:



Caged sulfate radicals also can be generated when using Mn(II) and Ni(II) to activate PMS according to eqs 2-20 and 2-21, and this explains in part the low reactivity of these two couples:



In Fe(III)/PMS system, Fe(III) is an electron acceptor (oxidant) would decompose peroxymonosulfate radical as shown in eqs 2-22:



These results indicate that PMS can be activated by different metal ions, and generating oxidants which have great potential in water treatment.

### *(2) PMS activated by metal oxides in heterogeneous systems*

Transition metal ions are usually applied in wastewater treatment in homogeneous systems. However, there are some disadvantages that limit the application of homogeneous catalyst [47-50]. For heterogeneous catalyst, most of which are mesoporous catalysts and play their role by the reactions occur at the surface, it can be considered for decomposition of PMS. Among heterogeneous catalysts, cobalt oxides such as CoO, Co<sub>2</sub>O<sub>3</sub> and Co<sub>3</sub>O<sub>4</sub> are usually used to activate PMS to degrade various pollutants [47]. Co<sub>3</sub>O<sub>4</sub> nano-particle exhibit excellent performance in PMS decomposition due to presence of Co(II) and Co(III) in molecule structure [51-53]. Various metal oxides (MgO, ZnO, Al<sub>2</sub>O<sub>3</sub>, ZrO<sub>2</sub>, TiO<sub>2</sub>) have been considered as support for cobalt species in order to activate PMS. Take MgO for example, the presence of hydroxyl groups on the surface of MgO formed CoOH<sup>+</sup> intermediate which could promote decomposition of PMS. The order of activity of supports was is MgO > ZnO > TiO<sub>2</sub> > ZrO<sub>2</sub> > Al<sub>2</sub>O<sub>3</sub>[54-47].

### *(3) PMS activation by UV irradiation*

The use of UV light can lead to the generation of SO<sub>4</sub><sup>•-</sup> and HO<sup>•</sup> radicals through the photolysis of the oxidants according to the eqs 2-23 [58-59];



The advantage of activation PMS by UV is due to its benign and economic properties for the purpose of peroxide activation via breaking of the chemical bonds [60-61]. The investigation of the parameters which affect the quantum yields of SO<sub>4</sub><sup>•-</sup> and HO<sup>•</sup> formation, shows that UV wavelength has significant influence on the generation of those radicals. The quantum yields of SO<sub>4</sub><sup>•-</sup> decreased with increase of UV wavelength in the range of 248 to 351 nm [62], and the maximal quantum yield can be gained at the wavelength of 254 nm. For this reasons, 254 nm is usually used for PMS activation [63-64].

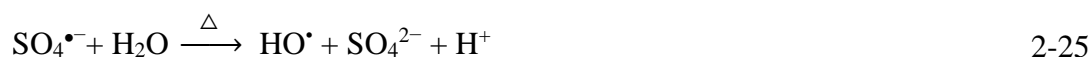
As an efficient AOPs method, the application of PMS/UV treatment is very beneficial not only for the complete elimination of the organic compounds, but also for the achievement of full oxidation (mineralization) [58, 65-66].

#### (4) Thermal activation of PMS

Temperature increase is an effective way to activate the PMS leading to the formation of  $\text{SO}_4^{\bullet-}$  and  $\text{HO}^{\bullet}$  [67-68] (eqs 2-24). In the heat/PMS system, temperature is the critical factor that affect the quantum yields of  $\text{SO}_4^{\bullet-}$  and  $\text{HO}^{\bullet}$  formation.



Furthermore,  $\text{HO}^{\bullet}$  could also be formed via the reaction of  $\text{SO}_4^{\bullet-}$  and  $\text{H}_2\text{O}$ , during the heat process based on the eqs. 2-25



Even though the reaction rate of this reaction is too slow to be important in most reaction systems [69], but higher temperature could significantly accelerate its reaction rate. In addition, at certain temperature, pH has also an influence on the transformation of  $\text{SO}_4^{\bullet-}$  to  $\text{HO}^{\bullet}$ .  $\text{SO}_4^{\bullet-}$  was the predominant radical at  $\text{pH} < 7$ ; both  $\text{SO}_4^{\bullet-}$  and  $\text{HO}^{\bullet}$  are present at  $\text{pH} = 9$ ;  $\text{HO}^{\bullet}$  is the predominant radical at  $\text{pH} = 12$  [69].

The popularity of  $\text{SO}_4^{\bullet-}$  for the purpose of pollutants degradation persuaded us to go for a comprehensive study on application of PMS as a promising source of  $\text{SO}_4^{\bullet-}$ . Following the current investigations, AOPs are shifting towards use of  $\text{SO}_4^{\bullet-}$  due to its unique characteristics. Hence, PMS is an effective and promising oxidant for producing hydroxyl and sulfate radicals. PMS-based advanced oxidation processes can open a new perspective of oxidative reactions to degrade the organic pollutants.

#### 2.2.2 PS-based advanced oxidation processes

Persulfate ion ( $\text{S}_2\text{O}_8^{2-}$ , PS) (the most common form is sodium PS ( $\text{Na}_2\text{S}_2\text{O}_8$ ) and potassium PS ( $\text{K}_2\text{S}_2\text{O}_8$ )), usually is colorless or white crystal, and has high stability [70]. It has symmetrical structure shown in Figure 2-2, the distance of O-O bond is 1.497 Å, and its bond energy is 140 kJ mol<sup>-1</sup> [71-72]. Recently, PS has received attention for water remediation due to its high stability, aqueous solubility, high efficiency and relatively low cost [73-74]. Persulfate is a strong oxidant ( $E_0(\text{S}_2\text{O}_8^{2-}/\text{SO}_4^{2-}) = 2.05 \text{ V/ENH}$ ) [75] and can act directly as an oxidant when activated by heat, UV, electron and transition metals to generate powerful  $\text{SO}_4^{\bullet-}$  radical.

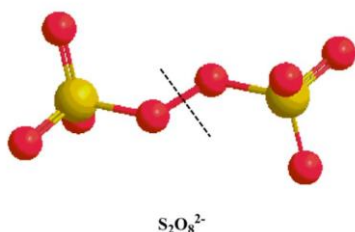


**Figure. 2-2.** Molecular structure of persulfate

*(1) Transition metal ions-activated persulfate*

Persulfate can be activated through one-electron transfer by using transition metal ions such as  $\text{Fe}^0$ ,  $\text{Fe}^{2+}$ ,  $\text{Cu}^{2+}$ ,  $\text{Co}^{2+}$  and  $\text{Ag}^+$  [76-79] as shown in eqs 2-26:



Among the different kinds of transition metal ions used for persulfate activation, the most commonly used is iron and iron complexes. These species have been proven to be efficient activators and can be easily injected into soils and groundwater due to their non-toxicity, and low cost [79-82].

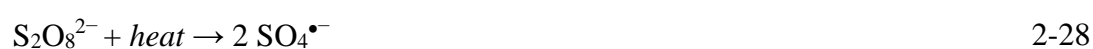
In Wu et al. paper [83], Fe(III)/PS system is used to degrade an emerging contaminant 4-tert-butylphenol (4tBP). The results show that, when experiments are conducted at a pH lower than 4 (to guarantee that all the Fe(III) is under dissolved form), 4tBP can be efficiently degraded. The pH has a significant effect on 4tBP degradation due to the speciation of Fe(III). When using Fe(II)/PS system to degrade other organic pollutants [84-85], it is shown that the activation of persulfate by Fe(II) generally results in a rapid degradation in the early stage, then follows by a decrease of efficiency due to the rapid depletion of  $\text{Fe}^{2+}$  by the sulfate radicals. This phenomenon can be explained by the eqs 2-27. When the concentration of Fe(II) is relatively high, it can react with  $\text{SO}_4^{\bullet-}$  to inhibit the reaction. Hence in this Fe(II)/PS system, the initial  $\text{Fe}^{2+}$  dosage is a crucial factor. In order to overcome this disadvantage, sequential and continuous addition of  $\text{Fe}^{2+}$  to activate persulfate could be an alternative strategy. The study by Jiang et al. [86] indicates that degradation of bisphenol A is enhanced from 49% to 97% using sequential additions of  $\text{Fe}^{2+}$ , and continuous  $\text{Fe}^{2+}$  addition achieved 100% removal using the same amount of total iron and reaction time.



Zero-valent iron (ZVI) can serve as an alternative source of  $\text{Fe}^{2+}$  under oxic or oxidation conditions [87] and so for PS activation. Except for  $\text{Fe}^{3+}/\text{Fe}^{2+}/\text{ZVI}$ , some researches show that iron sulfides such as amorphous FeS, mackinawite, troilite (FeS), greigite ( $\text{Fe}_3\text{S}_4$ ), pyrite ( $\text{FeS}_2$ ) and marcasite ( $\text{FeS}_2$ ) may also activate persulfate by serving as precursors of dissolved or surface  $\text{Fe}^{2+}$  to achieve in situ degradation of organic contaminants just like what  $\text{Fe}^{2+}$  or ZVI did [88-89].

### *(2) Thermal activation persulfate*

Several studies have demonstrated that persulfate can be thermally converted into  $\text{SO}_4^{\bullet-}$  (between the range 30-99°C) as shown in the following eqs 2-28 [90-91]:



The use of heat activation of PS for the degradation of emerging pollutants shows that, under appropriate conditions, most of the pollutants could be efficiently removed [92-94]. Waldemer et al explored the possible application of heat-activated persulfate on chlorinated ethene oxidation [95]. The results show that the disappearance of substrates follow the pseudo-first-order kinetics, and rate constants measured from 30 to 70 °C, fit the Arrhenius equation. Concerning the generated products after the reaction, it is observed that dechlorination is one of the most pathways.

Concerning the parameters that affect the efficiency of persulfate thermal activation, it is found that the increase of temperature can accelerate the decomposition of PS to  $\text{SO}_4^{\bullet-}$ .

However, excessive high temperature not facilitate the organic contaminants degradation all the time., In Wang's report, the degradation efficiency of polycyclic aromatic hydrocarbon decreased when the temperature increased over 60°C [96]. However, if the higher temperature enhances the degradation efficiency and solubility of the contaminants into the aqueous phase, temperature optimization is used to minimize the energy input required for achieving desired results. For example, if 100% removal of substrate is accomplished at 60°C and 90°C, 60°C was chosen for further experiments [97]. Moreover, microwave heating can also have the same better effect on persulfate activation [98], as microwave heating imparts the required energy more quickly to activate persulfate than conventional method.

### *(3) UV activated persulfate*

As an environmentally friendly and efficient method, UV irradiation activated persulfate to degrade a wide range of organic contaminants was reported by great quantity of previous studies [99-101]. In particular, PS irradiated by UV can generate both active oxidative species  $\text{SO}_4^{\bullet-}$  and  $\text{HO}^{\bullet}$  to be the oxidants as following eqs 2-29 and 2-30[102-103]:



The degradation kinetics and mechanism of the antiepileptic drug oxcarbazepine (OXC) by UV-activated persulfate oxidation are investigated. The results show that UV/persulfate process appeared to be more effective in degrading OXC than UV or PS alone, and its degradation exhibited a pseudo-first order kinetics pattern [104].  $\text{SO}_4^{\bullet-}$  and  $\text{HO}^{\bullet}$  are identified to be responsible for substrate degradation and  $\text{SO}_4^{\bullet-}$  made the predominant contribution in the process. For this UV/persulfate system, the most common wavelengths of the UV light are between 200 nm and 300 nm, as the maximum absorption of many organic contaminants occurs within this range [103,105]. Quantum yield is an important factor for characterizing the activation of PS, and UV wavelength has significant influence on the quantum yields. It was found that the quantum yields of sulfate radicals decreased with increase of UV wavelength in the range of 248 to 351 nm [106]. The maximal quantum yield is about 1.4 at the wavelength of 248 and 253.7 nm. In general, 254 nm is most used as the irradiation wavelength for persulfate, not only because which is in the energy absorbance of the ultraviolet range and can activate the PS to generate  $\text{SO}_4^{\bullet-}$  with a quantum yield up to 0.7 mol E/s[107], but also it can decrease reaction time requirements compared to other wavelengths. A comparative study using 254 nm and 365 nm UV activated persulfate for polyvinyl alcohol destruction found that 100% removal was achieved in less than 5 min at 254 nm but only 93% removal in 30 min was observed using 365 nm [108]. In addition, Gamma ray has been also demonstrated to be capable of activating the PS [109-110].

#### *(4) Electrochemically-activated persulfate*

Electrochemical activation of PS is a promising green technology with electrons acting as the reactant, which has drawn increasing attention in recent years [111-112]. Electrochemical reactions generate the sulfate radical at the cathode (eqs 2-31) following the same mechanism as the one electron transfer redox reaction for iron-activated persulfate [113]



Solid iron produces  $\text{Fe}^{2+}$  through chemical and anodic reactions (eqs 2-32), activates the persulfate (eqs 2-33), and can be regenerated at the cathode (eqs 2-34) for additional persulfate activation [114].



$\text{Fe}^{2+}$  generated from solubilized  $\text{Fe}^{3+}$  at the cathode can be used to activate persulfate (eqs 2-32). The synergistic effects of electro-activated persulfate and  $\text{Fe}^{3+}$  result in significant improvement over either method alone. In optimized conditions such as pH, persulfate concentration and current density, target pollutants could be completely removed. Furthermore, electrochemical regeneration of iron for persulfate activation can reduce the total iron used in these systems by using the current to control iron release, eliminating the need for further iron dosing [115]. Except for iron, electrochemical persulfate activation also can be accomplished by using platinum anodes and cathodes which can eliminate the need for iron addition [116]. Electrochemical techniques have proven to fully mineralize recalcitrant compounds not degraded via activated-persulfate alone [117]. Hence, combining electrochemistry and electrochemically-activated persulfate may achieve interesting results compared to either technique alone, thus reducing persulfate and/or electricity usage. However, more studies should be conducted to find the best suited electrode materials for activating persulfate, the relationship between current density and activation. Moreover, studies are needed to determine which electrode materials, the synergistic effects on degradation and mineralization of various classes of organics.

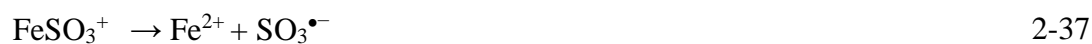
During the activation process of PS, PS itself can be decomposed. The decomposition of PS varied with the activation methods. Decomposition of PS is affected not only by activation methods but also by the experimental conditions. It is noted that high decomposition efficiency of PS or PMS does not mean the good performance for removing the organic compounds. Therefore, the decomposition efficiency of PS cannot be used to reflect the removal capacity of the selected process. Instead, the reaction stoichiometry efficiency (the

ratio of degraded organic compounds concentration to consumed oxidant concentration) could be used to evaluate the removal capacity of the selected process.

The activated PS has the potential for the degradation of emerging contaminants in soil, groundwater, water and wastewater. Among the various activation methods, ultraviolet and metal oxide activation are the most investigated methods according to the published references. In summary, UV/PS process is potential to application for removing the recalcitrant compounds from wastewater, but the effect of complex wastewater compositions should be pay attention too. For metal activated PS, Fe(II)-activated persulfate could be a promising process in terms of both economic and water safety. Although many methods can be used to activate PS and PMS, there is still a long way to go for the practical application.

### 2.2.3 Sulfite-based advanced oxidation processes

Sulfite ( $\text{SO}_3^{2-}$ ) or bisulfite ( $\text{HSO}_3^-$ ) are the most common S(IV) species. S(IV) is important for wine making, fruit preservation, or as dehydrated food additive and textural altering agents [118-120]. In early 1900's, accelerated aqueous S(IV) oxidation by  $\text{O}_2$  in the presence of trace transition metal ion,  $\text{M}^{n+}$ , has been observed [121], in the atmospheric liquid phase. Fe(II/III) catalyzes the conversion of S(IV) to S(VI) in the presence of dissolved oxygen. Many investigations of this process have extrapolated detailed mechanisms under various conditions, since it is very important for the generation of acid rain. On the basis of the mechanism of catalysis by iron, much attention has also been paid to flue gas desulfurization, which is an artificially enhanced process of transformation of S(IV) to S(VI) for the purpose of desulfurization. Kinetics and mechanisms have been proposed in eqs 2-35 to 2-37[122-124].



As the sulfite radical ( $\text{SO}_3^{\bullet-}$ ) is generated during this oxidation process, the autoxidation of sulfur(IV) in aqueous solution is involved in a chain reaction propagated by oxysulfur radicals [125] The species involved are the sulfite radical ( $\text{SO}_3^{\bullet-}$ ), the peroxomonosulfate radical ( $\text{SO}_5^{\bullet-}$ ), and the sulfate radical ( $\text{SO}_4^{\bullet-}$ ) as suggested by Hayon et al. [126]. The reaction chain is initiated by the formation of  $\text{SO}_3^{\bullet-}$ , which can be generated from eqs 2-35 to 2-37, In the

presence of oxygen,  $\text{SO}_3^{\bullet-}$  is rapidly converted to  $\text{SO}_5^{\bullet-}$ , which acts as the main chain carrier, then undergoes further reaction to form  $\text{SO}_4^{\bullet-}$ .

Nowadays, sulfite, a typical reducing agent, has been widely used for remediation of contaminated sites in many emergency cases. Moreover, the significant role of sulfite as an efficient source of active radicals via the reaction of an iron-sulfite-oxygen complex has been reported. Chen et al. reported this new process for dyes degradation with  $\text{SO}_4^{\bullet-}$  using an Fe(II)/sulfite system. Main results show that efficient degradation of dyes could be achieved using this novel system in acidic environment in comparison with the Fe(II)/persulfate and Fenton (Fe(II)/ $\text{H}_2\text{O}_2$ ) systems [118]. In Zhang et al's report [119], 84% of Orange II (10 mg  $\text{L}^{-1}$ ) can be efficiently decolorized within 60 min in an Fe(II)/sulfite-based photochemical system using a xenon lamp (350 W), whereas less efficiency (15%) was achieved without irradiation. Application of industrially available sulfite as a new source of sulfate radicals, instead of using expensive persulfate reagents, seems very promising in the practice of advanced oxidation technologies.

## References

- [1] Contreras-Ramos S M, Álvarez-Bernal D, Dendooven L. Removal of polycyclic aromatic hydrocarbons from soil amended with biosolid or vermicompost in the presence of earthworms (*Eisenia fetida*) [J]. *Soil Biology & Biochemistry*, 2008, 40(7): 1954-1959.
- [2] Wu J J, Muruganandham M, Chen S H. Degradation of DMSO by ozone-based advanced oxidation processes [J]. *Journal of Hazardous Materials*, 2007, 149(1): 218-225.
- [3] Buxton G V. Critical view of rate constants for reactions of hydrated electrons, hydrogen atoms and hydroxyl radicals in aqueous solution [J]. *Journal of Physical & Chemical Reference Data*, 1988, 17(2): 513-886.
- [4] Ribeiro A R, Nunes O C, Pereira M F, et al. An overview on the advanced oxidation processes applied for the treatment of water pollutants defined in the recently launched Directive 2013/39/EU [J]. *Environment International*, 2015, 75: 33-51.
- [5] Hoigné J. Inter-calibration of OH radical sources and water quality parameters [J]. *Water Science & Technology*, 1997, 35(4): 1-8.

- [6] Cheng M, Zeng G, Huang D, et al. Hydroxyl radicals based advanced oxidation processes (AOPs) for remediation of soils contaminated with organic compounds: A review [J]. Chemical Engineering Journal, 2016, 284: 582-598.
- [7] Ayoub K, van Hullebusch E D, Cassir M, et al. Application of advanced oxidation processes for TNT removal: A review [J]. Journal of Hazardous Materials, 2010, 178(1): 10-28.
- [8] Esplugas S, Yue P L, Pervez M I. Degradation of 4-chlorophenol by photolytic oxidation [J]. Water Research, 1994, 28(6): 1323-1328.
- [9] Wu J J, Muruganandham M, Chen S H. Degradation of DMSO by ozone-based advanced oxidation processes [J]. Journal of Hazardous Materials, 2007, 149(1): 218-225.
- [10] Vilhunen S, Vilve M, Vepsäläinen M, et al. Removal of organic matter from a variety of water matrices by UV photolysis and UV/H<sub>2</sub>O<sub>2</sub> method [J]. Journal of Hazardous Materials, 2010, 179(1-3): 776-782.
- [11] Puspita P, Roddick F, Porter N. Efficiency of sequential ozone and UV-based treatments for the treatment of secondary effluent [J]. Chemical Engineering Journal, 2015, 268(4): 337-347.
- [12] Crittenden J C, Hu S, Hand D W, et al. A kinetic model for H<sub>2</sub>O<sub>2</sub>/UV process in a completely mixed batch reactor [J]. Water Research, 1999, 33(10): 2315-2328.
- [13] Philippopoulos C J, Pouloupoulos S G. Photo-assisted oxidation of an oily wastewater using hydrogen peroxide [J]. Journal of Hazardous Materials, 2003, 98(1): 201-210.
- [14] Zangeneh H, Zinatizadeh A A L, Feizy M. A comparative study on the performance of different advanced oxidation processes (UV/O<sub>3</sub>/H<sub>2</sub>O<sub>2</sub>) treating linear alkyl benzene (LAB) production plant's wastewater [J]. Journal of Industrial & Engineering Chemistry, 2014, 20(4): 1453-1461.
- [15] Saritha P, Aparna C, Himabindu V, et al. Comparison of various advanced oxidation processes for the degradation of 4-chloro-2 nitrophenol [J]. Journal of Hazardous Materials, 2007, 149(3): 609-615.
- [16] Haber F, Weiss J. The Catalytic Decomposition of Hydrogen Peroxide by Iron Salts [J]. J Proc Roy Soc A, 1934, 147(147): 332-351.
- [17] Bautista P, Mohedano A F, Casas J A, et al. An overview of the application of Fenton oxidation to industrial wastewaters treatment [J]. Journal of Chemical Technology & Biotechnology Biotechnology, 2008, 83(10): 1323-1338.

- [18] Oturan M A, Aaron J J. Advanced Oxidation Processes in Water/Wastewater Treatment: Principles and Applications. A Review [J]. *Critical Reviews in Environmental Science & Technology*, 2014, 44(23): 2577-2641.
- [19] Flotron V, Delteil C, Padellec Y, et al. Removal of sorbed polycyclic aromatic hydrocarbons from soil, sludge and sediment samples using the Fenton's reagent process [J]. *Chemosphere*, 2005, 59(10): 1427-1437.
- [20] And J D L, Gallard H. Catalytic Decomposition of Hydrogen Peroxide by Fe(III) in Homogeneous Aqueous Solution: Mechanism and Kinetic Modeling [J]. *Environmental Science & Technology*, 1999, 33(16): 2726-2732.
- [21] Cheves W. Fenton's reagent revisited [J]. *Acc.chem.res*, 1975, 8(4): 125-131.
- [22] Joseph J. Pignatello, Esther Oliveros, Allison MacKay. Advanced Oxidation Processes for Organic Contaminant Destruction Based on the Fenton Reaction and Related Chemistry [J]. *Critical Reviews in Environmental Science & Technology*, 2006, 36(1): 71-84.
- [23] Nidheesh P V, Gandhimathi R. Trends in electro-Fenton process for water and wastewater treatment: An overview [J]. *Desalination*, 2012, 299(4): 1-15.
- [24] Nguyen T B, Coggon M M, Flagan R C, et al. Reactive uptake and photo-Fenton oxidation of glycol aldehyde in aerosol liquid water [J]. *Environmental Science & Technology*, 2013, 47(9): 4301-4307.
- [25] Iwasaki M, Hara M, Kawada H, et al. Cobalt Ion-Doped TiO<sub>2</sub> Photocatalyst Response to Visible Light [J]. *Journal of Colloid & Interface Science*, 2000, 224(1): 202-204.
- [26] Xie Z Q, Chen Y J. Hydrothermal synthesis and photocatalytic activity of zinc oxide nanorods [J]. *Chemical Research*, 2012.
- [27] Park H, Park Y, Kim W, et al. Surface modification of TiO<sub>2</sub>, photocatalyst for environmental applications [J]. *Journal of Photochemistry & Photobiology C Photochemistry Reviews*, 2013, 15(1): 1-20.
- [28] Dagher R, Drogui P, Robert D. Modified TiO<sub>2</sub> For Environmental Photocatalytic Applications: A Review [J]. *Industrial & Engineering Chemistry Research*, 2013, 52(10): 3581-3599.
- [29] Hoffmann M R, Choi W, Bahnemann D W. Environmental Applications of Semiconductor Photocatalysis [J]. *Chemical Reviews*, 1995, 95(1): 69-96.

- [30] Linsebigler A L, Lu G, Yates J T. Photocatalysis on TiO<sub>2</sub> Surfaces: Principles, Mechanisms, and Selected Results [J]. *Chemical Reviews*, 1995, 95(3): 735-758.
- [31] Ognier S, Rojo J, Liu Y, et al. Mechanisms of Pyrene Degradation during Soil Treatment in a Dielectric Barrier Discharge Reactor [J]. *Plasma Processes & Polymers*, 2015, 11(8): 734-744.
- [32] Anipsitakis G P, Tufano T P, Dionysiou D D. Chemical and microbial decontamination of pool water using activated potassium peroxymonosulfate [J]. *Water Research*, 2008, 42(12): 2899-2910.
- [33] Borgmann-Strahsen R. Comparative assessment of different biocides in swimming pool water [J]. *International Biodeterioration & Biodegradation*, 2003, 51(4): 291-297.
- [34] And G P A, Dionysiou D D. Degradation of Organic Contaminants in Water with Sulfate Radicals Generated by the Conjunction of Peroxymonosulfate with Cobalt [J]. *Environmental Science & Technology*, 2003, 37(20): 4790-4797.
- [35] Anipsitakis G P, Dionysiou D D. Radical generation by the interaction of transition metals with common oxidants [J]. *Environmental Science & Technology*, 2004, 38(13): 3705-3711.
- [36] Anipsitakis G P, Dionysiou D D. Transition metal/UV-based advanced oxidation technologies for water decontamination [J]. *Applied Catalysis B Environmental*, 2004, 54(3): 155-163.
- [37] Meunier B. ChemInform Abstract: Metalloporphyrins as Versatile Catalysts for Oxidation Reactions and Oxidative DNA Cleavage [J]. *Cheminform*, 1993, 24(12).
- [38] Saputra E, Utama P S, Muhammad S, et al. Catalytic Oxidation of Toxic Organics in Aqueous Solution for Wastewater Treatment: a Review [J]. 2011.
- [39] Chesney A R, Booth C J, Lietz C B, et al. Peroxymonosulfate Rapidly Inactivates the Disease-Associated Prion Protein [J]. *Environmental Science & Technology*, 2016, 50(13): 7095-8004.
- [40] Yu M, Teel A L, Watts R J. Activation of Peroxymonosulfate by Subsurface Minerals [J]. *Journal of Contaminant Hydrology*, 2016, 191: 33-43.
- [41] Flanagan J, Griffith W P, Skapski A C. The active principle of Caro's acid, HSO<sub>5</sub><sup>-</sup>: X-ray crystal structure of KHSO<sub>5</sub>·H<sub>2</sub>O [J]. *Journal of the Chemical Society Chemical Communications*, 1984, 23(23): 1574-1575.

- [42] Balakrishnan T, Kumar S D. The kinetics and mechanism of induced thermal decomposition of peroxomonosulphate by phase transfer catalysts [J]. *Journal of Chemical Sciences*, 2000, 112(4): 497-505.
- [43] Zhang Z, Edwards J O. Chain lengths in the decomposition of peroxomonosulfate catalyzed by cobalt and vanadium. Rate law for catalysis by vanadium [J]. *Inorganic Chemistry*, 1992, 31(17): 3514-3517.
- [44] Kim J, Edwards J O. A study of cobalt catalysis and copper modification in the coupled decompositions of hydrogen peroxide and peroxomonosulfate ion [J]. *Inorganica Chimica Acta*, 1995, 235(2): 9-13.
- [45] Mclachlan G A, Muller J G, Rokita S E, et al. Metal-mediated oxidation of guanines in DNA and RNA: a comparison of cobalt(II), nickel(II) and copper(II) complexes [J]. *Inorganica Chimica Acta*, 1996, 251: 193-199.
- [46] Hu P, Long M. Cobalt-catalyzed sulfate radical-based advanced oxidation: A review on heterogeneous catalysts and applications [J]. *Applied Catalysis B Environmental*, 2016, 181: 103-117.
- [47] Shukla P R, Wang S, Sun H, et al. Activated carbon supported cobalt catalysts for advanced oxidation of organic contaminants in aqueous solution [J]. *Applied Catalysis B Environmental*, 2010, 100(3): 529-534.
- [48] Chen X, Chen J, Qiao X, et al. Performance of nano-Co<sub>3</sub>O<sub>4</sub>/peroxymonosulfate system: Kinetics and mechanism study using Acid Orange 7 as a model compound [J]. *Applied Catalysis B Environmental*, 2008, 80(1-2): 116-121.
- [49] Yang B, Tian Z, Wang B, et al. Facile synthesis of Fe<sub>3</sub>O<sub>4</sub>/hierarchical-Mn<sub>3</sub>O<sub>4</sub>/graphene oxide as a synergistic catalyst for activation of peroxymonosulfate for degradation of organic pollutants [J]. *Rsc Advances*, 2015, 5(27): 20674-20683.
- [50] G P A, Elias Stathatos A. Heterogeneous Activation of Oxone Using Co<sub>3</sub>O<sub>4</sub> [J]. *Journal of Physical Chemistry B*, 2005, 109(27): 13052-13055.
- [51] Flanagan J, Griffith W P, Skapski A C. The active principle of Caro's acid, HSO<sub>5</sub><sup>-</sup>: X-ray crystal structure of KHSO<sub>5</sub>·H<sub>2</sub>O [J]. *Journal of the Chemical Society Chemical Communications*, 1984, 23(23):1574-1575.

- [52] Rao Y, Chen M, Zhou M. Degradation of Diclofenac by  $\text{Co}_3\text{O}_4$ -catalyzed Activation of Oxone Process [J]. *Journal of Advanced Oxidation Technologies*, 2014, 17(17): 145-151(7).
- [53] Wang Y, Zhou L, Duan X, et al. Photochemical degradation of phenol solutions on  $\text{Co}_3\text{O}_4$  nanorods with sulfate radicals [J]. *Catalysis Today*, 2015, 258: 576-584.
- [54] Ding Y, Zhu L, Huang A, et al. A heterogeneous  $\text{Co}_3\text{O}_4$ - $\text{Bi}_2\text{O}_3$  composite catalyst for oxidative degradation of organic pollutants in the presence of peroxymonosulfate [J]. *Catalysis Science & Technology*, 2012, 2(9): 1977-1984.
- [55] Stoyanova M, Slavova I, Christoskova S, et al. Catalytic performance of supported nanosized cobalt and iron-cobalt mixed oxides on MgO in oxidative degradation of Acid Orange 7 azo dye with peroxymonosulfate [J]. *Applied Catalysis A General*, 2014, 476(6): 121-132.
- [56] Zhu Y, Chen S, Quan X, et al. Cobalt implanted  $\text{TiO}_2$  nanocatalyst for heterogeneous activation of peroxymonosulfate [J]. *Rsc Advances*, 2013, 3(2): 520-525.
- [57] Zhang W, Tay H L, Lim S S, et al. Supported cobalt oxide on MgO: Highly efficient catalysts for degradation of organic dyes in dilute solutions [J]. *Applied Catalysis B Environmental*, 2010, 95(1): 93-99.
- [58] Olmez-Hanci T, Imren C, Kabdaşlı I, et al. Application of the UV-C photo-assisted peroxymonosulfate oxidation for the mineralization of dimethyl phthalate in aqueous solutions [J]. *Photochemical & Photobiological Sciences Official Journal of the European Photochemistry Association & the European Society for Photobiology*, 2011, 10(3): 408-413.
- [59] Anipsitakis G P, Dionysiou D D. Transition metal/UV-based advanced oxidation technologies for water decontamination [J]. *Applied Catalysis B Environmental*, 2004, 54(3): 155-163.
- [60] Jaafarzadeh N, Ghanbari F, Moradi M. Photo-electro-oxidation assisted peroxymonosulfate for decolorization of acid brown 14 from aqueous solution [J]. *Korean Journal of Chemical Engineering*, 2015, 32(3): 458-464.
- [61] Olmez-Hanci T, Imren C, Kabdaşlı I, et al. Application of the UV-C photo-assisted peroxymonosulfate oxidation for the mineralization of dimethyl phthalate in aqueous solutions [J]. *Photochemical & Photobiological Sciences Official Journal of the European Photochemistry Association & the European Society for Photobiology*, 2011, 10(3): 408-413.
- [62] Herrmann H. On the Photolysis of Simple Anions and Neutral Molecules as Sources of  $\text{SO}_x^-$  and Cl in Aqueous Solution [J]. *Physical Chemistry Chemical Physics Pccp*, 2007, 9(30): 3935-3942.

- [63] F.J. Beltran, Ozone-UV radiation-hydrogen peroxide oxidation technologies, Chemical Degradation Methods for Wastes and Pollutants: Environmental and Industrial Applications, Marcel Dekker, New York, USA, 2003, 1–76.
- [64] Getoff N. Purification of drinking water by irradiation. A review [J]. Journal of Chemical Sciences, 1993, 105(6): 373-391.
- [65] Sharma J, Mishra I M, Dionysiou D D, et al. Oxidative removal of Bisphenol A by UV-C/peroxymonosulfate (PMS): Kinetics, influence of co-existing chemicals and degradation pathway [J]. Chemical Engineering Journal, 2015, 276: 193-204.
- [66] Verma S, Nakamura S, Sillanpää M. Application of UV-C LED activated PMS for the degradation of anatoxin-a [J]. Chemical Engineering Journal, 2016, 284: 122-129.
- [67] Hori H, Nagaoka Y, Murayama M, et al. Efficient Decomposition of Perfluorocarboxylic Acids and Alternative Fluor chemical Surfactants in Hot Water [J]. Environmental Science & Technology, 2008, 42(19): 7438-7451.
- [68] Jia Q Z, Ma P S, Zhou H, et al. The effect of temperature on the solubility of benzoic acid derivatives in water [J]. Fluid Phase Equilibria, 2006, 250(1-2): 165-172.
- [69] Yang S Y, Wang P, Yang X, et al. Degradation efficiencies of azo dye Acid Orange 7 by the interaction of heat, UV and anions with common oxidants: persulfate, peroxymonosulfate and hydrogen peroxide [J]. Journal of Hazardous Materials, 2010, 179(1-3): 552-558.
- [70] C.J. Liang, C.J. Bruell, M.C. Marley, K.L. Sperry, Thermally activated PS oxidation of trichloroethylene (TCE) and 1,1,1-trichloroethane (TCA) in aqueous systems and soil slurries, Soil Sediment Contam. 12 (2003): 207-228.
- [71] Flanagan J, Griffith W P, Skapski A C. The active principle of Caro's acid,  $\text{HSO}_5^-$ : X-ray crystal structure of  $\text{KHSO}_5 \cdot \text{H}_2\text{O}$  [J]. Journal of the Chemical Society Chemical Communications, 1984, 23(23): 1574-1575.
- [72] I.M. Kolthoff, I.K. Miller, The Chemistry of PS. I. The kinetics and mechanism of the decomposition of the PS ion in aqueous medium<sup>1</sup>, J. Am. Chem. Soc. 73 (1951): 1-30.
- [73] Budaev S L, Batoeva A A, Tsybikova B A. Degradation of thiocyanate in aqueous solution by persulfate activated ferric ion [J]. Minerals Engineering, 2015, 81: 88-95.

- [74] Monteagudo J M, Durán A, González R, et al. In situ chemical oxidation of carbamazepine solutions using persulfate simultaneously activated by heat energy, UV light, Fe<sup>2+</sup> ions, and H<sub>2</sub>O<sub>2</sub> [J]. *Applied Catalysis B Environmental*, 2015, 176-177: 120-129.
- [75] Lau T K, Chu W, Graham N J. The aqueous degradation of butylated hydroxyanisole by UV/S<sub>2</sub>O<sub>8</sub><sup>2-</sup>: study of reaction mechanisms via dimerization and mineralization [J]. *Environmental Science & Technology*, 2007, 41(2): 613-619.
- [76] Anipsitakis G P, Dionysiou D D. Radical generation by the interaction of transition metals with common oxidants [J]. *Environmental Science & Technology*, 2004, 38(13): 3705-3711.
- [77] Jiang X, Wu Y, Wang P, et al. Degradation of bisphenol A in aqueous solution by persulfate activated with ferrous ion [J]. *Environmental Science & Pollution Research*, 2013, 20(7): 4947-4953.
- [78] Liang C, Guo Y Y. Mass transfer and chemical oxidation of naphthalene particles with zero valent iron activated persulfate [J]. *Environmental Science & Technology*, 2010, 44(21):8203-8211.
- [79] Ahmad M, Teel A L, Watts R J. Persulfate activation by subsurface minerals [J]. *Journal of Contaminant Hydrology*, 2010, 115(1-4): 34-45.
- [80] Liang C, Bruell C J, Marley M C, et al. Persulfate oxidation for in situ remediation of TCE. I. Activated by ferrous ion with and without a persulfate-thiosulfate redox couple [J]. *Chemosphere*, 2004, 55(9): 1213-1223.
- [81] Zhang Y Q, Huang W L, Fennell D E. In situ chemical oxidation of aniline by persulfate with iron(II) at ambient temperature [J]. *Chin Chem Lett*, 2010, 21: 911-913.
- [82] Rastogi A, Alabed S R, Dionysiou D D. Effect of inorganic, synthetic and naturally occurring chelating agents on Fe(II) mediated advanced oxidation of chlorophenols [J]. *Water Research*, 2009, 43(3): 684-94.
- [83] Wu Y, Prulho R, Brigante M, et al. Activation of persulfate by Fe(III) species: Implications for 4-tert-butylphenol degradation [J]. *Journal of Hazardous Materials*, 2017, 322: 380-386.
- [84] Liu C S, Shih K, Sun C X, et al. Oxidative degradation of propachlor by ferrous and copper ion activated persulfate [J]. *Science of the Total Environment*, 2012, 416: 507-512).
- [85] Pan X, Yan L, Qu R, et al. Degradation of the UV-filter benzophenone-3 in aqueous solution using persulfate activated by heat, metal ions and light [J]. *Chemosphere*, 2017, 196: 95-101.

- [86] Jiang X, Wu Y, Wang P, et al. Degradation of bisphenol A in aqueous solution by persulfate activated with ferrous ion [J]. *Environmental Science & Pollution Research*, 2013, 20(7): 4947-4953.
- [87] Zhao L, Ji Y, Kong D, et al. Simultaneous removal of bisphenol A and phosphate in zero-valent iron activated persulfate oxidation process [J]. *Chemical Engineering Journal*, 2016, 303: 458-466.
- [88] Oh S Y, Kang S G, Kim D W, et al. Degradation of 2,4-dinitrotoluene by persulfate activated with iron sulfides [J]. *Chemical Engineering Journal*, 2011, 172(2): 641-646.
- [89] Zhang Y, Tran H P, Du X, et al. Efficient pyrite activating persulfate process for degradation of p-chloroaniline in aqueous systems: a mechanistic study [J]. *Chemical Engineering Journal*, 2017, 308: 1112-1119.
- [90] Liang C, Wang Z S, Bruell C J. Influence of pH on persulfate oxidation of TCE at ambient temperatures [J]. *Chemosphere*, 2007, 66(1): 106-113.
- [91] Frontistis Z, Mestres E M, Konstantinou I, et al. Removal of cibacron black commercial dye with heat- or iron-activated persulfate: statistical evaluation of key operating parameters on decolorization and degradation by-products [J]. *Desalination & Water Treatment*, 2016, 57(6): 2616-2625.
- [92] Tan C, Gao N, Deng Y, et al. Heat-activated persulfate oxidation of diuron in water [J]. *Chemical Engineering Journal*, 2012, 203(5): 294-300.
- [93] Fan Y, Ji Y, Kong D, Lu J, Zhou Q. Kinetic and mechanistic investigations of the degradation of sulfamethazine in heat-activated PS oxidation process [J]. *Journal of Hazardous Materials*, 2015, 300: 39-47
- [94] Xu X, Pliego G, Zazo J A, et al. Mineralization of naphtenic acids with thermally-activated persulfate: The important role of oxygen.[J]. *Journal of Hazardous Materials*, 2016, 318:355-362.
- [95] Waldemer R H, Tratnyek P G, Johnson R L, et al. Oxidation of chlorinated ethenes by heat-activated persulfate: kinetics and products [J]. *Environmental Science & Technology*, 2007, 41(3): 1010-1015.
- [96] Wang L, Peng L, Xie L, et al. Compatibility of surfactants and thermally activated persulfate for enhanced subsurface remediation [J]. *Environmental Science & Technology*, 2017.

- [97] Costanza J, Otaño G, Callaghan J, et al. PCE oxidation by sodium persulfate in the presence of solids [J]. *Environmental Science & Technology*, 2010, 44(24): 9445-9451.
- [98] Lee Y, Shanglien L O, Kuo J, et al. Decomposition of perfluorooctanoic acid by microwave activated persulfate: Effects of temperature, pH, and chloride ions [J]. *Frontiers of Environmental Science & Engineering*, 2012, 6(1): 17-25.
- [99] Bu L, Zhou S, Zhou S, et al. Degradation of oxcarbazepine by UV-activated persulfate oxidation: kinetics, mechanisms, and pathways [J]. *Environmental Science & Pollution Research*, 2016, 23(3): 2848-2855.
- [100] Dhaka S, Kumar R, Khan M A, et al. Aqueous phase degradation of methyl paraben using UV-activated persulfate method [J]. *Chemical Engineering Journal*, 2017, 321: 11-19.
- [101] Hou S, Ling L, Shang C, et al. Degradation Kinetics and Pathways of Haloacetonitriles by the UV/Persulfate Process [J]. *Chemical Engineering Journal*, 2017.
- [102] Tan CQ, Gao NY, Deng Y, Zhang YJ, Sui MH, Deng J, Zhou SQ. Degradation of antipyrine by UV, UV/H<sub>2</sub>O<sub>2</sub> and UV/PS[J]. *Journal of Hazardous Materials*, 2013, 260: 1008-1016
- [103] Luo C, Ma J, Jiang J, et al. Simulation and comparative study on the oxidation kinetics of atrazine by UV/H<sub>2</sub>O<sub>2</sub>, UV/HSO<sub>5</sub><sup>-</sup> and UV/S<sub>2</sub>O<sub>8</sub><sup>2-</sup> [J]. *Water Research*, 2015, 80: 99-103.
- [104] Bu L, Zhou S, Zhou S, et al. Degradation of oxcarbazepine by UV-activated persulfate oxidation: kinetics, mechanisms, and pathways [J]. *Environmental Science & Pollution Research*, 2016, 23(3): 2848-2855.
- [105] Ao X, Liu W. Degradation of sulfamethoxazole by medium pressure UV and oxidants: Peroxymonosulfate, persulfate, and hydrogen peroxide [J]. *Chemical Engineering Journal*, 2017, 313: 629-637.
- [106] Herrmann H. On the Photolysis of Simple Anions and Neutral Molecules as Sources of SO<sub>x</sub><sup>-</sup> and Cl in Aqueous Solution [J]. *Physical Chemistry Chemical Physics Pccp*, 2007, 9(30): 3935-3942.
- [107] Mark G, Man N S, Schuchmann H P, et al. The photolysis of potassium peroxodisulphate in aqueous solution in the presence of tert-butanol: a simple acidometer for 254 nm radiation [J]. *Journal of Photochemistry & Photobiology A Chemistry*, 1990, 55(2): 157-168.
- [108] Lin C C, Wu M S. UV/S<sub>2</sub>O<sub>8</sub><sup>2-</sup>, process for degrading polyvinyl alcohol in aqueous solutions [J]. *Chemical Engineering & Processing Process Intensification*, 2014, 85: 209-215.
- [109] Devi P, Das U, Dalai A K. In-situ chemical oxidation: Principle and applications of peroxide and

- persulfate treatments in wastewater systems [J]. *Science of the Total Environment*, 2016, 571: 643-657.
- [110] L.W. Matzek, K.E. Carter, Activated PS for organic chemical degradation: a review, *Chemosphere*, 2016, 151: 178–188
- [111] Bu L, Zhou S, Shi Z, et al. Removal of 2-MIB and geosmin by electrogenerated persulfate: Performance, mechanism and pathways [J]. *Chemosphere*, 2017, 168: 1309-1316.
- [112] Farhat A, Keller J, Tait S, et al. Removal of Persistent Organic Contaminants by Electrochemically Activated Sulfate [J]. *Environmental Science & Technology*, 2015, 49(24): 14326-14333.
- [113] Zhao J, Zhang Y, Xie Q, et al. Enhanced oxidation of 4-chlorophenol using sulfate radicals generated from zero-valent iron and peroxydisulfate at ambient temperature [J]. *Separation & Purification Technology*, 2010, 71(3): 302-307.
- [114] Yuan S, Liao P, Alshwabkeh A N. Electrolytic manipulation of persulfate reactivity by iron electrodes for trichloroethylene degradation in groundwater [J]. *Environmental Science & Technology*, 2014, 48(1): 656-663.
- [115] Lin H, Wu J, Zhang H. Degradation of bisphenol A in aqueous solution by a novel electro/Fe<sup>3+</sup>/peroxydisulfate process [J]. *Separation & Purification Technology*, 2013, 117(4):18-23.
- [116] Chen W S, Jhou Y C, Huang C P. Mineralization of dinitrotoluenes in industrial wastewater by electro-activated persulfate oxidation [J]. *Chemical Engineering Journal*, 2014, 252(5): 166-172.
- [117] Carter K E, Farrell J. Oxidative destruction of perfluorooctane sulfonate using boron-doped diamond film electrodes [J]. *Environmental Science & Technology*, 2008, 42(16): 6111-6115.
- [118] Long C, Peng X, Liu J, et al. Decolorization of Orange II in Aqueous Solution by an Fe(II)/sulfite System: Replacement of Persulfate [J]. *Industrial & Engineering Chemistry Research*, 2016, 51(42): 13632–13638.
- [119] Zhang L, Chen L, Xiao M, et al. Enhanced Decolorization of Orange II Solutions by the Fe(II)–Sulfite System under Xenon Lamp Irradiation [J]. *Industrial & Engineering Chemistry Research*, 2013, 52(30): 10089-10094.

**Chapter 3 A simple Cr(VI)-S(IV)-O<sub>2</sub> system for rapid and simultaneous reduction of Cr(VI) and oxidative degradation of organic pollutants**

### 3.1 Introduction

Chromium, a common heavy-metal contaminant, is known as a hazardous material. It normally occurs as hexavalent chromium (Cr(VI)) and trivalent chromium (Cr(III))[1]. As Cr(VI) is more toxic than Cr(III), reduction of Cr(VI) to Cr(III) is the principal strategy for pollution control for industrial emissions containing Cr(VI)[2]. Because of the high standard reduction potential of Cr(VI)/Cr(III) at acidic pH (e.g.,  $E^0: \text{Cr}_2\text{O}_7^{2-}/\text{Cr}^{3+} = 1.36 \text{ V}$ )[3], Cr(VI) can be easily reduced by chemical reductants [4,5] and biological processes [6]. Among its known reductants, ferrous iron (Fe(II),  $E^0: \text{Fe}^{3+}/\text{Fe}^{2+} = 0.771 \text{ V}$ ) [3] has been extensively used over the past several decades because it is abundant, reliable, inexpensive, and efficient [7,8]. Another advantage of using Fe(II) as reductant in wastewater is the simple separation of reduced Cr(III) via Cr(OH)<sub>3</sub> formation and coprecipitation with Fe(OH)<sub>3</sub> at high pH.

Industrial wastewaters usually contain more than one type of contaminant. Even effluents from electroplating and textile industries contain heavy metals and organic additives [9,10]. Therefore, heavy metals and organic contaminants must be removed to meet the requirement of discharge standards. Dual functions have been developed for simultaneous removal of heavy metals and organic contaminants. Methods such as biodegradation, biosorption, adsorption, and nanotechnology using Pd(II) and Cr(VI) for removing organic pollutants such as benzoate, as well as phenol catabolism, have received much attention [11-13]. Kaur and Crimi designed a system using in situ chemical oxidation and persulfate to treat soils and groundwater contaminated with organic and metal contaminants [14]; however, its degradation processes take much time and involve many complex technical procedures to achieve the goal. Semiconductor photocatalytic systems (e.g., TiO<sub>2</sub>) can produce reductive and oxidative species (e.g., electron-hole pair) simultaneously [15]. The photo-Fenton-like process induced by the Fe(III)-OH complex [16] produces reductive Fe(II) and oxidative HO• radicals. These photochemical systems have been applied in simultaneous reduction of Cr(VI) and oxidation of organic contaminants (e.g., dye and surfactant); however, they are more expensive and complicated.

Studies have also used sulfur species such as sulfides (hydrogen sulfide [17] and calcium polysulfide [18]) and sulfite [19] for Cr(VI) reduction. These works focused on the kinetics of Cr(VI) reduction but did not probe the mechanism of transformation of sulfur species. Cr(VI)-catalyzed autoxidation of S(IV) [20,21] had been investigated during 1960s and 1990s. Formation of oxysulfur radicals (mainly SO<sub>3</sub>•<sup>-</sup>, SO<sub>4</sub>•<sup>-</sup>, and SO<sub>5</sub>•<sup>-</sup>) in this reaction has been confirmed; however, the potential application of such oxysulfur radicals in the oxidation of

organic or inorganic contaminants, except in the Fe(III)/Fe(II)-S(IV)-O<sub>2</sub> system, has been very limited [22,23]. Recently, we showed that the rapid decolorization of azo dyes by the Fe(III)/Fe(II)-S(IV)-O<sub>2</sub> system with or without UV-vis irradiation [24-26] is a promising alternative to an advanced oxidation process using persulfate [27]. The possibility of oxidation of organic contaminants by a S(IV)-O<sub>2</sub> system using Cr(VI) induction and Cr(VI) reduction has not yet been explored.

The aim of this work was to propose the simultaneous reduction of Cr(VI) and oxidation of organic contaminants by sulfite ions in the presence of oxygen. The Cr(VI)-S(IV)-O<sub>2</sub> system reduces Cr(VI) during S(IV) autoxidation, which means that it can utilize inorganic waste Cr(VI) to degrade organic waste. A rapid reaction using the azo dye acid orange 7 (AO7, the organic substrate) that is comparable to Cr(VI) reduction was used in oxidative decolorization at various pH values and Cr(VI)/S(IV) molar ratios. We examined the effect of oxygen and different kinds of radical scavengers used to quench radicals generated in this system. The mechanism of the system and the contribution of reactive oxygen species and reactive sulfur species were preliminarily probed. Furthermore, aniline, phenol, bisphenol A and their substituted analogs were selected to testify the possible application of this system. This work provides a novel and low-cost system for waste treatment using waste Cr(VI) to achieve simultaneous reduction of Cr(VI) and oxidation of organic contaminants.

## 3.2 Material and methods

### 3.2.1 Chemicals.

A Cr(VI) solution was prepared by dissolving analytical-grade (AR) potassium dichromate (K<sub>2</sub>Cr<sub>2</sub>O<sub>7</sub>). AO7, 1,5-diphenylc arbazide used to detect the concentration of Cr(VI), the radical scavengers *tert*-butyl alcohol (TBA) and aniline, as well as NaOH (AR) and H<sub>2</sub>SO<sub>4</sub> (AR) which were used to adjust the pH of the solutions, were obtained from Sinopharm Chemical Reagent Co., Ltd. Na<sub>2</sub>SO<sub>3</sub> (AR) (Shanghai Zhanyun Chemical Co., Ltd.) was prepared just prior to measurements. Analytical-grade o-Nitroaniline, p-Nitroaniline, p-Chloroaniline, Sulfonamides, Phenol, Bisphenol A, 2-Bromophenol, Paracetamol, p-aminophenol, Catechol, o-Nitrophenol, 2,6-Dinitrophenol, which were used to testify the possible application of this system were also purchased from Sinopharm Chemical Reagent Co., Ltd. Acetonitrile and methanol were HPLC grade and purchased from Fisher Corporation. All chemicals were used without further purification. Ultrapure water with 18.2 MΩ cm resistivity used in this work was obtained through a water purification system (Liyuan Electric

Instrument Co., Beijing, China).

### 3.2.2 Reaction procedures.

All experiments were performed by using a 200 mL beaker at about  $20 \pm 2$  °C and under normal laboratory lighting. Predetermined amounts of AO7 and Na<sub>2</sub>SO<sub>3</sub> were added to the beaker. The pH of reaction solutions thus prepared was adjusted to the desired values with dilute NaOH and H<sub>2</sub>SO<sub>4</sub>. Each solution was constantly stirred with a Polytetrafluoroethylene (PTFE)-coated magnetic stirrer, and each run was performed by careful addition of the desired amount of Cr(VI) that was prepared beforehand. The pH was not controlled during the reaction. Samples were withdrawn at specific time intervals and analyzed immediately in order to avoid further reaction. The initial concentration of the substrates in all batch experiments was 0.029 mM. In the radical-scavenging experiments, specific concentrations of TBA or aniline, scavengers for HO• or oxysulfur radicals, respectively, were added to the reaction solutions (the procedure for preparation of their solutions is similar to that for substrates and Na<sub>2</sub>SO<sub>3</sub>). The concentrations of TBA and aniline in the solutions were 11.6 and 2.9 mM, respectively. The effect of oxygen was also investigated. Nitrogen introduced through a gas-purging tube was used to exclude oxygen from the solution. To maintain constant conditions, the total flow rate of nitrogen was maintained at 1 L min<sup>-1</sup>. All experiments were carried out in parallel. All relative errors were <5%.

### 3.2.3 Analysis.

An optical-fiber spectrometer (Shimadzu, Japan) was used to measure AO7 concentrations by absorbance detection at 485 nm. The Cr(VI) concentration was determined spectrophotometrically at 540 nm by using 1,5-diphenylcarbazide, and the calibration of Cr(VI) was shown in Figure 3-1. In addition, spectra of the remaining AO7 were obtained on a UV-1601 spectrophotometer (Shimadzu, Japan) using a cuvette with 1 cm width. A LC-10A HPLC system (Shimadzu, Japan) equipped with a SIL-10A auto sampler, an SPD-10A UV detector and a C18 reverse-phase column (4.6 × 250 mm, 5 μm, Dalian Elite Analytical Instruments Co., LTD., PRC) was used to monitor residual aniline, phenol, bisphenol A etc. The injected volume was 100 μL, the UV detection and the corresponding mobile phase with a 1 mL min<sup>-1</sup> flow rate were as follows: aniline and o-Nitroaniline: 230 nm with water/acetonitrile mixture (45/55 v/v); p-Nitroaniline: 272 nm with water/methanol mixture (45/55 v/v), p-Chloroaniline: 260 nm with water/acetonitrile mixture (45/55 v/v), Sulfonamides: 270 nm with water/acetonitrile mixture (45/55 v/v), Phenol: 270 nm with water/methanol mixture (45/55 v/v), Bisphenol A: 278 nm with water/methanol mixture

(40/60 v/v), 2-Bromophenol: 278nm with water/acetonitrile mixture (45/55 v/v), Paracetamol: 241 nm with water/ methanol mixture (75/25 v/v), p-aminophenol: 225nm with water/methanol mixture (50/50 v/v), Catechol: 270 nm with water/methanol mixture (70/30 v/v), o-Nitrophenol: 278 nm with water/ methanol mixture (35/65 v/v), 2,6-Dinitrophenol: 225 nm with water/ methanol mixture (35/65 v/v). The pH was measured on a pHs-3C pH meter (Hinotek, Ningbo, China). TOC (Total Organic Carbon) analysis was performed on an Analytik Jena multi N/C 2100.

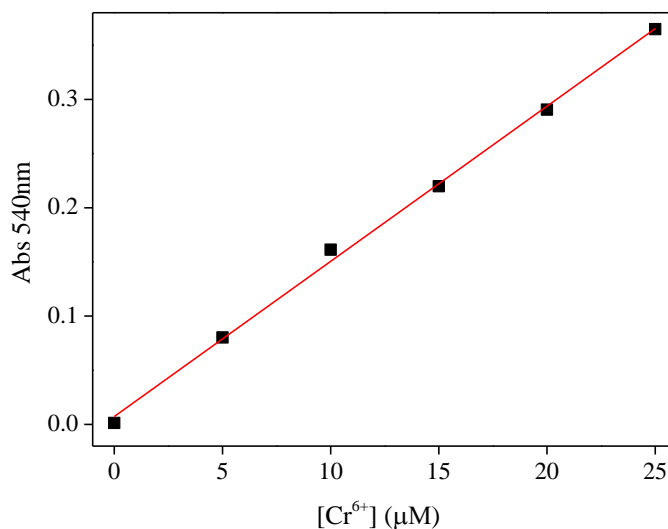


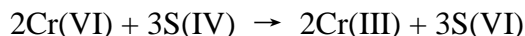
**Figure. 3-1.** The calibration of Cr(VI)

### 3.3 Results and discussion

#### 3.3.1 Control experiments.

As shown in Figure. 3-2a, neither S(IV) nor Cr(VI) added to the reagent had an effect on AO7 decolorization. Although Cr(VI) becomes a stronger oxidant at acidic pH, it could not oxidize AO7 at pH 3.0 when it is at low concentration (0.1 mM). S(IV), a common reductant, could reduce Cr(VI) under these conditions but could not decolorize AO7. These results suggest that AO7 decolorization depends on the reaction between S(IV) and Cr(VI). As shown in Figure.3-2b, AO7 could not reduce Cr(VI) in the absence of S(IV); but with S(IV) and Cr(VI) in solution in the absence of AO7, there was almost no difference in the amount of Cr(VI) reduced and that in the presence of AO7. All of these findings indicate that AO7 decolorization and Cr(VI) reduction proceeded only when S(IV) and Cr(VI) were present. Thus, the well-known reaction in eqs (3-1)[19] and reactions leading to AO7 decolorization

occurred in the Cr(VI)–S(IV)–O<sub>2</sub> system were as follows:



3-1

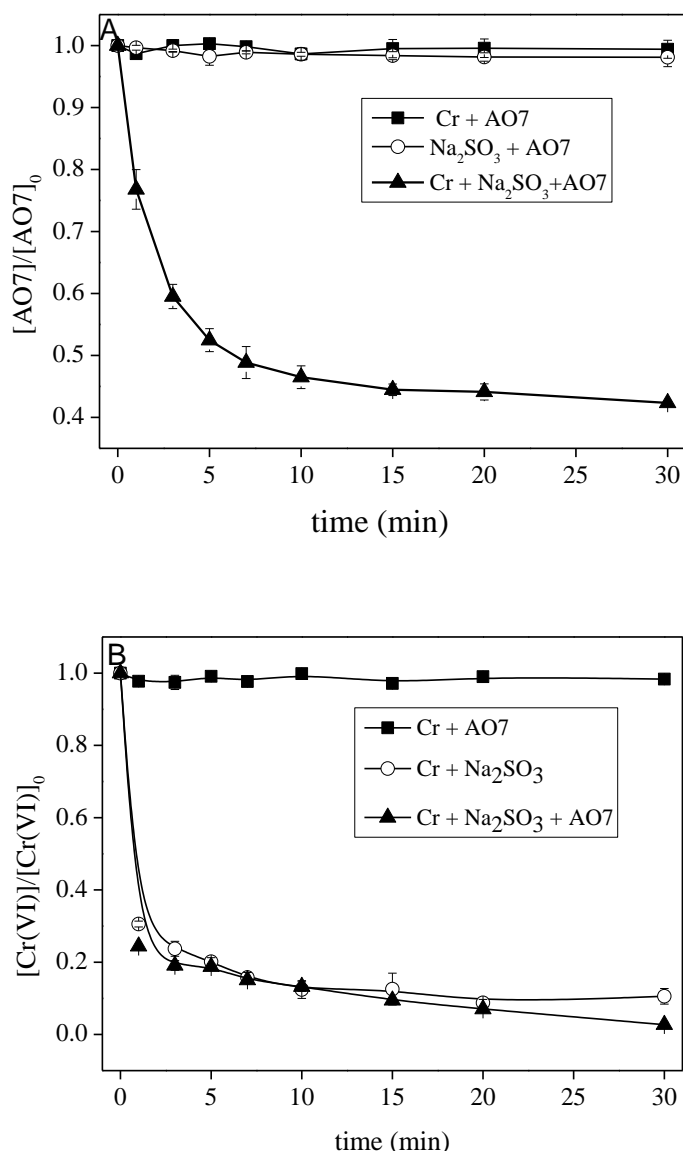
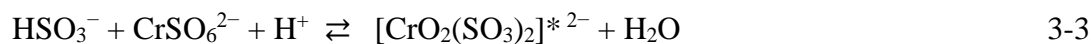


**Figure. 3-2(a).** Change in AO7 concentration in the control experiments under various conditions. Conditions: [AO7]<sub>0</sub> = 0.029 mM, [Cr(VI)]<sub>0</sub> = 0.1 mM, [Na<sub>2</sub>SO<sub>3</sub>]<sub>0</sub> = 0.55 mM, pH<sub>ini</sub> = 3.0. **(b).** Change in Cr(VI) concentration in the control experiments under various conditions. Conditions: [AO7]<sub>0</sub> = 0.029 mM, [Na<sub>2</sub>SO<sub>3</sub>]<sub>0</sub> = 0.55 mM, [Cr(VI)]<sub>0</sub> = 0.1 mM, pH<sub>ini</sub> = 3.0.

Early in 1965, Haight et al.[20] investigated the mechanism of S(IV) oxidation by Cr(VI) in acidic solution. They proposed the formation of active CrSO<sub>6</sub><sup>2-</sup> and the intermediate complex [CrO<sub>2</sub>(SO<sub>3</sub>)<sub>2</sub>]<sup>\*2-</sup> via reactions between Cr(VI) and S(IV) (eqs (3-2) and (3-3)). The intermediate complex [CrO<sub>2</sub>(SO<sub>3</sub>)<sub>2</sub>]<sup>\*2-</sup> is unstable and undergoes further intermolecular electron-transfer reaction (eqs (3-4)) to produce sulfite radical (SO<sub>3</sub><sup>\*-</sup>) and Cr(III). The net

reaction of the reactions in eqs ((3-2)–(3-4)) may be expressed as eqs (3-5) or simply as eqs (3-6), which indicates the reaction between Cr(VI) and S(IV) that produces  $\text{SO}_3^{\bullet-}$ . A study conducted by Hollyer et al.[28], gave further evidence of the generation of sulfite radicals,  $\text{SO}_3^{\bullet-}$ , rather than  $\text{SO}_4^{2-}$ ; they found that upon addition of barium chloride to the reaction between Cr(VI) and S(IV), no precipitation occurred immediately. The rapid increase in Cr(VI) reduction within several minutes may be explained by the rapid formation of a Cr(III)–S(VI) complex[29]. Subsequent transformation of oxysulfur radicals ( $\text{SO}_3^{\bullet-}$ ,  $\text{SO}_4^{\bullet-}$ , and  $\text{SO}_5^{\bullet-}$ ) occur in the presence of dissolved oxygen, as mainly shown by eqs ((3-7)–(3-10)). The study of Brandt and Elding[29] also supports such mechanism; they propose the role of Cr(VI) in the atmospheric oxidation of S(IV). Therefore, the formation reactions of oxysulfur radicals in the Cr(VI)–S(IV)– $\text{O}_2$  system that lead to AO7 decolorization are similar to those in the Fe(III)–S(IV)– $\text{O}_2$  system (eqs (3-11))[24-26].



### 3.3.2 Effect of pH.

To determine the optimum initial pH of the Cr(VI)–S(IV)– $\text{O}_2$  system, experiments at initial pH values ( $\text{pH}_{\text{init}}$ ) between 3.0 and 7.0 were conducted. As seen in Figure. 3-3a and 3-3b, the initial pH of the reagent mixture had a strong effect on Cr(VI) reduction and AO7 decolorization. As depicted in Figure. 3-3a, Cr(VI) was quickly reduced to Cr(III) in ~5 min. When the pH increased from 3.0 to 7.0, the reduction efficiency decreased from 97.8% to 83.5%. The rate of AO7 decolorization increased with the decrease in pH. The efficiency of AO7 decolorization after 30 min reached 57.7%, 51.8%, and 48.8% at pH 3.0, 4.0, and 5.0, respectively, but the decolorization efficiency was less than 7% at the initial pH above 6.

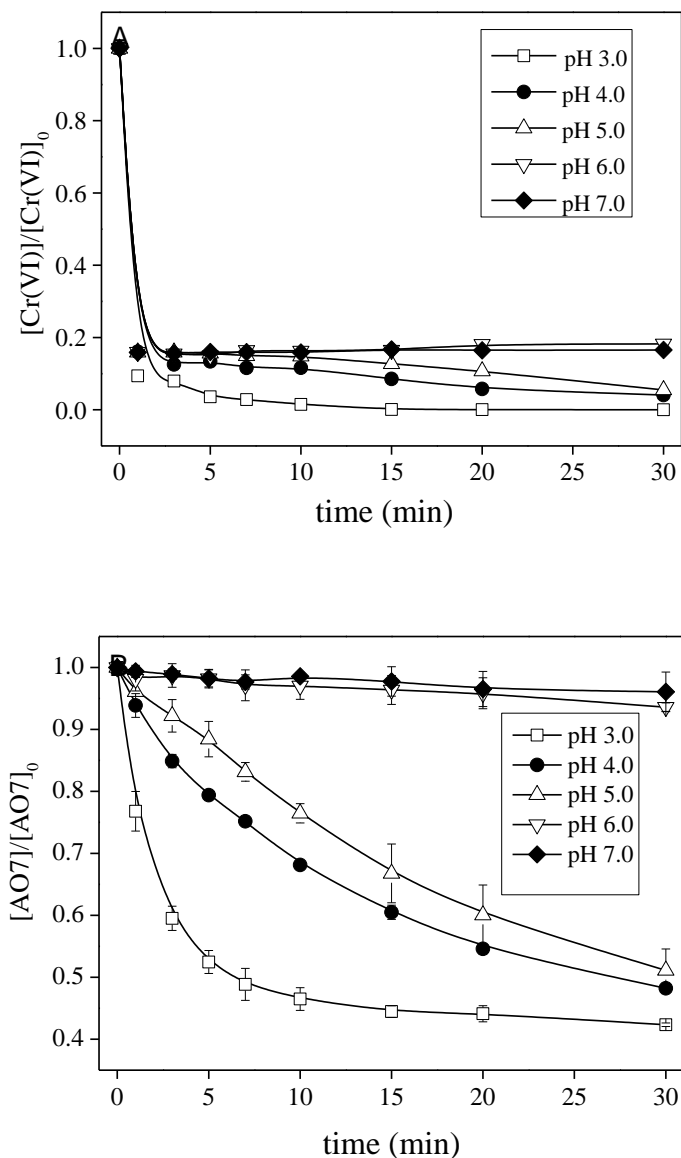


**Figure. 3-3.** (a) Change in Cr(VI) concentration and in (b) AO7 concentration during Cr(VI) reduction in the Cr(VI)–S(IV)–O<sub>2</sub> system at various pH values. Conditions:  $[\text{AO7}]_0 = 0.029$  mM,  $[\text{Cr(VI)}]_0 = 0.1$  mM,  $[\text{Na}_2\text{SO}_3]_0 = 0.55$  mM.

Speciation of both Cr(VI) and S(IV) under the aforementioned conditions may primarily account for the increase in reaction rate with decreasing pH. Both pH and the total concentration of Cr(VI) determine the species distribution. Figure 3-4 and 3-5 show that the predominant Cr(VI) species at pH 1.0–6.0 is  $\text{HCrO}_4^-$  when the initial total concentration of Cr(VI) is 0.1–2.0 mM.  $\text{HCrO}_4^-$  has higher standard electrode potential at low pH ( $E^0(\text{HCrO}_4^-/\text{Cr}^{3+}) = 1.20$  V) compared with that of  $\text{CrO}_4^{2-}$  ( $E^0(\text{CrO}_4^{2-}/\text{Cr}(\text{OH})_4^-) = -0.13$  V) for higher pH[3], and thus more easily undergoes reduction by S(IV) than does  $\text{CrO}_4^{2-}$ . Moreover, the fraction of  $\text{HCrO}_4^-$  increased with decreasing pH from 7 to 3, which resulted in faster reduction of Cr(VI) at lower pH. As shown in Figure. 3-6 and Figure. 3-7, the

predominant S(IV) species at pH 3.0–6.0 is  $\text{HSO}_3^-$ . Thus, lower pH facilitated AO7 decolorization and Cr(VI) reduction; but to assume that 2.0 (or a lower pH value) is the optimum pHini value for industrial applications might be erroneous, since S(IV) volatilizes at  $\text{pH}_{\text{ini}} < 2.0$ [24].

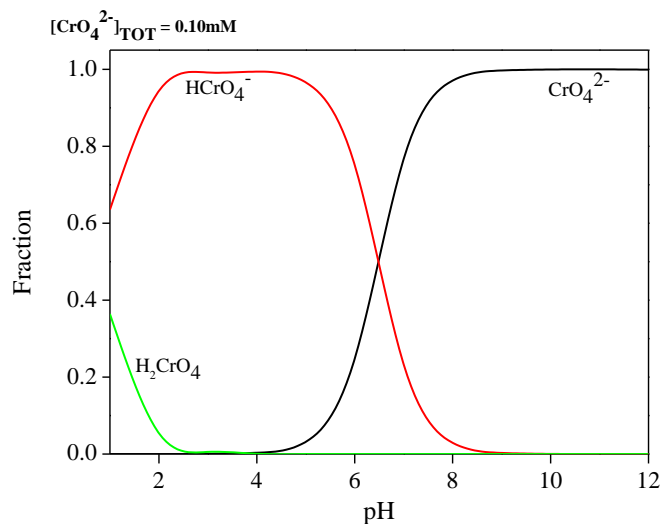


**Figure. 3-4.** Species distribution of 0.1 mM Cr(VI) in aqueous solutions at pH in the range of 1 – 12.  $\text{HCrO}_4^-$  ion is the only predominant species of Cr(VI) at pH 1 – 6, while the fraction of  $\text{HCrO}_4^-$  drops sharply when increasing pH from 6 to 9. This figure was created by the special software MEDUSA.

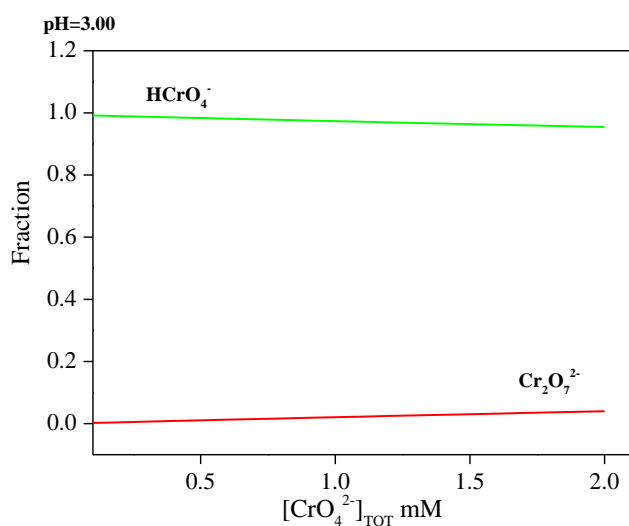


**Figure. 3-5.** Species distribution of Cr(VI) in aqueous solutions at pH 3 containing Cr(VI) at the concentration in the range of 0.1 – 2.0 mM. In the concentration range of 0.1 – 2.0 mM,  $\text{HCrO}_4^-$  ion is the only predominant species of Cr(VI) (> 90%) at pH 3. The fraction of  $\text{Cr}_2\text{O}_7^{2-}$  increases with increasing the total concentration of Cr(VI) and it is about 0.5 when the total concentration of Cr(VI) is at ca. 25 mM. This means in the Cr(VI)-S(IV)- $\text{O}_2$  system investigated in this work,  $\text{HCrO}_4^-$  ion is

the only predominant species.

Besides the distributions of Cr(VI) and S(IV) species, reactions in eqs (3-3) and (3-4) are also pH-dependent; the latter have higher rates at acidic pH. These are the original source of  $\text{SO}_3^{\bullet-}$ , which requires sufficient amounts of  $\text{H}^+$  to form the stable Cr(III)–S(VI) complex. The rate of  $\text{SO}_3^{\bullet-}$  production may determine the subsequent production rates of the oxysulfur radicals  $\text{SO}_4^{\bullet-}$  and  $\text{SO}_5^{\bullet-}$  in the presence of a fixed concentration of S(IV) and atmospheric oxygen. As Brandt and Elding [21] indicated, the overall rate of this reaction decreases as the pH increases within the range of 4–6. In the present work, the overall efficiencies of AO7 decolorization and Cr(VI) reduction at pH 3.0 were higher than those at other pH values. Consequently, pH 3.0 was deemed as the optimal pH and was used in subsequent experiments.

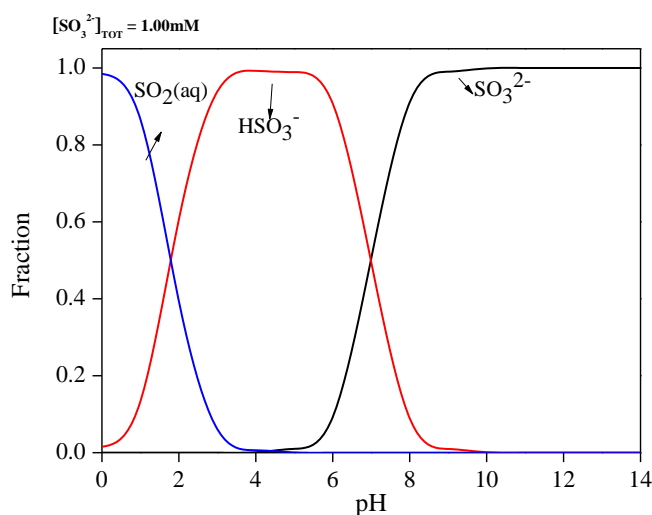


**Figure. 3-6.** Species distribution of 1 mM S(IV) in aqueous solutions at pH in the range of 1 – 12.  $\text{HSO}_3^-$  ion is the only predominant species of S(IV) at pH 3 – 6, while the fraction of  $\text{HSO}_3^-$  drops sharply when increasing pH from 1 to 3 or 6 to 9.

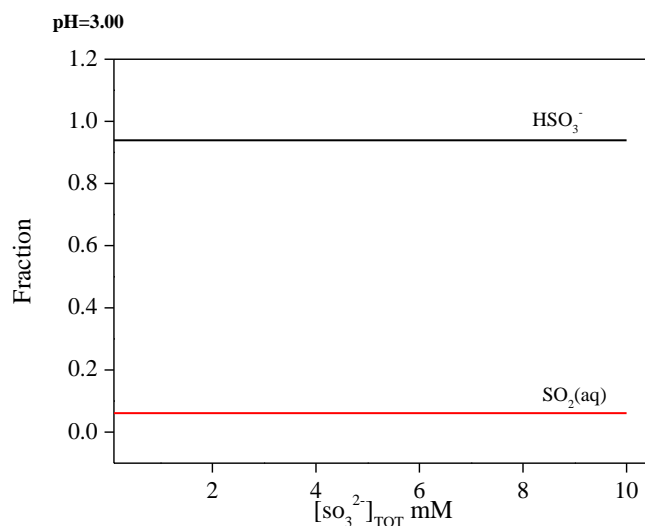


**Figure. 3-7.** Species distribution of S(IV) in aqueous solutions at pH 3 containing S(IV) at the concentration in the range of 0.1 – 10.0 mM. In the concentration range of 0.1 – 10.0 mM, HSO<sub>3</sub><sup>-</sup> ion is the only predominant species of S(IV) (> 90%) at pH 3. Less than 10% S(IV) is dissolved SO<sub>2</sub>. This means in the Cr(VI)-S(IV)-O<sub>2</sub> system investigated in this work, HSO<sub>3</sub><sup>-</sup> ion is the only predominant species.

### 3.3.3 Effect of the Cr(VI)/S(IV) molar ratio.

As shown in the previous section, the initial pH of the reaction mixture is of great importance to AO7 decolorization and Cr(VI) reduction in the aqueous Cr(VI)–S(IV)–O<sub>2</sub> system. For the sake of practicality, the Cr(VI)/S(IV) molar ratio needed to ensure complete reaction at the optimum pH<sub>init</sub> was determined. The efficiency of AO7 decolorization at various Cr(VI)/S(IV) molar ratios at initial AO7 concentration of 0.029 mM and at pH 3.0 was determined. Results in Figure 3-8a and 3-8b clearly show that the Cr(VI)/S(IV) molar ratio greatly influenced the efficiency of AO7 decolorization. The efficiency of AO7 decolorization increased with the increase in Cr(VI) dosage under the same conditions (Figure. 3-8a). When the concentrations of added Cr(VI) were 0.05, 0.1 and 0.15mM, at 0.55 mM initial concentration of S(IV), the efficiencies of AO7 decolorization after 30 min were 33.3%, 57.7%, and 71.5% respectively. When both concentration are double, 0.3 mM of Cr(VI) and 1.1 mM of S(IV), 95.6% of AO7 decolorization was achieved. However, considering its high cost, potential for causing serious pollution, potential application, and feasibility of use in industrial processes or engineered systems, 0.1 mM was used as the Cr(VI) dosage when other individual effects were investigated.

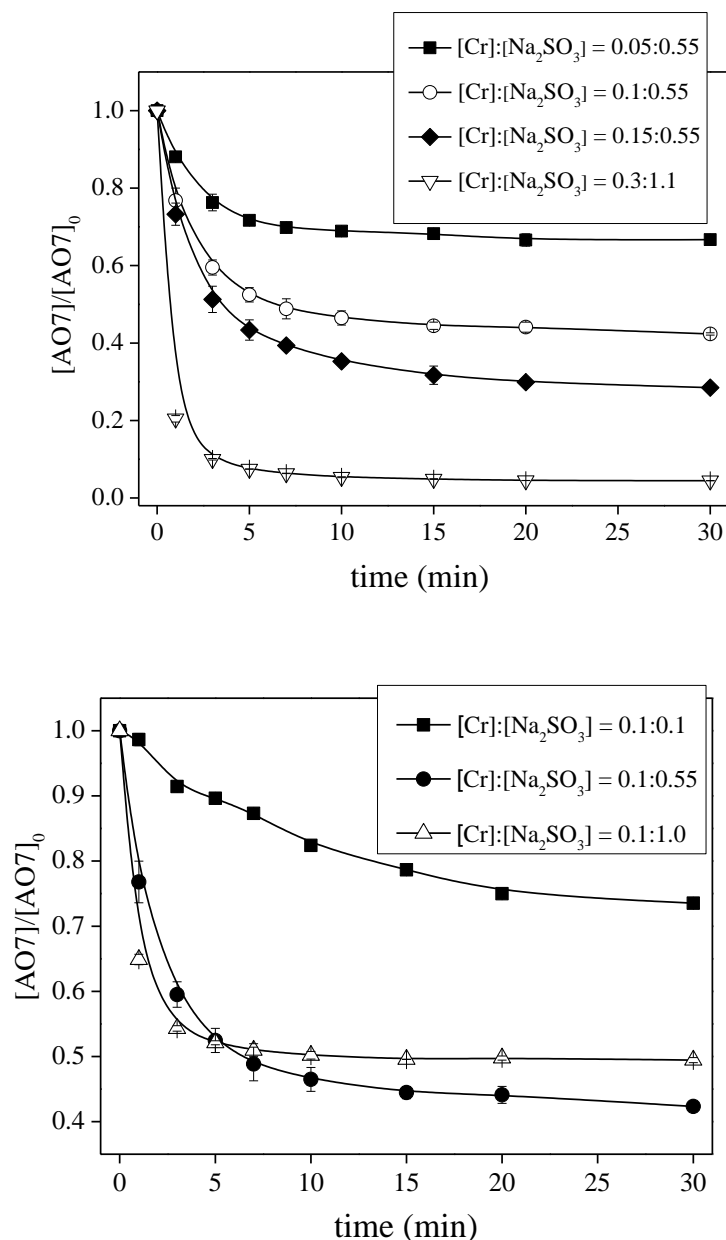


**Figure. 3-8.** Changes in AO7 concentration in the Cr(VI)–S(IV)–O<sub>2</sub> system (a) at various initial concentrations of Cr(VI) and (b) at various initial concentrations of S(IV). Conditions: [AO7]<sub>0</sub> = 0.029 mM, pH<sub>ini</sub> = 3.0.

Experimental results for different concentrations of added S(IV) indicate that the efficiency of AO7 decolorization at S(IV) dosage of 0.55 mM (57.7%) after 30 min was higher than that at S(IV) dosages of 0.1 mM (26.5%) (Figure. 3-8b) and 1 mM (50.6%). However, AO7 was completely decolorized (>95% decolorization efficiency; Figure. 3-8a) at relatively high concentrations of Cr(VI) and S(IV) (0.3 and 1.1 mM, respectively). For the investigation of the Cr(VI) reduction under different Cr(VI)/S(IV) molar ratios, the results in Figure. 3-9a and Figure. 3-9b indicate that when both S(IV) and Cr(VI) were added, Cr(VI) could be quickly reduced to Cr(III) regardless of Cr(VI)/S(IV) molar ratio, consistent with the results for pH

value discussed in the section 3.2. The low concentration of S(IV) (0.1 mM) was very insufficient for the reduction of all Cr(VI) (Figure. 3-9a). The variation of Cr(VI) concentration in both Figure. 3-9a and 3-9b implies that traces of Cr(VI) remained when the Cr(VI)/S(IV) molar ratio in the reagent was 0.1:0.55 mM.

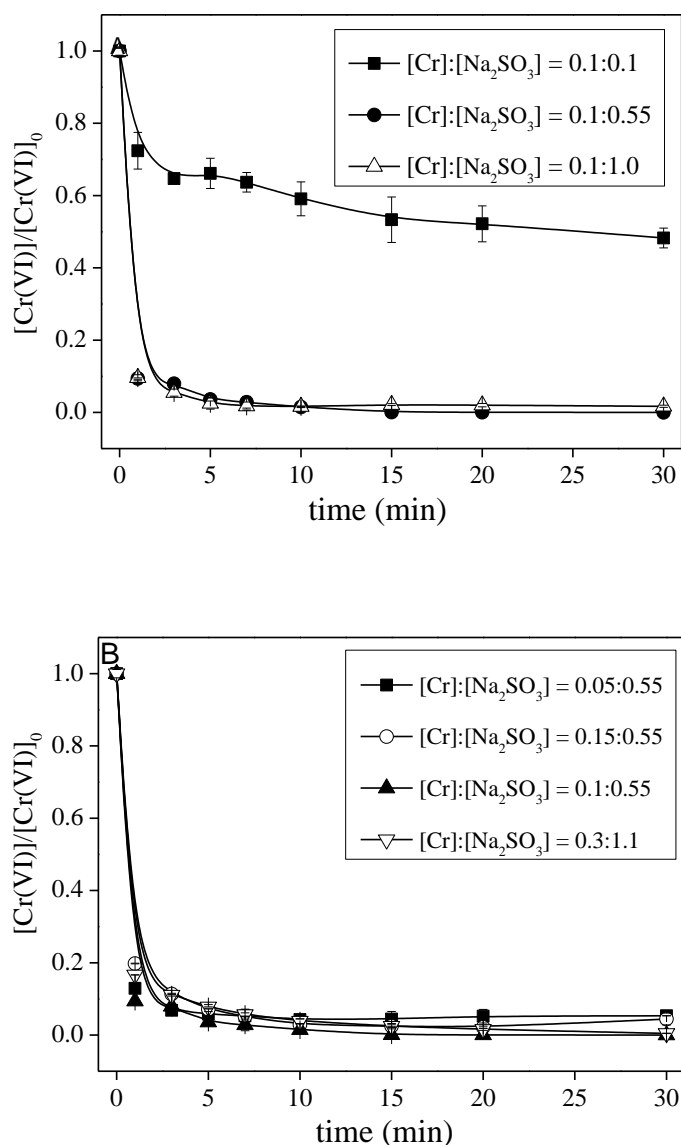


**Figure. 3-9.** Changes in Cr(VI) concentration in the Cr(VI)–S(IV)–O<sub>2</sub> system (a) at various initial concentrations of S(IV) and (b) at various initial concentrations of Cr(VI). Conditions: [AO7]<sub>0</sub> = 0.029 mM, pH<sub>init</sub> = 3.0.

The aforementioned results illustrate that an increase in S(IV) dosage did not always enhance AO7 decolorization; excessively high S(IV) concentrations (such as 1.0 mM) could retard the subsequent reaction in the system. Several scholars [28,29] have confirmed that at high  $[\text{M}(n)]/[\text{S(IV)}]$  and low  $[\text{S(IV)}]/[\text{O}_2]$  ratios ( $\text{M}(n)$ : heavy-metal ion), the system undergoes oxidation. Otherwise, the system tends to predominantly undergo reduction. Therefore,

elevated concentrations of S(IV), a reducing species, may prevent the system from undergoing oxidation. However, an increase in S(IV) concentration could facilitate AO7 decolorization because it generates oxysulfur radicals. Hence, the balance between the reducing nature of S(IV) and its catalytic character is critical. Considering the factors above, we deemed 0.1:0.55 mM as the optimum Cr(VI)/S(IV) molar ratio for this system.

### 3.3.4 Effect of oxygen and radical scavengers.

The effect of oxygen on AO7 decolorization in the Cr(VI)-S(IV)-O<sub>2</sub> system was investigated (results are presented in Figure 3-10). When the experiment was conducted in the presence of air, the decolorization efficiency was nearly 57.7%. The efficiency dropped to 14.6% upon exclusion of oxygen from the solution by purging with nitrogen. This result implies that oxygen plays an important role in AO7 decolorization in the system. Furthermore, as long as there is dissolved oxygen in the solution, SO<sub>3</sub>•<sup>-</sup> could react rapidly with oxygen, forming SO<sub>5</sub>•<sup>-</sup> and SO<sub>4</sub>•<sup>-</sup> (eqs ((3-5)–(3-9)), [26,28] which can oxidatively decolorize AO7. In addition, reaction of SO<sub>4</sub>•<sup>-</sup> with H<sub>2</sub>O can produce HO• (reaction (3-12)), which is alternative for AO7 decolorization either [30].



3-12

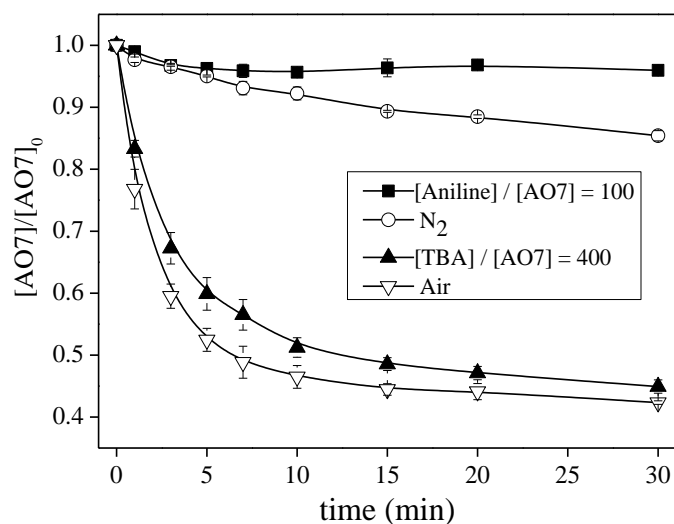


**Figure. 3-10.** Change in AO7 concentration in the Cr(VI)-S(IV)-O<sub>2</sub> system in the presence of various radical scavengers. Conditions: [AO7]<sub>0</sub> = 0.029 mM, [Cr(VI)]<sub>0</sub> = 0.1 mM, [Na<sub>2</sub>SO<sub>3</sub>]<sub>0</sub> = 0.55 mM, pH<sub>ini</sub> = 3.0.

To shed light onto the reaction mechanism, we conducted quenching studies to identify the activity of the added radicals, TBA and aniline. In our previous studies [31], TBA could completely inhibit the reaction of AO7 with HO• when [TBA]<sub>0</sub> = 400×[AO7]<sub>0</sub>. HO• is an

extremely potent oxidizing agent that unselectively oxidizes various kinds of organic pollutants [32, 33]. However as shown in Figure 3-10, inhibition with TBA resulted in only a slight decrease in decolorization rate, indicating that HO• did not play a significant role in AO7 decolorization in the Cr(VI)–S(IV)–O<sub>2</sub> system. The pseudo-first-order kinetic law was applied to analyze the decolorization process of AO7 (examples of the regression analysis of the pseudo-first-order kinetic curves were shown in Figure 3-11). The pseudo-first-order rate ( $k_{\text{obs}}$ ) in Table 3-1 suggest that the contribution of HO• to AO7 decolorization was only ~21.7%. Aniline may be an appropriate scavenger for SO<sub>4</sub>•<sup>-</sup>, as the rate constant ( $k$ ) with aniline and SO<sub>4</sub>•<sup>-</sup> is on the order of 10<sup>9</sup> L mol<sup>-1</sup> s<sup>-1</sup> (data estimated in our other work not shown). The rate constant for the reaction between aniline and HO• ( $k = 1.7 \times 10^{10}$  L mol<sup>-1</sup> s<sup>-1</sup>)[34] is nearly three orders of magnitude larger than those for the reactions between aniline and SO<sub>5</sub>•<sup>-</sup> ( $k = 3.0 \times 10^6$  L mol<sup>-1</sup> s<sup>-1</sup>) and between aniline and SO<sub>3</sub>•<sup>-</sup> ( $k < 1.0 \times 10^6$  L mol<sup>-1</sup> s<sup>-1</sup>)[35]. However, when the concentration of aniline added to the reaction was high enough, almost all of the oxysulfur radicals (SO<sub>4</sub>•<sup>-</sup> and SO<sub>5</sub>•<sup>-</sup>) and HO• could be quenched completely [31]. When [aniline]<sub>0</sub> = 100[AO7]<sub>0</sub>, <5% of AO7 was decolorized, confirming that oxysulfur radicals are the main active species in the Cr(VI)-S(IV)-O<sub>2</sub> system under acidic conditions. The contribution of oxysulfur radicals (SO<sub>4</sub>•<sup>-</sup> and SO<sub>5</sub>•<sup>-</sup>) to AO7 decolorization was nearly 72.5% (Table 3-1), which confirms that oxysulfur radicals were the oxidants that mainly led to decolorization.

**Table 3-1.**

Pseudo-first-order Rate ( $k_{\text{obs}}$ ) of AO7 in the Cr(VI)–S(IV)–O<sub>2</sub> System in the Presence of Various Radical Scavengers

| parameter  | concentration ratio of radical scavengers                             |  |  |
|--|---|--|--|
|  | none  | [TBA] <sub>0</sub> /[AO7] <sub>0</sub> = 400 | [aniline] <sub>0</sub> /[AO7] <sub>0</sub> = 100 |
| $k_{\text{obs}}$ (min <sup>-1</sup> )                | 0.120   | 0.094  | 0.007  |
| contribution of HO• + SO <sub>x</sub> • <sup>-</sup> | $(1 - k_{\text{obs,aniline,AO7}}/k_{\text{obs}}) \times 100 = 94.2\%$ |  |  |
| contribution of HO•                                  | $(1 - k_{\text{obs,TBA,AO7}}/k_{\text{obs}}) \times 100 = 21.7\%$     |  |  |
| contribution of SO <sub>x</sub> • <sup>-a</sup>      | $93.4\% - 22.8\% = 72.5\%$  |  |  |
| contribution of other oxidant                        | $100\% - 94.2\% = 5.8\%$  |  |  |

<sup>a</sup>SO<sub>x</sub>•<sup>-</sup> refers to oxysulfur radicals (mainly SO<sub>4</sub>•<sup>-</sup> and SO<sub>5</sub>•<sup>-</sup>).

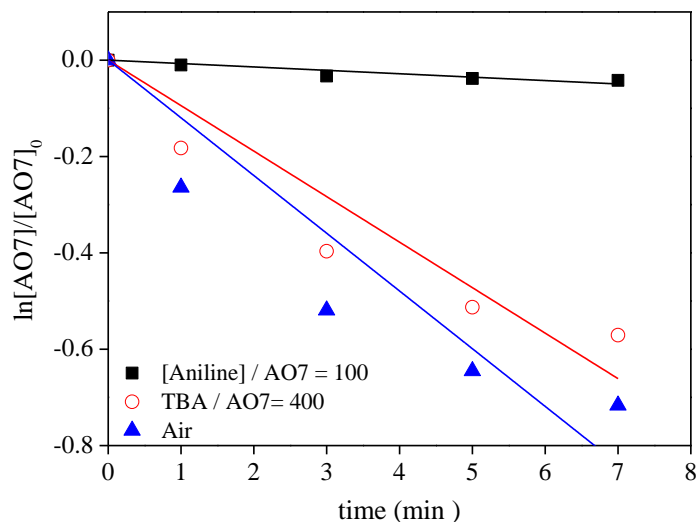
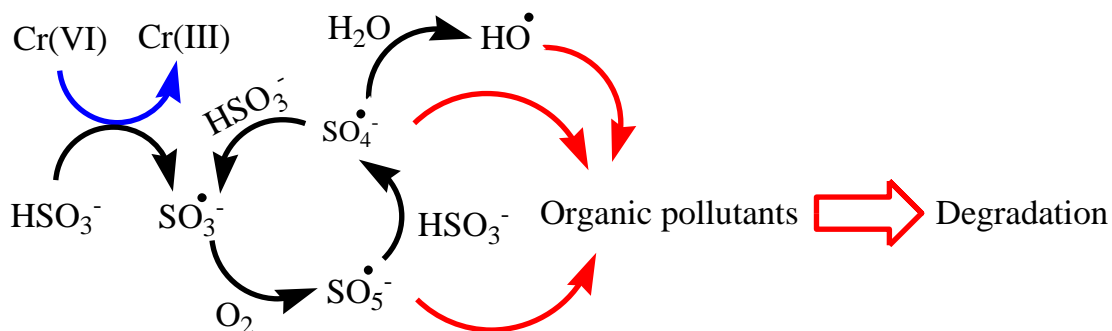


**Figure. 3-11.** Examples of the regression analysis of the pseudo-first-order kinetic curves of AO7 during decolorization with scavengers in the Cr(VI)–S(IV)–O<sub>2</sub> system. Conditions: [AO7]<sub>0</sub> = 0.029 mM, [Cr(VI)]<sub>0</sub> = 0.1 mM, [Na<sub>2</sub>SO<sub>3</sub>]<sub>0</sub> = 0.55 mM, pH<sub>ini</sub> = 3.0.

### 3.3.5 Preliminary study of the mechanism.

The proposed mechanism of rapid and simultaneous reduction of Cr(VI) and oxidative decolorization of AO7 by sulfite ions based on the results above is shown in Scheme 3-1. In experiments using the Cr(VI)–S(IV)–O<sub>2</sub> system in the absence of O<sub>2</sub> under acidic conditions, Cr(VI) readily underwent reduction to Cr(III), and SO<sub>3</sub><sup>•-</sup> that formed oxidatively decolorized AO7. In the presence of molecular O<sub>2</sub>, SO<sub>3</sub><sup>•-</sup> radical is unstable and reacts rapidly with it, producing the active oxysulfur radicals SO<sub>5</sub><sup>•-</sup> and SO<sub>4</sub><sup>•-</sup>. SO<sub>4</sub><sup>•-</sup> produces HO<sup>•</sup> by reaction with water. SO<sub>4</sub><sup>•-</sup>, SO<sub>5</sub><sup>•-</sup>, and HO<sup>•</sup> contribute to AO7 decolorization.



**Scheme. 3-1.** Proposed mechanism of simultaneous Cr(VI) reduction and oxidative degradation of organic pollutants in the Cr(VI)–S(IV)–O<sub>2</sub> system. Blue, black, and red arrows denote Cr(VI) reduction, S(IV) autoxidation to oxysulfur radicals and HO<sup>•</sup>, and oxidative degradation of organic pollutants, respectively.

UV–vis absorption spectra of the remaining AO7 during the reaction (Figure. 3-12) indicate a decline in absorbance at 485 nm, which suggests that the Cr(VI)–S(IV)–O<sub>2</sub> system could effectively destroy the azo bond, the AO7 chromophore, resulting in decolorization. However, the efficiency of TOC removal, which was the general index used to investigate the mineralization of organic pollutants, did not decline even after 48 h of reaction. The efficiency of TOC removal in the Fe(II)–S(IV)–O<sub>2</sub> system in our previous studies[24,25], is very similar to that in this work (data not shown). Therefore, the Cr(VI)–S(IV)–O<sub>2</sub> system is more reliable for decolorization than for mineralization.

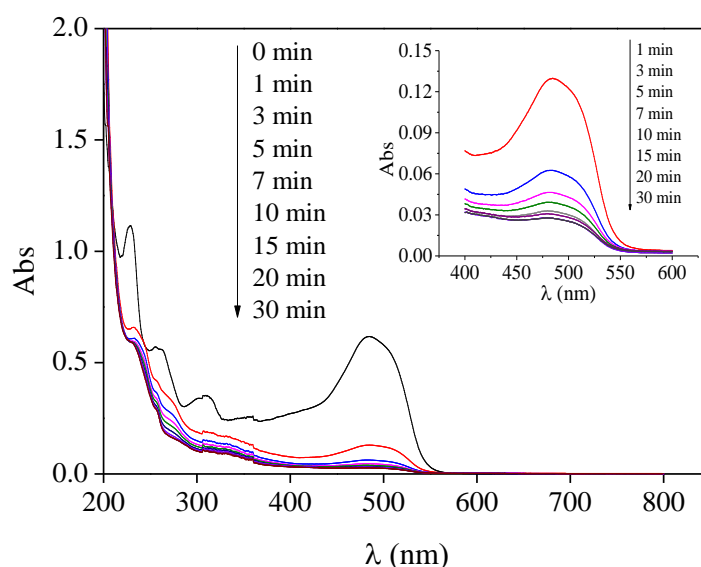


**Figure.3-12.** UV–vis spectra of AO7 at specific time intervals during the reaction. Conditions: [AO7]<sub>0</sub> = 0.029 mM, [Cr(VI)]<sub>0</sub> = 0.3 mM, [Na<sub>2</sub>SO<sub>3</sub>]<sub>0</sub> = 1.1 mM, pH<sub>ini</sub> = 3.0.

### 3.3.6 Appliance of Cr(VI)–S(IV)–O<sub>2</sub> system for degrading other organic compounds

Cr(VI)–S(IV)–O<sub>2</sub> system not only has strong decolorization effect on azo dye, similarly, rapid degradation of other organic pollutants such as aniline, phenol, bisphenol A and their substituted analogs (more than 10 derivatives) within 60 min can also be achieved. As shown in Table 3-2, the experiments were conducted at specific Cr(VI)/S(IV) molar ratios (0.1: 0.55 mM) at initial substrates concentration of 0.029 mM and at pH 3.0. After 30 min reaction, all the pollutants selected in this study underwent different degree of degradation, and almost no further degradation occurred after 60 min reaction. However, the degradation rate of organic pollutants is quite different, and the reason may be explained by the existence of different substituted groups.

**Table 3-2**

Degradation efficiency of various kinds of organic pollutants used in this work

| Compounds         | Degradation efficiency at 30 | Degradation efficiency at 60 |
|-------------------|------------------------------|------------------------------|
|                   | min                          | min                          |
| Aniline           | 38.2 ± 1.7 %                 | 42.2 ± 1.2 %                 |
| o-Nitroaniline    | 24.1 ± 0.2 %                 | 25.0 ± 0.5 %                 |
| p-Nitroaniline    | 13.3 ± 0.5 %                 | 13.8 ± 0.7 %                 |
| p-Chloroaniline   | 37.4 ± 0.8 %                 | 38.0 ± 0.6 %                 |
| Sulfonamides      | 42.6 ± 0.7 %                 | 43.1 ± 0.1 %                 |
| Phenol            | 64.9 ± 0.6 %                 | 65.9 ± 1.7 %                 |
| Bisphenol A       | 54.9 ± 1.1 %                 | 56.7 ± 0.1 %                 |
| 2-Bromophenol     | 71.5 ± 1.9 %                 | 75.3 ± 1.6 %                 |
| Paracetamol       | 46.2 ± 1.0 %                 | 46.3 ± 1.4 %                 |
| p-aminophenol     | 80.8 ± 1.4 %                 | 84.1 ± 1.0 %                 |
| Catechol          | 73.5 ± 0.2 %                 | 75.4 ± 0.3 %                 |
| o-Nitrophenol     | 58.7 ± 1.8 %                 | 61.5 ± 2.4 %                 |
| 2,6-Dinitrophenol | 4.80 ± 0.2 %                 | 5.90 ± 0.1 %                 |

In general, the degradation efficiency of phenol and its derivatives are much higher than aniline and its derivatives in the same condition. However, referring to the influence of functional group, for both aromatic amines and phenols, the same substituted group has the same trend on degradation. As shown in Table 3-2, the reactions after 30 min significantly slowed down when the substituted group of nitro substituent existed (o-Nitroaniline 24.1±0.2 %, p-Nitroaniline 13.3±0.5 %, and o-Nitrophenol 58.7±1.8 %) compared to aniline (38.2±1.7 %) and phenol (64.9±0.6 %), especially the degradation ratio of 2,6-Dinitrophenol was less than 5%. Thus the substituted group of nitro may have a negative effect on degradation of substituted phenols and amines in this Cr(VI)-S(IV)-O<sub>2</sub> system. In contrast, from the data in Table 3-2, the substituted group of amino can promote the degradation. After 30 min, there was 80.8 ± 1.4 % p-aminophenol degraded, which was nearly 15 % higher than that of phenol. Similarly, halogen group Br<sup>-</sup> has slightly promoting effects on this kind of pollutants in this system.

**Table 3-3.**The pseudo-first-order rate ( $k_{\text{obs1}}$ ) and the Hammett  $\sigma$  values for the compounds

| Compounds         | $k_{\text{obs1}}$ (min <sup>-1</sup> ) | $\sigma$ |
|-------------------|--|----------|
| p-Nitroaniline    | 0.06737                                | 0.58     |
| o-Nitroaniline    | 0.04746                                | 0.11     |
| p-Chloroaniline   | 0.03277                                | -0.45    |
| Aniline           | 0.0321                                 | -0.67    |
| Sulfonamides      | 0.02844                                | -0.07    |
| 2,6-Dinitrophenol | 0.10129                                | 1.18     |
| o-Nitrophenol     | 0.01775                                | 0.4      |
| 2-Bromophenol     | 0.01119                                | -0.15    |
| Paracetamol       | 0.02578                                | -0.38    |
| Phenol            | 0.01442                                | -0.38    |
| Bisphenol A       | 0.01998                                | -0.58    |
| Catechol          | 0.01026                                | -0.75    |
| p-aminophenol     | 0.00712                                | -1.04    |

In addition, the results in Table 3-2 also show that the degradation efficiency exhibited a significant difference for aniline, phenol and their derivatives with the same substituents but at different substituted positions. Electronic parameter such as Hammett  $\sigma$  constants, simply obtained from the ionization of organic acids in solution, can frequently predict successfully equilibrium and rate for a variety of families of reactions in solution [36]. The combination of electronic, steric, hydrophobic/hydrophilic, and hydrogen-bonding parameters has been used to derive quantitative structure-activity relationships (QSAR) for a host of reactions of organic compounds in aqueous solutions [37]. In this study, the relationship between the Hammett  $\sigma$  values for each compound and the pseudo-first-order rate ( $k_{\text{obs1}}$ ) has been investigated. The  $k_{\text{obs1}}$  were listed for the substituents with Hammett  $\sigma$  values [38-39] in Table 3-3, which showed that the reaction rate dramatically increased with abundant electron. Furthermore, the  $\sigma$  corresponds to the effect that a substituted group would have upon a benzene ring if it was substituted at different position. Figure 3-13 illustrated the pseudo-first-order rate constants versus their associated Hammett  $\sigma$  values for the substituted groups at the *para* or *meta* position. A trend line has been plotted to show the linear

relationship between logarithmic value of the initial reaction rate and  $\sigma$  values of the substituent. However, as uncertain spatial structure and ionization effects of molecules, the substrates with *ortho* position substituted by functional group has still been a mystery.

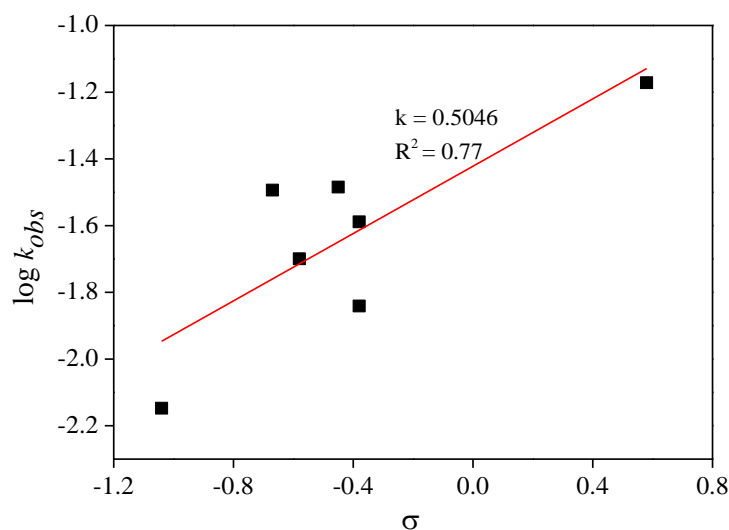


**Figure. 3-13.** The pseudo-first-order rate constants( $k_{obs1}$ ) versus their associated Hammett  $\sigma$  values which the functional group was substituted at the *para* and *meta* position. Substrates: [p-Nitroaniline]<sub>0</sub> = [Paracetamol]<sub>0</sub> = [Phenol]<sub>0</sub> = [p-Chloroaniline]<sub>0</sub> = [Bisphenol A]<sub>0</sub> = [Aniline]<sub>0</sub> = [p-aminophenol]<sub>0</sub> = 10 $\mu$ M, [Cr(VI)]<sub>0</sub> = 0.1 mM, [Na<sub>2</sub>SO<sub>3</sub>]<sub>0</sub> = 0.55 mM, pHini = 3.0. The correlation coefficient R is calculated to be 0.77, which is above the critical value of R, 0.755 (N = 7, Significance test (T-test) shows that the calculated t value is 2.70, which is above the critical value of t, 2.571 (N= 7, significance level = 0.05 (two tails)).

### 3.4 Conclusions

The Cr(VI)–S(IV)–O<sub>2</sub> system is an efficient system for rapid and simultaneous reduction of Cr(VI) and oxidative degradation of organic pollutants in aqueous solution with dioxygen under acidic conditions. We have considered effects such as pH, concentration of added Cr(VI) and S(IV), as well as the presence of O<sub>2</sub> or N<sub>2</sub> and various radical scavengers. Our results show that the reaction of Cr(VI) and degradation of organic pollutants depended heavily on the pH and initial concentrations of Cr(VI) and S(IV). In addition, oxysulfur radicals were the dominant oxidants for AO7 decolorization. Thus, our Cr(VI)–S(IV)–O<sub>2</sub> system may be a new candidate for use in the efficient treatment of waste using waste chromium via simultaneous reduction of Cr(VI) and oxidation of organic contaminants.

## References

- [1] Alidokht L, Khataee A R, Reyhanitabar A, et al. Reductive removal of Cr(VI) by starch-stabilized Fe<sup>0</sup>, nanoparticles in aqueous solution [J]. *Desalination*, 2011, 270(1–3): 105-110.
- [2] Barrera C E. A review of chemical, electrochemical and biological methods for aqueous Cr(VI) reduction [J]. *Journal of Hazardous Materials*, 2012, 223-224(2): 1-12.
- [3] Dean J.A. *Lange's Handbook of chemistry*; McGraw-Hill: New York, 1999.
- [4] Guo J, Li Y, Dai R, et al. Rapid reduction of Cr(VI) coupling with efficient removal of total chromium in the coexistence of Zn(0) and silica gel [J]. *Journal of Hazardous Materials*, 2012, 243(4): 265-271.
- [5] Zhilin D M, Schmitt-Kopplin P, Perminova I V. Reduction of Cr(VI) by peat and coal humic substances [J]. *Environmental Chemistry Letters*, 2004, 2(3): 141-145.
- [6] Poopal A C, Laxman R S. Studies on biological reduction of chromate by *Streptomyces griseus* [J]. *Journal of Hazardous Materials*, 2009, 169(1–3): 539-545.
- [7] Buerge I J, Hug S J. Kinetics and pH Dependence of Chromium(VI) Reduction by Iron(II) [J]. *Environmental Science & Technology*, 1997, 31(5): 1426-1432.
- [8] Fendorf S E, Li G. Kinetics of Chromate Reduction by Ferrous Iron [J]. *Environmental Science & Technology*, 1996, 30(5): 1614-1617.
- [9] Singh P, Iyengar L, Pandey A. Bacterial Decolorization and Degradation of Azo Dyes [J]. *International Biodeterioration & Biodegradation*, 2007, 59(2): 73-84.
- [10] Dermentzis K, Christoforidis A, Valsamidou E, et al. Removal of hexavalent chromium from electroplating wastewater by electrocoagulation with iron electrodes [J]. *Global Nest Journal*, 2011, 13(4): 412-418.
- [11] Suja E, Nancharaiyah Y V, Venugopalan V P. Biogenic nanopalladium production by self-immobilized granular biomass: application for contaminant remediation [J]. *Water Research*, 2014, 65: 395-401.
- [12] Song H, Liu Y, Xu W, et al. Simultaneous Cr(VI) reduction and phenol degradation in pure cultures of *Pseudomonas aeruginosa* CCTCC AB91095 [J]. *Bioresour Technol*, 2009, 100(21): 5079-5084.
- [13] Shen H, Pritchard P H. Microbial Reduction of Cr(VI) during Anaerobic Degradation of Benzoate [J]. *Environmental Science & Technology*, 1996, 30(5): 1667-1674.
- [14] Kaur K, Crimi M. Release of chromium from soils with persulfate chemical oxidation [J]. *Groundwater*, 2014, 52(5): 748–755.
- [15] Dozzi M V, Saccomanni A, Selli E. Cr(VI) photocatalytic reduction: effects of simultaneous organics oxidation and of gold nanoparticles photodeposition on TiO<sub>2</sub> [J]. *Journal of Hazardous Materials*, 2012, 211-212(2): 188-195.
- [16] Liu Y, Deng L, Chen Y, et al. Simultaneous photocatalytic reduction of Cr(VI) and oxidation of bisphenol A induced by Fe(III)–OH complexes in water [J]. *Journal of Hazardous Materials*, 2007,

139(2): 399-402.

- [17] Chulsung K, Zhou Q, et al. Chromium(VI) Reduction by Hydrogen Sulfide in Aqueous Media: Stoichiometry and Kinetics [J]. *Environmental Science & Technology*, 2001, 35(11): 2219-2225.
- [18] Chrysochoou M, Ting A. A kinetic study of Cr(VI) reduction by calcium polysulfide [J]. *Science of the Total Environment*, 2011, 409(19): 4072-4077.
- [19] Beukes J P, Pienaar J J, Lachmann G, et al. The reduction of hexavalent chromium by sulphite in wastewater [J]. *Water S A*, 1999, 25((3)): 363-370.
- [20] Haight G P, Perchonock E, Emmenegger F, et al. The Mechanism of the Oxidation of Sulfur(IV) by Chromium (VI) in Acid Solution [J]. *Journal of the American Chemical Society*, 1965, 87(17): 3835-3840.
- [21] Brandt C, Elding L I. Role of chromium and vanadium in the atmospheric oxidation of sulfur(IV) [J]. *Atmospheric Environment*, 1998, 32(4): 797-800.
- [22] Lee Y J, Rochelle G T. Oxidative degradation of organic acid conjugated with sulfite oxidation in flue gas desulfurization: products, kinetics, and mechanism [J]. *Environmental Science & Technology*, 1987, 21(3): 266-72.
- [23] Kulkarni U S, Dixit S G. Destruction of phenol from wastewater by oxidation with  $\text{SO}_3^{2-}\text{-O}_2$  [J]. *Industrial & Engineering Chemistry Research*, 1991, 30(8): 1916-1920.
- [24] Long C, Peng X, Liu J, et al. Decolorization of Orange II in Aqueous Solution by an Fe(II)/sulfite System: Replacement of Persulfate [J]. *Industrial & Engineering Chemistry Research*, 2016, 51(42): 13632-13638.
- [25] Zhang L, Chen L, Xiao M, et al. Enhanced Decolorization of Orange II Solutions by the Fe(II)–Sulfite System under Xenon Lamp Irradiation [J]. *Industrial & Engineering Chemistry Research*, 2013, 52(30): 10089-10094.
- [26] Zhou D, Chen L, Zhang C, et al. A novel photochemical system of ferrous sulfite complex: kinetics and mechanisms of rapid decolorization of Acid Orange 7 in aqueous solutions [J]. *Water Research*, 2014, 57(5): 87-95.
- [27] Zhou D, Zhang H, Chen L. Sulfur-replaced Fenton systems: can sulfate radical substitute hydroxyl radical for advanced oxidation technologies? [J]. *Journal of Chemical Technology & Biotechnology*, 2015, 90(5): 775-779.
- [28] Zhang W, Singh P, Muir D. Iron(II) oxidation by  $\text{SO}_2/\text{O}_2$  in acidic media: - Part I. Kinetics and mechanism [J]. *Hydrometallurgy*, 2000, 55(3): 229-245.
- [29] Kuo D T F, Kirk D W, Jia C Q. The chemistry of aqueous S(IV)-Fe-O<sub>2</sub> system: state of the art [J]. *Sulfur Reports*, 2006, 27(5): 461-530.
- [30] Wine P H, Tang Y, Thorn R P, et al. Kinetics of aqueous phase reactions of the  $\text{SO}_4^-$  radical with potential importance in cloud chemistry [J]. *Journal of Geophysical Research Atmospheres*, 1989, 94: 1085-1094.
- [31] Zhou D, Yuan Y, Yang S, et al. Roles of oxysulfur radicals in the oxidation of acid orange 7 in the Fe(III)–Sulfite system [J]. *Sulfur Reports*, 2015, 36(4): 373-384.

- [32] Mestankova H, Mailhot G, Jirkovsky J, et al. Mechanistic approach of the combined (iron–TiO<sub>2</sub>) photocatalytic system for the degradation of pollutants in aqueous solution: an attempt of rationalization [J]. *Applied Catalysis B Environmental*, 2005, 57(4): 257-265.
- [33] Pozdnyakov I P, Melnikov A A, Tkachenko N, et al. Ultrafast photophysical processes for Fe(III)-carboxylates [J]. *Dalton Transactions*, 2014, 43(47): 17590-17595.
- [34] Zuo Y, Hoigne J. Formation of hydrogen peroxide and depletion of oxalic acid in atmospheric water by photolysis of iron(III)-oxalato complexes [J]. *Environmental Science & Technology*, 1992, 26(5):1014-1022.
- [35] Hayon E, Treinin A, Wilf J. Electronic spectra, photochemistry, and autoxidation mechanism of the sulfite-bisulfite-pyrosulfite systems. The SO<sub>2</sub><sup>-</sup>, SO<sub>3</sub><sup>-</sup>, SO<sub>4</sub><sup>-</sup>, and SO<sub>5</sub><sup>-</sup> radicals [J]. *Journal of the American Chemical Society*, 1972, 94(1): 47-57.
- [36] Osborne D, Lawson P A, Adams N, et al. Trends in electron–ion dissociative recombination of benzene analogs with functional group substitutions: Negative Hammett  $\sigma_{\text{para}}$  values [J]. *Icarus*, 2014, 235(1): 1-4.
- [37] Osborne D, Dotan I, Adams N, et al. Trends in electron–ion dissociative recombination of benzene analogs with functional group substitutions: Positive Hammett  $\sigma_{\text{para}}$  constants [J]. *Int J Mass Spectrom*, 2014, 360: 24-27.
- [38] Hansch C, Leo A, Taft R W. ChemInform Abstract: A Survey of Hammett Substituent Constants and Resonance and Field Parameters [J]. *Cheminform*, 1991, 22(39): 165-195.
- [39] Schwarzenbach R P, Gschwend P M, Imboden D M. 8. Organic Acids and Bases: Acidity Constant and Partitioning Behavior[M], *Environmental Organic Chemistry*. John Wiley & Sons, Inc. 2005: 245-274.

**Chapter 4 Rapid oxidation of paracetamol by cobalt(II)  
catalyzed sulfite at alkaline pH**

## 4.1 Introduction

Advanced oxidation processes based on sulfate radical (SR-AOPs) have emerged as a promising method in the field of oxidative decontamination of polluted water and soil [1-3]. Sulfate radical ( $\text{SO}_4^{\bullet-}$ ), a strong one-electron oxidant, has relatively high standard redox potential ( $E^0 = 2.6 \text{ V vs NHE}$ ) with an oxidation potential comparable to or even higher than that of hydroxyl radical [4]. Moreover,  $\text{SO}_4^{\bullet-}$  can react *via* electron transfer, by addition to C-C double bonds and H-abstraction [5, 6], thus, it is able to oxidize a large number of pollutants such as phenol derivatives and aniline in water [7-9].  $\text{SO}_4^{\bullet-}$  can be generated in homogeneous or heterogeneous systems *via* photolysis, thermolysis and radiolysis [10, 11] or *via* transition metal activation of persulfate ( $\text{S}_2\text{O}_8^{2-}$ , PS) [7, 12-15] and peroxymonosulfate ( $\text{SO}_5^{2-}$ , PMS) [16, 17].

In fact, PMS can be activated by various transition metals such as Fe, Mn, Ni and Co in the homogenous systems [1, 18]. Among them, Co and Fe are the most commonly used metal to promote radical formation due to their occurrence in natural media and low cost. Huang and Huang investigated the ability of Co(II) and PMS system to degrade Bisphenol A at pH 7, and achieved an efficient detoxification and mineralization method [19]. A process based on the sulfate radicals generation through iron (Fe(II), Fe(III)) activation of PMS or PS was studied for polychlorinated biphenyls degradation in aqueous system [20]. The high oxidation efficiency and slow rate of consumption of the oxidants make metal-mediated activation system a feasible strategy for degradation of recalcitrant organic compounds. Furthermore, PMS activation using cobalt oxide or cobalt-metal oxide as heterogeneous catalysts also gains significant relevance in water treatment applications [21]. The cobalt oxides such as CoO, CoO<sub>2</sub>, CoO(OH), Co<sub>2</sub>O<sub>3</sub> and Co<sub>3</sub>O<sub>4</sub>, Fe-Co mixed oxide nanocatalysts, cobalt oxide supported on MgO (Co/MgO), on TiO<sub>2</sub> (Co/TiO<sub>2</sub>) and Co<sub>3</sub>O<sub>4</sub>/TiO<sub>2</sub> and combined with other metals were used as efficient heterogeneous catalysts for activation of PMS [22-25]. The most advantage of heterogeneous catalyst is that solid particles can be easily removed from liquid phase and, in some cases, reused.

Recently, sulfite ions were found to react with transition metals such as Fe(II), Fe(III) and Cr(VI) to generate  $\text{SO}_4^{\bullet-}$  and application for the azo dyes and amine compounds

decontamination was tested [17, 26-30].

In our previous work, we reported some novel AOPs using Fe(II)-sulfite, Fe(III)-sulfite, photo-Fe(II)-sulfite system able to produce oxysulfur radicals (including  $\text{SO}_3^{\bullet-}$ ,  $\text{SO}_4^{\bullet-}$  and  $\text{SO}_5^{\bullet-}$ ). Combined with the work conducted by other researchers [31-33], the basic chain oxidation mechanisms of oxysulfur radicals generation has been investigated.

In this work, Co(II)-sulfite ions (S(IV)) system has been investigated to promote the paracetamol degradation in water. Paracetamol (PARA) is a widely used analgesic and antipyretic drug and an important material for the manufacturing of azo dyes. PARA was chosen as a target contaminant in this work due to its presence in the environment from several emissions from manufacturing facilities, consumer use and disposal, and hospital waste [34, 35]. The effect of pH, initial PARA concentration, Co(II)/S(IV) molar ratio, the presence of oxygen were investigated. Moreover, the activation mechanism and contribution of reactive oxygen and sulfur species were elucidated by using different kinds of radical scavengers and transient absorption spectroscopy.

## **4.2 Materials and methods**

### **4.2.1 Chemicals**

Cobalt(II) sulfate ( $\text{CoSO}_4 \cdot 7\text{H}_2\text{O}$ , analytical reagent grade), Cobalt(II) oxide (CoO) and Paracetamol ( $\text{C}_8\text{H}_9\text{NO}_2$ ), were purchased from Sinopharm Chemical Reagent Co., Ltd. Sulfite solutions (from  $\text{Na}_2\text{SO}_3$ , Sinopharm Chemical Reagent Co., Ltd) were prepared just prior to measurements. The radical scavengers tert-butyl alcohol (TBA), ethanol (EtOH) as well as NaOH and  $\text{H}_2\text{SO}_4$  which were used to adjust the pH of the solutions, were obtained from Sinopharm Chemical Reagent Co., Ltd. Methanol was HPLC grade and purchased from Fisher Corporation. Ammonium thiocyanate ( $\text{NH}_4\text{SCN}$ ) and Methyl isobutyl ketone (MIK) used to determine the concentration of Co(II), were obtained from Sigma, France. All chemicals were used without further purification. Ultrapure water with 18.2 M $\Omega$  cm resistivity used in this work was obtained through a water purification system.

### **4.2.2 Degradation experiments**

All experiments were conducted in a 250 mL open cylindrical reactor cooled by an external jacket water circulation at a constant temperature of 25°C. Appropriate amounts of the PARA,

scavengers and  $\text{Na}_2\text{SO}_3$  were mixed in the solution and the pH was adjusted using a pHS-3C pH meter by adding dilute NaOH and  $\text{H}_2\text{SO}_4$  until desired value. Each solution was constantly stirred with a Polytetrafluoroethylene (PTFE)-coated magnetic stirrer and purged with air with a fixed flow of  $0.8 \text{ L min}^{-1}$ .

Each experiment was initiated spiking with Co(II) or CoO into the solution. Samples were withdrawn at fixed interval times and analyzed immediately to determine the remaining concentration of PARA and Co(II). For radical-scavenging experiments, specific concentrations of TBA or EtOH were added to the solutions before Co(II) addition. In order to assess the role of oxygen during Co(II)-sulfite solution were purged by bubbling  $\text{N}_2$  (99.99%) or  $\text{O}_2$  (99.99%) for 30 min before and throughout the experiment. A dissolved oxygen (DO) meter (8403, AZ Instrument Co. Ltd.) was used to determine the oxygen concentration in solution. During anoxic reaction, the DO was  $0.01 \text{ mg L}^{-1}$  while for  $\text{O}_2$  saturated solution a concentration of  $20 \text{ mg L}^{-1}$  was determined. All experiments were carried at least two times.

#### 4.2.3 Chemical analysis

The concentration of PARA was determined using a high-performance liquid chromatography (HPLC) Shimadzu LC-10A system equipped with UV-vis detector (SPD-10AV; Shimadzu) and an ODS-C18 column ( $25 \text{ cm} \times 4.6 \text{ mm}$ ,  $5 \mu\text{m}$ ; Shimadzu, Kyoto, Japan). The separation was carried out using methanol: water (25:75 v/v) as isocratic mobile phase at a flow rate of  $1.0 \text{ mL min}^{-1}$ . The detector was set at 241 nm. An optical-fiber coupled to a spectrophotometer (UV-1601 Shimadzu, Japan) was used to scan the UV-vis absorption spectra of Co(II)- $\text{SO}_3^{2-}$  complex. The concentration of Co(II) in solution was determined by Methyl isobutyl ketone and Ammonium thiocyanate, and the method description is like this: The calibration of Cobalt(II) was measured by preparing a series of standard solutions, firstly, 5 mL cobalt(II) and 1 mL  $\text{NH}_4\text{SCN}$  (566g/L) was added to a 10 mL centrifuge tube and hand shaken for 1 min, then another 4 mL pure MIK was added to the mixture, and ultrasonic shaking for 1min and equilibrating until stratification occurred. Using the UV-Vis spectrophotometer for the absorbance at 620 nm for the upper layer complex which containing Cobalt(II). The calibration curve is presented in Figure 4-1[36].

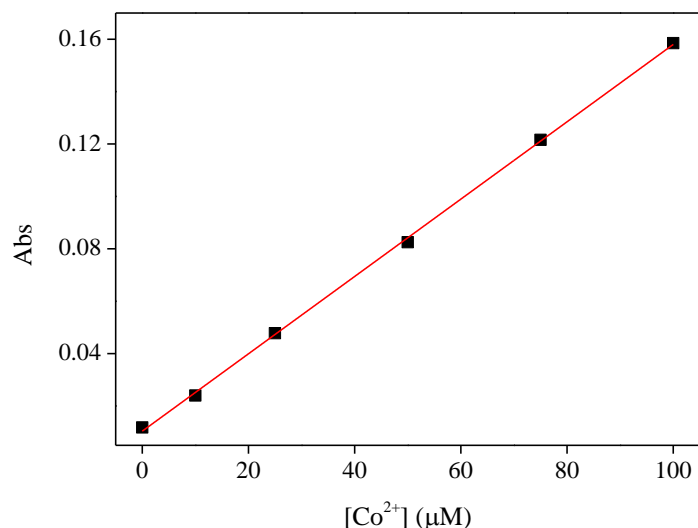


**Figure. 4-1.** Co(II) calibration curves at 620 nm.

The calibration equation is:

$$[\text{Co}^{2+}] \text{ (M)} = (6.77 \times 10^{-4} \times \text{Abs}_{620 \text{ nm}}) - 7.02 \times 10^{-6}$$

For  $\text{SO}_4^{\bullet-}$  reactivity a laser flash photolysis (LFP) system was used with 266 nm excitation following the procedure reported by Wu et al. [15]. Analysis of transient decay and second order rate constant determination (using PARA concentrations from 0 to 0.1 mM) were determined at 470 nm corresponding to the maximum absorption of  $\text{SO}_4^{\bullet-}$ . The second order rate constants were determined at pH 5.0 and 11.0 corresponding to the molecular and deprotonated forms respectively of PARA ( $\text{pK}_a = 9.5$ ).

## 4.3 Results and discussion

### 4.3.1 Control experiments

A typical degradation of Paracetamol by three different kinds of system (only Co(II), only sulfite(S(IV), Co(II)+S(IV)) is presented in Figure.4-2. The result showed that when the experiment conducted in the presence of S(IV) without any catalyst, negligible change in paracetamol concentration was observed. A similar trend was also achieved in the experiment by only using Co(II) even after being centrifuged for 15 min at 9000 rpm. There was no precipitation occurred, which illustrated that there is no adsorption in this system and neither S(IV) nor Co(II) added to the reagent had an effect on Paracetamol. However, when both S(IV)

and Co(II) were in solution, Paracetamol can be degraded to more than 80% in 10 min. These results suggest that Paracetamol degradation depends heavily on the reaction between S(IV) and Co(II), it proceeded only when S(IV) and Co(II) were present.

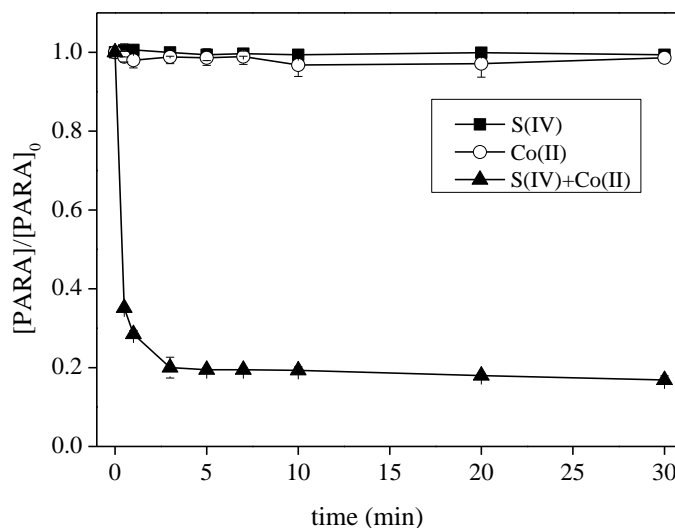


**Figure. 4-2.** The effect of control experiments under various conditions on paracetamol degradation.

Condition:  $[\text{PARA}]_0 = 10\mu\text{M}$ ,  $[\text{Co(II)}]_0 = 0.1\text{ mM}$ ,  $[\text{Na}_2\text{SO}_3]_0 = 1.0\text{ mM}$ ,  $\text{pH}_0 = 9.0$ ,  $T = 25^\circ\text{C}$ ,  $F_{\text{air}} = 0.8\text{ L min}^{-1}$ .

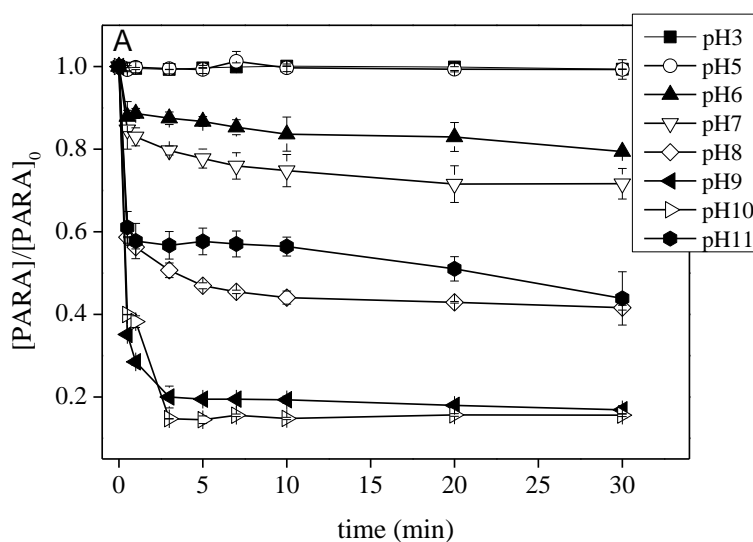
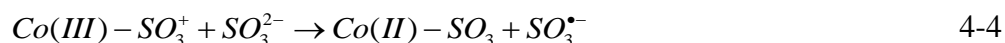
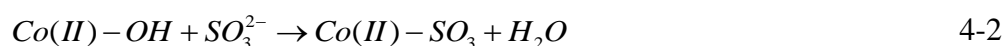
### 4.3.2 Effect of initial pH on PARA degradation

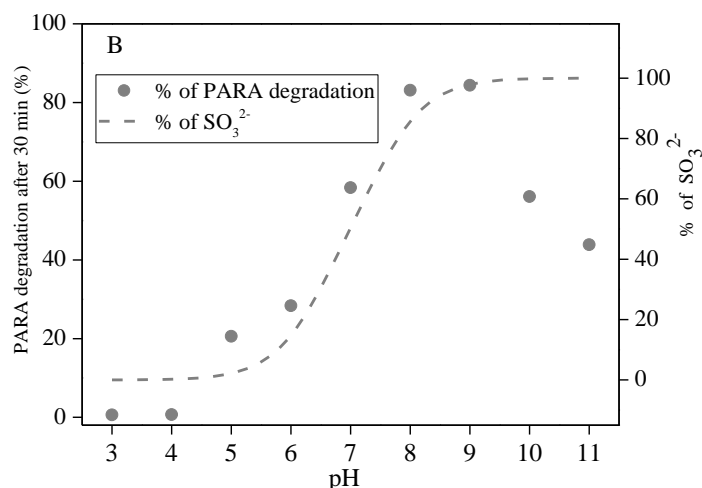
The effect of the initial pH on the Co(II)-S(IV) system oxidation of PARA was investigated from 3.0 to 11.0. The initial concentrations of Co(II) and  $\text{SO}_3^{2-}$  were 0.1 mM and 1.0 mM, respectively and during the reaction, air (otherwise stated) was constantly bubbled at a flow rate of  $0.8\text{ L min}^{-1}$ . The PARA degradation shows a strong pH-dependence as illustrated in Figure.4-3a. Despite a negligible degradation at relatively acidic values (pH 3.0 – 5.0), PARA degradation is enhanced from pH 5.0 to pH 10.0 while a decrease is observed at pH 11.0. It is interesting to observe that degradation efficiency between pH 3.0 and 10 is strongly correlated to the  $\text{HSO}_3^-/\text{SO}_3^{2-}$  speciation in solution ( $\text{pK}_a = 7.2$ ) as shown in Figure.4-3b in which degradation of PARA after 30 min at different pH values is correlated to the concentration of  $\text{SO}_3^{2-}$  in solution. However, at pH 11, the inhibition of PARA degradation can be attributed to the formation of insoluble Cobalt-hydroxide ( $\text{Co(OH)}_2$ ) complex that is expected to precipitate in solution [37].

Moreover, it has been reported that deprotonated complexes ( $\text{Co(II)-OH}$ ), which is more

reactive toward  $\text{SO}_3^{2-}$  compared to  $\text{HSO}_3^-$  would be formed at alkaline pH values (eqs 4-1) leading to the formation of a  $\text{Co(II)-SO}_3$  complex [27].  $\text{Co(II)-SO}_3$  could be oxidized to  $\text{Co(III)-SO}_3^+$  complex in the presence of dissolved oxygen as reported in different works (eqs 4-2 and eqs 4-3) [38].  $\text{SO}_3^{\bullet-}$  could be generated during the redox reaction between the  $\text{Co(III)-SO}_3^+$  complex and  $\text{SO}_3^{2-}$  (eqs 4-4).

UV-vis absorption spectra of  $\text{Co(II)}$ ,  $\text{S(IV)}$ ,  $\text{Co(II)}$  and  $\text{S(IV)}$  during the reaction (Figure.4-4) were acquired to investigate the complexation between  $\text{Co(II)}$  and  $\text{S(IV)}$ . The result showed that: only  $\text{Co(II)}$  or  $\text{S(IV)}$  at pH 9.0 did not show absorption in the range 250-600 nm. However, when  $\text{S(IV)}$  was added to the solution containing 0.1 mM  $\text{Co(II)}$  an absorption band absorbing up to ~ 600 nm is present. The presence of this new absorption band demonstrates that the  $\text{Co(II)-S(IV)}$  complex could be formed and decreasing in the absorption during time proved the reaction between  $\text{Co(II)}$  and  $\text{S(IV)}$ , and corresponding depletion of  $\text{S(IV)}$ .

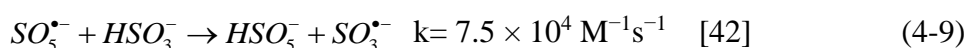
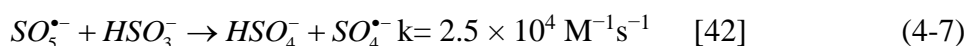




**Figure. 4-3.** (A) Effect of initial pH values on PARA degradation.; (B) Degradation of PARA at different pH values correlated to the concentration of  $\text{SO}_3^{2-}$ . Condition:  $[\text{PARA}]_0 = 10 \mu\text{M}$ ,  $[\text{Co(II)}]_0 = 0.1 \text{ mM}$ ,  $[\text{Na}_2\text{SO}_3]_0 = 1.0 \text{ mM}$ ,  $T = 25^\circ\text{C}$ ,  $F_{\text{air}} = 0.8 \text{ L min}^{-1}$ .

The pH represents also a key factor influencing the  $\text{SO}_3^{\bullet-}$  reactivity in water. In fact, the primary step is the oxygen-mediated oxidation of  $\text{SO}_3^{\bullet-}$  to  $\text{SO}_5^{\bullet-}$  (eqs 4-5), this latter can react with  $\text{HSO}_3^-/\text{SO}_3^{2-}$  leading to the formation of  $\text{SO}_3^{\bullet-}$  and  $\text{SO}_4^{\bullet-}$  (eqs 4-1 to 4-9).

As reported in eqs 4-6 and eqs 4-8,  $\text{SO}_5^{\bullet-}$  could react with  $\text{SO}_3^{2-}$  to generate  $\text{SO}_3^{\bullet-}$  and  $\text{SO}_4^{\bullet-}$  at a rate constant around  $10^5$ – $10^6 \text{ M}^{-1}\text{s}^{-1}$ .  $\text{SO}_4^{\bullet-}$  could react with PARA or with  $\text{SO}_3^{2-}$  leading to the generation  $\text{SO}_3^{\bullet-}$  (eqs 4-10), then a  $\text{SO}_x^{\bullet-}$  ( $\text{SO}_3^{\bullet-}$ ,  $\text{SO}_4^{\bullet-}$  and  $\text{SO}_5^{\bullet-}$ ) cycle can be achieved. However, in the presence of  $\text{HSO}_3^-$  (acidic conditions),  $\text{SO}_5^{\bullet-}$  reacts with  $\text{HSO}_3^-$  to generate  $\text{SO}_4^{\bullet-}/\text{SO}_3^{\bullet-}$  with a relatively shower rate constants (eqs 4-7 and eqs 4-9) compared to the reactivity with  $\text{SO}_3^{2-}$ . The overall reaction rate between  $\text{SO}_5^{\bullet-}$  and  $\text{SO}_3^{2-}$  is  $\sim 1$ – $2$  orders of magnitude higher than between  $\text{SO}_5^{\bullet-}$  and  $\text{HSO}_3^-$ .



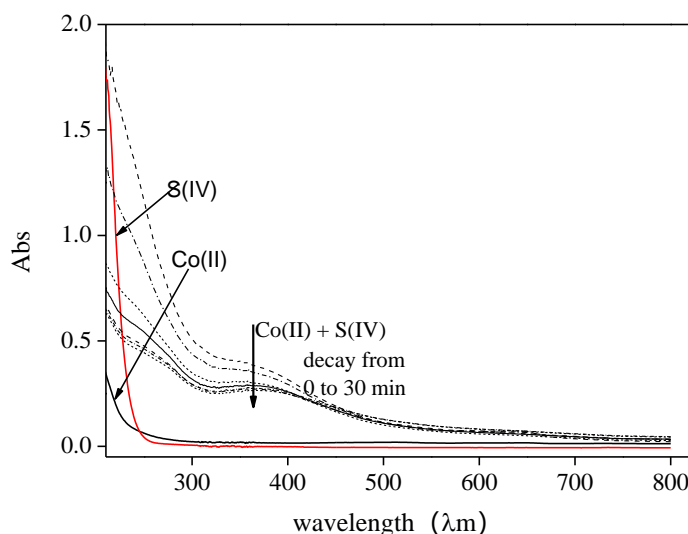


**Figure.4-4.** UV–vis spectra of reaction solution at specific time intervals during the reaction. Conditions:

$$[Co(II)]_0 = 0.1 \text{ mM}, [Na_2SO_3]_0 = 1.0 \text{ mM}, pH_0 = 9.0, T = 25^\circ\text{C}, F_{air} = 0.8 \text{ L min}^{-1}.$$

### 4.3.3 S(IV) and Co(II) effect on the PARA degradation

Different amounts of Co(II) were used to investigate the effect of Co(II) concentration on the PARA removal at pH 9.0 (Figure.4-5). When experiments were conducted using a Co(II) concentration between 0.05 and 0.15 mM and a fixed sulfite concentration of 1.0 mM, no significant differences were observed on the PARA degradation profile. One of reasons explaining the slightly effect of Co(II) concentration may be the fast recycle of Co(II) and Co(III) in the presence of a stoichiometry excess of S(IV) concentrations in aerated solution (eqs 4-3 and eqs 4-4). Moreover, when the concentration of Co(II) was monitored during the reaction, it was found that its concentration was nearly stable (Figure. 4-6). Such results suggest that in the presence of enough sulfite in solution, the cobalt cycle could achieved very fast leading to the generation of  $SO_3^{\bullet-}$  at the same time. Even the addition of Co(II) didn't play a relevant role on the paracetamol degradation, but for the sake of feasibility and accuracy, 0.1 mM Co(II) was employed during all experiments, as when the experiments were conducted under low concentration of Co(II) such as 0.05 mM, the repeatability could not be ensured every time.

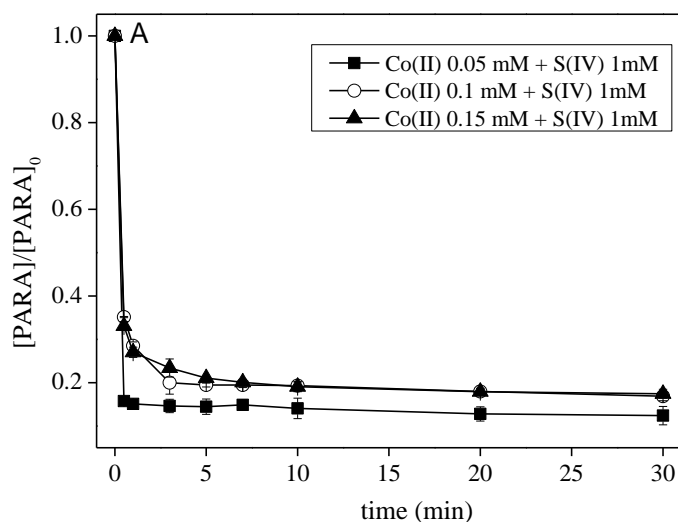


**Figure.4-5.** Effect of Co(II) concentrations on PARA degradation. Condition:  $[\text{PARA}]_0 = 10\mu\text{M}$ ,

$[\text{Na}_2\text{SO}_3]_0 = 1.0 \text{ mM}$ ,  $\text{pH}_0 = 9.0$ ,  $T = 25^\circ\text{C}$ ,  $F_{\text{air}} = 0.8 \text{ L min}^{-1}$ .

The dependence of the PARA degradation on the initial concentration of S(IV) was also investigated (Figure.4-7). An increase in S(IV) concentration (between 0.5 to 1 mM) accelerate the PARA degradation being , through Co(II) reactivity, a source of  $\text{SO}_3^{\bullet-}$ . However, at higher sulfite ions concentrations (2 mM) there is no more enhancement of PARA degradation and this effect could be attributed to the reactivity competition of  $\text{SO}_4^{\bullet-}/\text{SO}_5^{\bullet-}$  between PARA and  $\text{SO}_3^{2-}$  (eqs 4-8 and eqs 4-10). Hence, the balance between S(IV) concentration and its catalytic character is a key factor for the oxidative system efficiency.

In all these experiments (Figure.4-5 and 4-7) it is impossible to obtain more than 90% of PARA degradation. This observation is certainly due to a competition reaction of the sulfate radicals on PARA, the excess of sulfite and the degradation products of PARA. After a short period of time sulfate radicals react no more on paracetamol due to its low concentration.

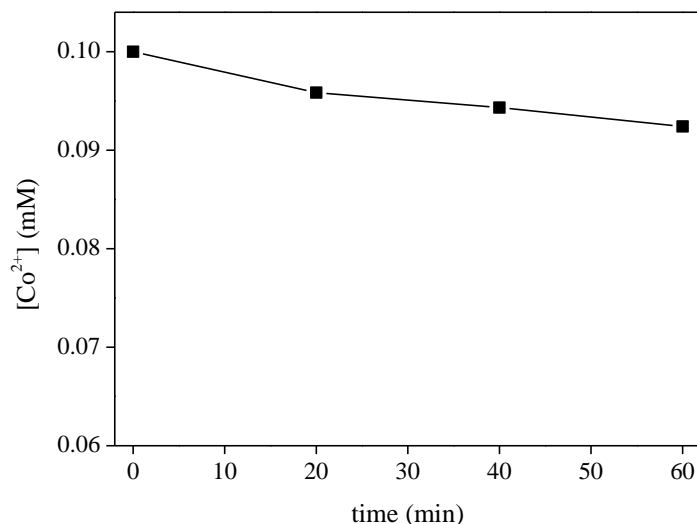


**Figure.4-6.** Co(II) concentration during the reaction. Condition:  $[\text{PARA}]_0 = 10\mu\text{M}$ ,  $[\text{Co(II)}]_0 = 0.1\text{ mM}$ ,  $[\text{Na}_2\text{SO}_3]_0 = 1.0\text{ mM}$ ,  $\text{pH}_0 = 9.0$ ,  $T = 25^\circ\text{C}$ ,  $F_{\text{air}} = 0.8\text{ L min}^{-1}$ .

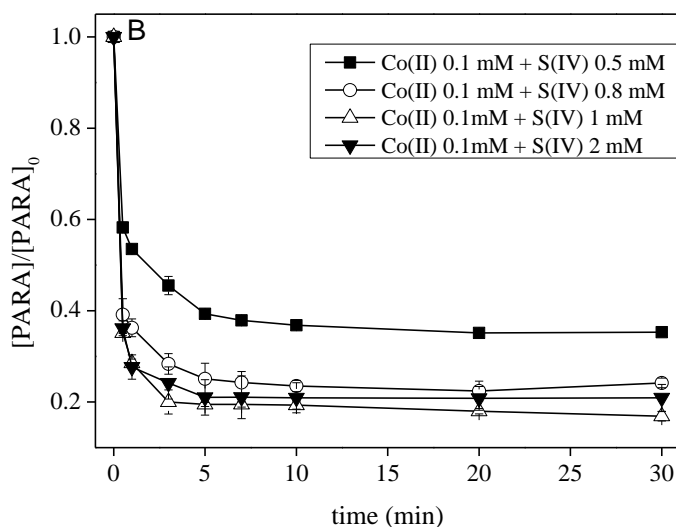


**Figure.4-7.** Effect of S(IV) concentrations on PARA degradation. Condition:  $[\text{PARA}]_0 = 10\mu\text{M}$ ,  $[\text{Co(II)}]_0 = 0.1$ ,  $\text{pH}_0 = 9.0$ ,  $T = 25^\circ\text{C}$ ,  $F_{\text{air}} = 0.8\text{ L min}^{-1}$ .

#### 4.3.4 Effect of PARA initial concentration on the PARA degradation

To investigate the effect of initial PARA concentration on PARA degradation in the Co(II)-S(IV) system, experiments were conducted at different initial PARA concentrations (5.0 - 100 $\mu\text{M}$ ) in the presence of Co(II) 0.1mM and S(IV) 1.0mM at PH 9.0. The results show in Figure. 4-8 suggested that degradation rate were increased with the increasing initial PARA

concentration and markedly higher during the first stage of reaction, and the relationship between initial PARA concentration ( $C_0$ ) and initial reaction rate ( $R_0$ ) in the first 3min is depicted in Figure. 4-8 Insert. Its fitted equation is  $R_0=0.1689[\text{PARA}]_0$  (correlation coefficient  $R = 0.974$ ), which confirms that the degradation of PARA by the Co(II)-S(IV) system followed pseudo-first-order kinetics.

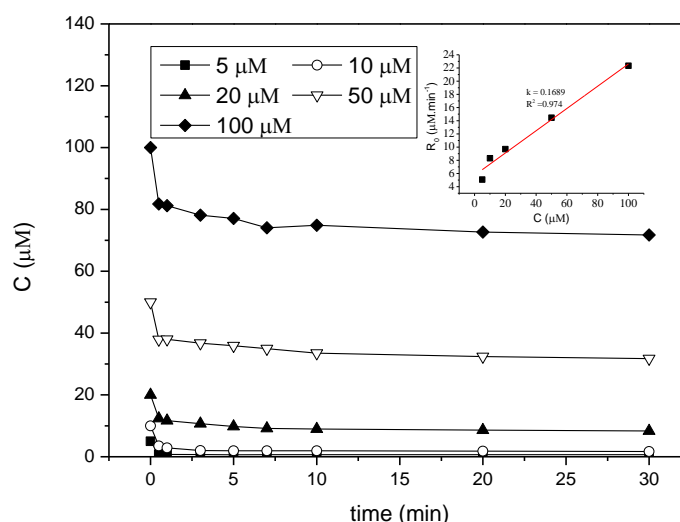


**Figure. 4-8.** Effect of different initial concentration of PARA. Inset: the initial reaction rate for different paracetamol concentration. Condition:  $[\text{Co(II)}]_0 = 0.1 \text{ mM}$ ,  $[\text{Na}_2\text{SO}_3]_0 = 1.0 \text{ mM}$ ,  $\text{pH}_{\text{ini}} = 9.0$ ,  $T = 25^\circ\text{C}$ ,  $L_{\text{air}} = 0.8\text{L}/\text{min}$ .

#### 4.3.5 Effect of $\text{O}_2$

The effect of oxygen concentration on the PARA degradation using 0.1 mM of Co(II) and 1 mM of S(IV) was investigated comparing results from aerated and nitrogen-purged solutions. When experiment was conducted in aerated solution (under air bubbling), a PARA degradation plateau was reached after first 10 min corresponding to ~82% of degradation (Figure. 4-9). However, under nitrogen-saturated solution, the efficiency dropped to less than 8% confirming that oxygen is a crucial parameter. Oxygen strongly favors the degradation of pollutant through  $\text{SO}_3^{\bullet-}$  oxidation into  $\text{SO}_5^{\bullet-}$  that undergo further reaction to form  $\text{SO}_4^{\bullet-}$  in the solution (eqs 4-5 - eqs 4-7).

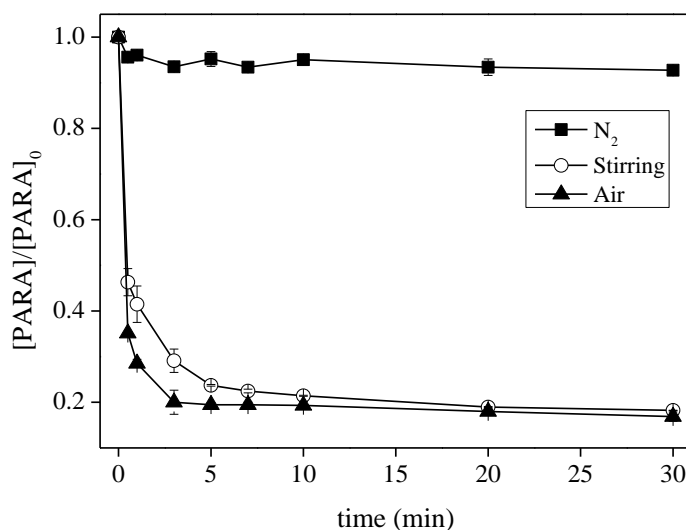


**Figure. 4-9.** Effect of oxygen on PARA degradation. Condition:  $[\text{PARA}]_0 = 10\mu\text{M}$ ,  $[\text{Co(II)}]_0 = 0.1\text{ mM}$ ,  $[\text{Na}_2\text{SO}_3]_0 = 1.0\text{ mM}$ ,  $\text{pH}_0 = 9.0$ ,  $T = 25^\circ\text{C}$ ,  $F_{\text{air}} = 0.8\text{ L min}^{-1}$ .

#### 4.3.6 Radical species involvement

The second order rate constants of sulfate radical with molecular and deprotonated PARA (at pH 9.0, pH used in our experiments, about 25 % of PARA is under deprotonated form) were determined from the linear fit of pseudo-first order decay monitored at 470 nm (corresponding to the maximum absorption of sulfate radical) vs concentration of PARA in solution (Figure.4-10). The second order rate constant was estimated to be  $1.33 \pm 0.79 \times 10^9\text{ M}^{-1}\text{ s}^{-1}$  (at pH 5) and  $6.14 \pm 0.99 \times 10^8\text{ M}^{-1}\text{ s}^{-1}$  (at pH = 11.0) corresponding respectively to the molecular and deprotonated form, on the phenol group, of PARA.

To shed light onto radical mechanism involved in such system, EtOH and TBA were used as radical scavengers. This competition kinetic approach is based on the different second-order rate constant with  $\text{HO}^\bullet$  and  $\text{SO}_4^{\bullet-}$  ( $k_{\text{TBA},\text{HO}^\bullet} = 6.0 \times 10^8\text{ M}^{-1}\text{ s}^{-1}$  [44] which is nearly three orders of magnitude higher than  $k_{\text{TBA},\text{SO}_4^{\bullet-}} = 8.5 \times 10^5\text{ M}^{-1}\text{ s}^{-1}$  [45] and  $k_{\text{EtOH},\text{HO}^\bullet} = 1.9 \times 10^9\text{ M}^{-1}\text{ s}^{-1}$  [44],  $k_{\text{EtOH},\text{SO}_4^{\bullet-}} = 5.6 \times 10^7\text{ M}^{-1}\text{ s}^{-1}$  [41]). In the

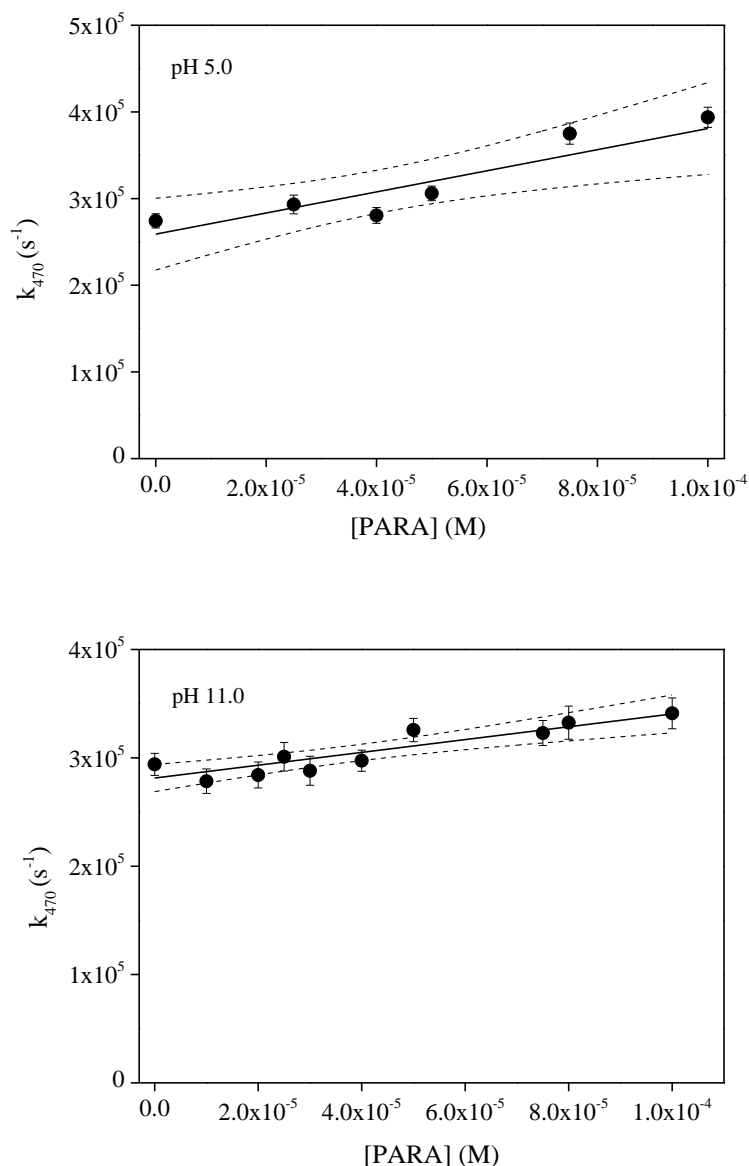


**Figure. 4-10.** Pseudo-first order decay of sulfate radical monitored at 470 nm vs PARA concentration for molecular (pH 5.0) and deprotonated form (pH 11.0).solid line represents the linear fit of the experimental data and the dashed lines denote the 95% confidence interval of this fit.

presence of TBA (up to 6 mM) no effect was observed on the PARA degradation [Figure. 4-11] indicating that hydroxyl radical are not generated using Co(II) 0.1 mM and  $\text{SO}_3^{2-}$  1 mM at pH 9.0. Indeed, if hydroxyl radical were produced in the system, addition of 1 mM TBA should be scavenged about 98 %  $\text{HO}^\bullet$  reducing drastically the PARA degradation. However, when EtOH was used as radical scavenger in solution (Figure. 4-12) PARA degradation rate and efficiency (after 30 min) were modified. In the presence of 500 mM of EtOH, a complete

inhibition of PARA degradation should be expected on the basis of second order rate constant reported before. But, PARA is still degraded with ~ 29% of disappearance after 30 min.

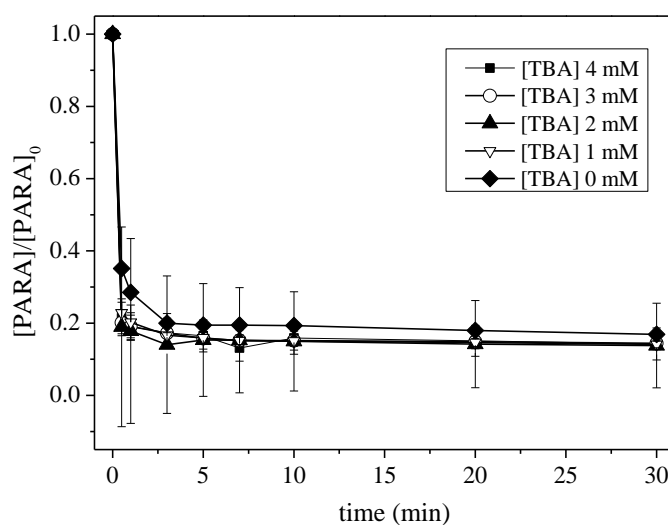


**Figure.4-11.** Effect of TBA on paracetamol degradation. Condition:  $[PARA]_0 = 10\mu\text{M}$ ,  $[Co(II)]_0 = 0.1$  mM,  $[Na_2SO_3]_0 = 1.0$  mM,  $pH_0 = 9.0$ ,  $T = 25^\circ\text{C}$ ,  $F_{air} = 0.8$  L  $\text{min}^{-1}$ .

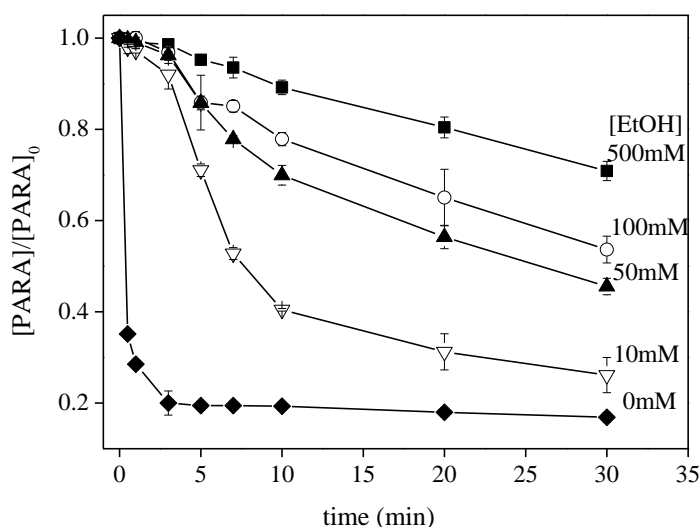


**Figure.4-12.** Effect of radical scavenger of EtOH on PARA degradation. Condition:  $[PARA]_0 = 10\mu\text{M}$ ,  $[Co(II)]_0 = 0.1$  mM,  $[Na_2SO_3]_0 = 1.0$  mM,  $pH_0 = 9.0$ ,  $T = 25^\circ\text{C}$ ,  $F_{air} = 0.8$  L  $\text{min}^{-1}$ .

Such trend could be explained considering the possible involvement of  $SO_5^{\bullet-}$  during PARA degradation. In fact, EtOH is not able to scavenge strongly  $SO_5^{\bullet-}$  due to the very low rate constant ( $k_{EtOH,SO_5^{\bullet-}} < 10^3$   $\text{M}^{-1} \text{s}^{-1}$  [46]). Such results suggest that  $SO_4^{\bullet-}$  represent the main radical leading to the degradation, but also possible implication of  $SO_5^{\bullet-}$  during degradation

of PARA is possible.

#### 4.3.7 Heterogeneous reaction between CoO and $\text{SO}_3^{2-}$

Cobalt oxide such as CoO,  $\text{CoO}_2$ ,  $\text{CoO}(\text{OH})$ ,  $\text{Co}_2\text{O}_3$  and  $\text{Co}_3\text{O}_4$  were usually used to react with PMS to oxidize different kinds of organic pollutants [24]. Experiments to prove the efficiency of sulfite activation by CoO were conducted at pH 9.0 with the paracetamol concentration of  $10 \mu\text{M}$  and  $\text{SO}_3^{2-}$  at 1.0 mM. As shown in Figure. 4-13, when 0.1 mM and 1.0 mM CoO were added to the solution, the degradation efficiency were 32.9% and 71.7%, after 30 min respectively, which indicates that CoO exhibit a good catalytic activity. One of heterogeneous catalysts advantages belong to their stability and their reusability as catalyst. However, oxide can easily agglomerate during catalytic reaction, resulting in the reduction of catalytic performance [47], also cobalt ion leaching and dissolving problem can cause the same potential environmental and health problem as homogeneous catalysts do. As reported in Figure. 4-13 and Figure. 4-5, the initial degradation rate is completely different in the two systems, very fast with soluble Co(II) and much slower with CoO. This observation shows that the reactivity of sulfite with cobalt is efficient in homogeneous phase and so with cobalt oxide a first process of solubilisation seems necessary.

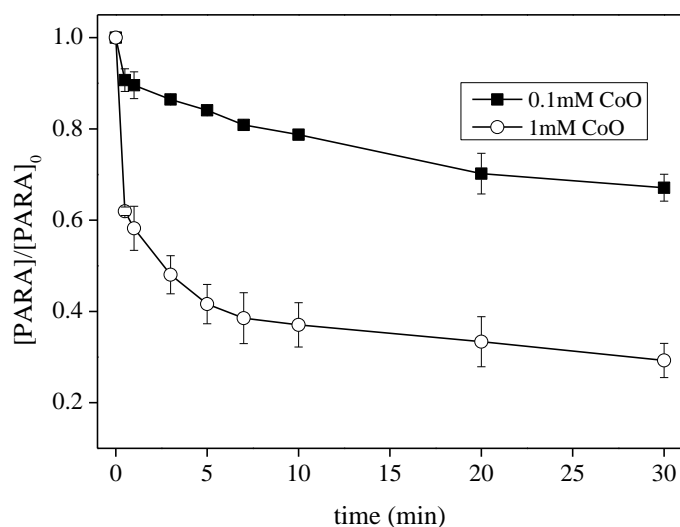


**Figure. 4-13.** Effect of heterogeneous catalyst CoO react with S(IV) to degrade PARA. Condition:

$$[\text{PARA}]_0 = 10 \mu\text{M}, [\text{Na}_2\text{SO}_3]_0 = 1.0 \text{ mM}, \text{pH}_0 = 9.0, T = 25^\circ\text{C}, F_{\text{air}} = 0.8 \text{ L min}^{-1}$$

### 4.3.8 Sequential experiments for high concentration PARA

Sequential experiments were performed with multiple additions of S(IV) to enhance the degradation of high concentration of PARA in this Co(II)-S(IV) system. In the experiment, the concentration of PARA was 500  $\mu\text{M}$ , Co(II) was 0.5 mM, and the initial pH value of solution was adjusted to 9.0 and then controlled during the whole reaction. 5 mM S(IV) was added to the solution at the beginning, while 0.5 mM were spiked every 20 min. After 200 min of reaction, (Figure. 4-14) nearly complete PARA degradation was archived. Compared to Co(II), which is recycled during the reaction, sulfite is consumed as transforms into  $\text{SO}_3^{\bullet-}$  and subsequently into  $\text{SO}_4^{2-}$ . So due to the depletion of S(IV), multiple additional sulfite is necessary to promote sequential treatment.

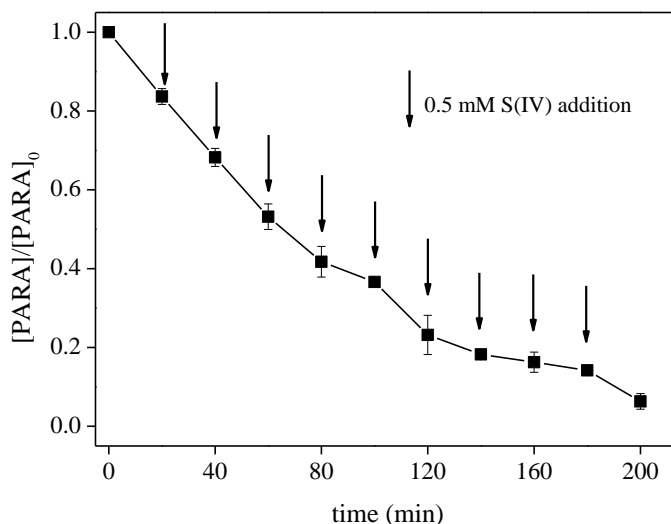


**Figure. 4-14.** Changes in paracetamol concentration over time in sequential experiments for the oxidation of paracetamol at high concentration. Initial conditions:  $[\text{PARA}]_0 = 500 \mu\text{M}$ ,  $[\text{Co(II)}]_0 = 0.5 \text{ mM}$ ,  $[\text{Na}_2\text{SO}_3]_0 = 5.0 \text{ mM}$ ,  $\text{pH}_0 = 9.0$ ,  $T = 25^\circ\text{C}$ ,  $F_{\text{air}} = 0.8 \text{ L min}^{-1}$ . Multiple additions of 0.5 mM S(IV) every 20 min.

## 4.4 Conclusions

Our results showed the high efficiency of this Co(II)-S(IV) system using PARA as organic pollutant model in aqueous solution at alkaline pH. In this system, the degradation of paracetamol depend on initial concentrations of S(IV) and strongly the pH. In fact, it is clear that dissolved oxygen plays a crucial role allowing the oxysulfure radicals oxidation to initiate

the reaction. The results of radical scavenger experiments demonstrate that  $\text{SO}_4^{\bullet-}$  and also  $\text{SO}_5^{\bullet-}$  (to a lesser extent) are involved during the paracetamol degradation. Furthermore, heterogeneous catalyst CoO also could react with sulfite to degrade paracetamol to a large extent. In general, this research work provides a new promising strategy by using sulfite and transition metal Co(II) to degrade organic compounds in wastewater under alkaline environment. One of the perspectives of this work is to perform same experiments with other metals in order to assess their ability to promote the radical generation from sulfite under dark and light conditions.

## References

- [1] Anipsitakis G P, Dionysiou D D. Degradation of organic contaminants in water with sulfate radicals generated by the conjunction of peroxymonosulfate with cobalt [J]. *Environmental Science & Technology*, 2017, 37(20): 4790-4797.
- [2] Shukla P, Sun H, Wang S, et al. Co-SBA-15 for heterogeneous oxidation of phenol with sulfate radical for wastewater treatment [J]. *Catalysis Today*, 2011, 175(1): 380-385.
- [3] Zuo Y, Zhan J, Wu T. Effects of Monochromatic UV-Visible Light and Sunlight on Fe(III)-Catalyzed Oxidation of Dissolved Sulfur Dioxide [J]. *Journal of Atmospheric Chemistry*, 2005, 50(2): 195-210.
- [4] Neta P, Huie R E, Ross A B. Rate Constants for Reactions of Peroxyl Radicals in Fluid Solutions [J]. *Journal of Physical & Chemical Reference Data*, 1990, 19(2): 413-513.
- [5] Lutze H V, Bircher S, Rapp I, et al. Degradation of chlorotriazine pesticides by sulfate radicals and the influence of organic matter.[J]. *Environmental Science & Technology*, 2015, 49(3): 1673-1680.
- [6] Ren Y, Lin L, Ma J, et al. Sulfate radicals induced from peroxymonosulfate by magnetic ferrosphenel  $\text{MFe}_2\text{O}_4$ , (M = Co, Cu, Mn, and Zn) as heterogeneous catalysts in the water [J]. *Applied Catalysis B Environmental*, 2015, 165: 572-578.
- [7] Anipsitakis G P, Dionysiou D D, Gonzalez M A. Cobalt-mediated activation of peroxymonosulfate and sulfate radical attack on phenolic compounds. implications of chloride ions [J]. *Environmental Science & Technology*, 2006, 40(3): 1000-1007.

- [8] Lin Y T, Liang C, Chen J H. Feasibility study of ultraviolet activated persulfate oxidation of phenol [J]. *Chemosphere*, 2011, 82(8): 1168-1172.
- [9] Xie X, Zhang Y, Huang W, et al. Degradation kinetics and mechanism of aniline by heat-assisted persulfate oxidation[J]. *Journal of Environmental Sciences*, 2012, 24(5): 821-829.
- [10] Antoniou M G, Cruz A A D L, Dionysiou D D. Degradation of microcystin-LR using sulfate radicals generated through photolysis, thermolysis and  $e^-$ , transfer mechanisms [J]. *Applied Catalysis B Environmental*, 2010, 96(3): 290-298.
- [11] Criquet J, Leitner N K V. Electron beam irradiation of aqueous solution of persulfate ions [J]. *Chemical Engineering Journal*, 2011, 169(1-3): 258-262.
- [12] Guo H, Gao N, Yang Y, et al. Kinetics and Transformation Pathways on Oxidation of Fluoroquinolones with Thermally Activated Persulfate [J]. *Chemical Engineering Journal*, 2016, 292: 82-91.
- [13] Matzek L W, Carter K E. Activated persulfate for organic chemical degradation: A review [J]. *Chemosphere*, 2016, 151: 178-188.
- [14] Wu Y, Prulho R, Brigante M, et al. Activation of persulfate by Fe(III) species: Implications for 4-tert-butylphenol degradation [J]. *Journal of Hazardous Materials*, 2017, 322: 380-386.
- [15] Wu Y, Bianco A, Brigante M, et al. Sulfate Radical Photogeneration Using Fe-EDDS: Influence of Critical Parameters and Naturally Occurring Scavengers [J]. *Environmental Science & Technology*, 2015, 49(24): 14343-14349.
- [16] Qi C, Liu X, Ma J, et al. Activation of peroxymonosulfate by base: Implications for the degradation of organic pollutants [J]. *Chemosphere*, 2016, 151: 280-288.
- [17] Zhang T, Zhu H, Croué J P. Production of sulfate radical from peroxymonosulfate induced by a magnetically separable  $CuFe_2O_4$  spinel in water: efficiency, stability, and mechanism [J]. *Environmental Science & Technology*, 2013, 47(6): 2784-2791.
- [18] Reddy D R, Dinesh G K, Anandan S, et al. Sonophotocatalytic treatment of Naphthol Blue Black dye and real textile wastewater using synthesized Fe doped  $TiO_2$  [J]. *Chemical Engineering & Processing Process Intensification*, 2016, 99: 10-18.
- [19] Huang Y F, Huang Y H. Behavioral evidence of the dominant radicals and intermediates involved in Bisphenol A degradation using an efficient  $Co^{2+}$ /PMS oxidation process [J]. *Journal of Hazardous Materials*, 2009, 167(1-3): 418-426.

- [20] Rastogi A, Al-Abed S R, Dionysiou D D. Sulfate radical-based ferrous-peroxymonosulfate oxidative system for PCBs degradation in aqueous and sediment systems [J]. *Applied Catalysis B Environmental*, 2009, 85(3): 171-179.
- [21] Ghanbari F, Moradi M, Mohseni-Bandpei A, et al. Simultaneous application of iron and aluminum anodes for nitrate removal: a comprehensive parametric study [J]. *International Journal of Environmental Science & Technology*, 2014, 11(6): 1653-1660.
- [22] Liang H, Sun H, Patel A, et al. Excellent performance of mesoporous  $\text{Co}_3\text{O}_4/\text{MnO}_2$  nanoparticles in heterogeneous activation of peroxymonosulfate for phenol degradation in aqueous solutions [J]. *Applied Catalysis B Environmental*, 2012, 127(1): 330-335.
- [23] Stoyanova M, Slavova I, Christoskova S, et al. Catalytic performance of supported nanosized cobalt and iron–cobalt mixed oxides on MgO in oxidative degradation of Acid Orange 7 azo dye with peroxymonosulfate [J]. *Applied Catalysis A General*, 2014, 476(6): 121-132.
- [24] Wang Y, Zhou L, Duan X, et al. Photochemical degradation of phenol solutions on  $\text{Co}_3\text{O}_4$  nanorods with sulfate radicals [J]. *Catalysis Today*, 2015, 258: 576-584.
- [25] Zhu Y, Chen S, Quan X, et al. Cobalt implanted  $\text{TiO}_2$  nanocatalyst for heterogeneous activation of peroxymonosulfate [J]. *Rsc Advances*, 2013, 3(2): 520-525.
- [26] Long C, Peng X, Liu J, et al. Decolorization of Orange II in Aqueous Solution by an Fe(II)/sulfite System: Replacement of Persulfate [J]. *Industrial & Engineering Chemistry Research*, 2016, 51(42): 13632–13638.
- [27] Liu Z, Yang S, Yuan Y, et al. A novel heterogeneous system for sulfate radical generation through sulfite activation on a  $\text{CoFe}_2\text{O}_4$  nanocatalyst surface [J]. *Journal of Hazardous Materials*, 2016, 324.
- [28] Yuan Y, Yang S, Zhou D, et al. A simple Cr(VI)–S(IV)– $\text{O}_2$  system for rapid and simultaneous reduction of Cr(VI) and oxidative degradation of organic pollutants [J]. *Journal of Hazardous Materials*, 2016, 307: 294-301.
- [29] Zhou D, Chen L, Zhang C, et al. A novel photochemical system of ferrous sulfite complex: kinetics and mechanisms of rapid decolorization of Acid Orange 7 in aqueous solutions [J]. *Water Research*, 2014, 57(5): 87-95.
- [30] Zhou D, Yuan Y, Yang S, et al. Roles of oxysulfur radicals in the oxidation of acid orange 7 in the Fe(III)-sulfite system [J]. *Sulfur Reports*, 2015, 36(4): 373-384.

- [31] Kuo D T F, Kirk D W, Jia C Q. The chemistry of aqueous S(IV)-Fe-Osystem: state of the art [J]. *Journal of Sulfur Chemistry*, 2006, 27(27): 461-530.
- [32] Zuo Y. Kinetics of photochemical/chemical cycling of iron coupled with organic substances in cloud and fog droplets [J]. *Geochimica Et Cosmochimica Acta*, 1995, 59(15): 3123-3130.
- [33] Zuo Y, Zhan J. Effects of oxalate on Fe-catalyzed photooxidation of dissolved sulfur dioxide in atmospheric water [J]. *Atmospheric Environment*, 2005, 39(1): 27-37.
- [34] Benotti M J, Trenholm R A, Vanderford B J, et al. Pharmaceuticals and endocrine disrupting compounds in U.S. drinking water [J]. *Environmental Science & Technology*, 2009, 43(3): 597-603.
- [35] Zhang L, Hu J, Zhu R, et al. Degradation of paracetamol by pure bacterial cultures and their microbial consortium [J]. *Applied Microbiology & Biotechnology*, 2013, 97(8): 3687-3698.
- [36] Katakis D, Allen A O. Radiolysis of acid aqueous solutions of aquopentaammine- and hexaamminecobaltic ions [J]. *Journal of Physical Chemistry*, 1964, 68(6): 1359-1362.
- [37] Chan K H, Chu W. Degradation of atrazine by cobalt-mediated activation of peroxymonosulfate: Different cobalt counteranions in homogenous process and cobalt oxide catalysts in photolytic heterogeneous process [J]. *Water Research*, 2009, 43(9): 2513-2521.
- [38] Pasiukbronikowska W, Bronikowski T, Ulejczyk M. Mechanism and kinetics of autoxidation of calcium sulfite slurries [J]. *Environmental Science & Technology*, 1992, 26(10): 1976-1981.
- [39] Huie R E, Neta P. Chemical behavior of  $\text{SO}_3^{\cdot-}$  and  $\text{SO}_5^{\cdot-}$  radicals in aqueous solutions [J]. *J. Phys. Chem*, 1984, 88: 5665-5669.
- [40] Buxton G V, Mcgowan S, Salmon G A, et al. A study of the spectra and reactivity of oxysulphur-radical anions involved in the chain oxidation of S(IV): A pulse and  $\gamma$ -radiolysis study [J]. *Atmospheric Environment*, 1996, 30(14): 2483-2493.
- [41] Deister U, Warneck P. Photooxidation of sulfite ( $\text{SO}_3^{2-}$ ) in aqueous solution [J]. *Journal of Physical Chemistry*, 1990, 94(5): 2191-2198.
- [42] Huie R E, Neta P. Rate constants for some oxidations of S(IV) by radicals in aqueous solutions [J]. *Atmospheric Environment*, 1987, 21(8): 1743-1747.
- [43] Wine P H, Tang Y, Thorn R P, et al. Kinetics of aqueous phase reactions of the  $\text{SO}_4^{\cdot-}$  radical with potential importance in cloud chemistry [J]. *Journal of Geophysical Research Atmospheres*, 1989, 94: 1085-1094.

- [44] Buxton G V, Greenstock C L, Helman W P, Ross A B, Critical review of rate constants for reaction of hydrated electrons, hydrogen atoms and hydroxyl radicals in aqueous solution [J]. *J. Phys. Chem. Ref. Data*, 1988, 17: 513-886.
- [44] Buxton G V, Greenstock C L, Helman W P, et al. Critical Review of rate constants for reactions of hydrated electrons *Chemical Kinetic Data Base for Combustion Chemistry. Part 3: Propane* [J]. *Journal of Physical & Chemical Reference Data*, 1988, 17(2): 513-886.
- [45] Clifton C L, Huie R E. Rate constants for hydrogen abstraction reactions of the sulfate radical,  $\text{SO}_4^{\cdot-}$  Alcohols [J]. *International Journal of Chemical Kinetics*, 1989, 21(8): 677-687.
- [46] Hayon E, Treinin A, Wilf J. Electronic spectra, photochemistry, and autoxidation mechanism of the sulfite-bisulfite-pyrosulfite systems.  $\text{SO}_2^{\cdot-}$ ,  $\text{SO}_3^{\cdot-}$ ,  $\text{SO}_4^{\cdot-}$ , and  $\text{SO}_5^{\cdot-}$  radicals [J]. *Journal of the American Chemical Society*, 1972, 94(1): 47-57.
- [47] Deng J, Feng S F, Zhang K, et al. Heterogeneous Activation of Peroxymonosulfate Using Ordered Mesoporous  $\text{Co}_3\text{O}_4$ , for the Degradation of Chloramphenicol at Neutral pH [J]. *Chemical Engineering Journal*, 2016, 308: 505-515.

**Chapter 5 Enhanced oxidation of aniline using Fe(III)-S(IV)  
system: simultaneous enhancement of Fe(III)/Fe(II) cycle  
and oxysulfur radicals**

## 5.1 Introduction

Sulfate radical (SR,  $\text{SO}_4^{\bullet-}$ ) based advanced oxidation process (AOPs), namely SR-AOPs, has currently drawn much attention in the field of oxidative decontamination of polluted waters and soils [1-5]. Persulfate (PS,  $\text{S}_2\text{O}_8^{2-}$ ) and peroxymonosulfate (PMS,  $\text{HSO}_5^-$ ) have been used as  $\text{SO}_4^{\bullet-}$  precursors in previously reported investigations [6-14] using homogeneous or heterogeneous catalysts containing transition metal such as Fe(II) and Co(II) [15, 16]. Recently, bisulfite ( $\text{HSO}_3^-$ ) has been used to replace PS or PMS for new transition-metal-catalyzed SR-AOPs systems for oxidation of several contaminants such as azo dyes [14, 17-19], phenols, aromatic amines, and arsenite [20-22]. Mechanism of radical chain reactions involving oxysulfur radicals (mainly sulfite radical ( $\text{SO}_3^{\bullet-}$ ), peroxymonosulfate radical ( $\text{SO}_5^{\bullet-}$ ), and  $\text{SO}_4^{\bullet-}$ ) during S(IV) autoxidation have been investigated. Generally,  $\text{SO}_5^{\bullet-}$  is formed from the reaction of  $\text{SO}_3^{\bullet-}$  with molecular oxygen leading to the formation  $\text{SO}_4^{\bullet-}$  through further reaction with another  $\text{SO}_5^{\bullet-}$ . However, the involvement of  $\text{SO}_5^{\bullet-}$  during the oxidation of contaminants has not been completely demonstrated. Neta and Huie reported one-electron redox reactions between  $\text{SO}_5^{\bullet-}$  and aromatic amines, hydroquinone and other hydroxyphenols [23]. The authors suggested that  $\text{SO}_5^{\bullet-}$  and not  $\text{SO}_3^{\bullet-}$  was responsible for the observed degradation of aniline in solution. On the basis of the oxidation potential,  $\text{SO}_5^{\bullet-}$  can be used to achieve the degradation of organic compounds. Moreover,  $\text{SO}_5^{\bullet-}$  can improve the Fe(III)/Fe(II) cycle, even if the mechanisms remain unclear. In the absence of oxygen, nearly no oxidation of organic contaminants has been observed, which exclude the role played by  $\text{SO}_3^{\bullet-}$  [20, 21]. The evidence of Fe(III)/Fe(II) cycle in the presence of saturated oxygen solutions was provided by Brandt et al., [24]. The authors suggested that  $\text{SO}_5^{\bullet-}$  could be the main oxidant during Fe(II) oxidation into Fe(III). Since the formation of  $\text{SO}_5^{\bullet-}$  is the main oxygen-consuming step during the overall redox process in Fe(III)-S(IV) system, the role of oxygen during the regeneration of Fe(III) from Fe(II) is not still elucidated as well as the enhancement of the contaminant oxidation through the activation by iron of S(IV).

In this work, the mechanism of the aniline (AN) (used as contaminant compound model) oxidation is investigated in the Fe(III)-S(IV) system, with emphasizing the dual role of oxygen. The changes in concentrations of Fe(III) and sulfite, initial pH value of reaction solution are investigated; the second-order rate constants between aniline and  $\text{SO}_4^{\bullet-}$ / $\text{SO}_5^{\bullet-}$  are also measured, then the contribution made by  $\text{SO}_4^{\bullet-}$  and  $\text{SO}_5^{\bullet-}$  are all evaluated in this work.

On the basis of the above results and experiments performed in this work, the role of oxygen as oxidant to degrade the aniline directly and accelerating the cycle between Fe(III) and Fe(II) are analyzed accurately. Furthermore, the sequential experiments are also conducted to degrade high concentration of aniline which provide a facile route for decontamination of organic compounds in industrial water with high concentration. Results of this work help to understand the relevance and mechanism of organic contaminants oxidation by  $\text{SO}_5^{\bullet-}$ , which has not been paid much attentions in the conventional SR-AOPs using PMS.

## 5.2 Materials and methods

### 5.2.1 Chemicals

Ferrous sulfate ( $\text{FeSO}_4 \cdot 7\text{H}_2\text{O}$ , analytical reagent grade), ferric sulfate ( $\text{Fe}_2(\text{SO}_4)_3$ ), Aniline (AN), Benzotriazole (BTA), N,N-dimethylaniline (DMA), tert-butyl alcohol (TBA), ethanol (EtOH), isopropanol and diphenylamine (DPA), 1,10-phenantroline, NaOH and  $\text{H}_2\text{SO}_4$  were purchased from Sinopharm Chemical Reagent Co., Ltd. Sodium sulfite ( $\text{Na}_2\text{SO}_3$ ) from Shanghai Zhanyun Chemical Co., Ltd. was prepared just prior to measurements. Peroxymonosulfate ( $2\text{KHSO}_5 \cdot \text{KHSO}_4 \cdot \text{K}_2\text{SO}_4$  (PMS)), and potassium persulfate ( $\text{K}_2\text{S}_2\text{O}_8$  (PS)) purchased from Sigma-Aldrich, were served as the compounds providing the strong oxidant, peroxymonosulfate ion ( $\text{HSO}_5^-$ ). Analytical-grade o-Nitroaniline, p-Nitroaniline, p-aminophenol, p-Chloroaniline, Sulfonamides, Phenol, Paracetamol, NN-dimethylaniline, which were used to testify the possible application of this system were also purchased from Sinopharm Chemical Reagent Co., Ltd. Acetonitrile and methanol were HPLC grade and purchased from Fisher Corporation.  $\text{Na}_2\text{CO}_3$  and  $\text{NaHCO}_3$  were used to determine the concentration of  $\text{Na}_2\text{SO}_3$ . Ammonium acetate used to prepare buffer solution for Fe(II) titration, were purchased from Sinopharm Chemical Reagent Co., Ltd.

All chemicals were used without further purification. Ultrapure water with 18.2 M $\Omega$  cm resistivity used in this work was obtained through a water purification system (Liyuan Electric Instrument Co., Beijing, China).

### 5.2.2 Experimental setup

Experiments were conducted in a 250 mL open cylindrical reactor held at a constant temperature of 25°C by circulating thermostatically controlled water through an outer water-jacketed. Appropriate amounts of compounds were mixed in the solution, and the pH was adjusted using a PHS-3C pH meter (Hinotek, Ningbo, China) by adding of NaOH or  $\text{H}_2\text{SO}_4$  concentrated solutions. Solutions were continuously stirred with a

Polytetrafluoroethylene (PTFE)-coated magnetic stirrer, and each run was started by careful addition of the desired volume of a Fe(III) or Fe(II) stock solution. Samples were withdrawn at fixed interval times and analyzed immediately to determine the remaining concentration of Aniline, S(IV) and Fe(II) in solution to avoid further reaction. If necessary, predetermined amounts of radical scavengers were added to the solution before aniline. In order to investigate the effect of oxygen on the aniline degradation, N<sub>2</sub> (99.99%) or pure O<sub>2</sub> (99.99%) were bubbled for 30 min before and throughout the experiment using a constant flow rate kept at 1 L min<sup>-1</sup>. A dissolved oxygen meter (8403, AZ Instrument Co. Ltd.) was used to determine the concentration of oxygen in solution.

### 5.2.3 Analytical methods

Aniline disappearance was monitored by high-performance liquid chromatography Shimadzu LC-10A system (Kyoto, Japan) equipped with a UV-vis detector (SPD-10AV; Shimadzu) set at 230 nm, a LC-10AT liquid pump, a SIL-10A auto-injector and a ODS-C18 column (25 cm × 4.6 mm, 5 μm; Shimadzu, Kyoto, Japan). The eluent was mixture of acetonitrile/water (v/v, 55/45) with a flow rate of 1.0 mL min<sup>-1</sup>. The injection volume was 20 μL and the retention time for aniline was 4.7 min in these experimental conditions. The condition of monitoring the residual of other aromatic amines by HPLC were as follow: o-Nitroaniline: 230nm with water/acetonitrile mixture (45/55 v/v); p-Nitroaniline: 272nm with water/methanol mixture (45/55 v/v), p-Chloroaniline: 260nm with water/acetonitrile mixture (45/55 v/v), Sulfonamides: 270nm with water/acetonitrile mixture (45/55 v/v), Phenol: 270nm with water/methanol mixture (45/55 v/v), Paracetamol: 241nm with water/ methanol mixture (75/25 v/v), p-aminophenol: 225nm with water/methanol mixture (50/50 v/v), NN-dimethylaniline: 254 nm with water/acetonitrile mixture (45/55 v/v).

The concentration of Fe(II) was determined using a colorimetric complexant the 1,10-phenanthroline coupled with spectrophotometric detection at 510 nm using a Shimadzu spectrophotometer UV-1601 [25]. The sulfite concentration was determined by ion chromatography (ICS-90, Dionex, China) using 1mM NaHCO<sub>3</sub> and 8 mM Na<sub>2</sub>CO<sub>3</sub> as eluent and dilute H<sub>2</sub>SO<sub>4</sub> as regenerator. The sample loop size was 50 μL and the eluent flow rate was 1.0 mL min<sup>-1</sup>.

## 5.3 Results and discussion

### 5.3.1 Effects of Fe(III)/S(IV) ratio and pH

AN concentration disappearance is monitored in the presence of 0.1 mM of Fe(III) and 1 mM

of S(IV) at pH 4.0. No significant degradation is determined when Fe(III) and S(IV) are present separately in solution while, in the presence of both species, AN undergoes significant degradation. In the first 30 minutes about 65 % of AN are degraded while a slowly degradation rate can be observed up to 80 min (Figure 5-1). The initial pseudo-first order degradation rate can be estimated to be  $(1.32 \pm 0.08) \times 10^{-1} \text{ min}^{-1}$ .

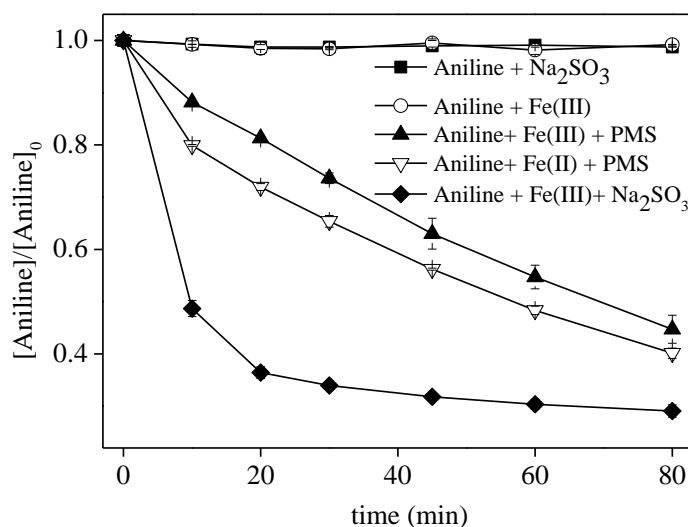


**Figure 5-1.** Degradation of aniline in the control experiments under various conditions under aerated solution. Condition:  $[\text{AN}]_0 = 10 \mu\text{M}$ ,  $[\text{Fe(III)}]_0 = 0.1 \text{ mM}$ ,  $[\text{S(IV)}]_0 = 1.0 \text{ mM}$ ,  $\text{pH}_{\text{ini}} = 4.0$ .

In order to investigate the effect of iron and sulfite concentration on degradation, sulfite concentration was modified using 0.1 mM of Fe(III) in solution at pH 4.0. Increasing S(IV) concentration from 1 to 1.2 mM, the AN degradation is strongly inhibited with initial pseudo-first order degradation rate decreasing to  $(8.16 \pm 0.48) \times 10^{-2} \text{ min}^{-1}$  and degradation after 80 min is about 42 %. Increasing the S(IV) concentration inhibits the oxidation of aniline through the scavenging reaction between S(IV) and generated radicals  $\text{SO}_4^{\bullet-}$  or  $\text{SO}_5^{\bullet-}$ . Moreover, decreasing the S(IV) concentration to 0.6 mM no significant change of AN disappearance is noticed (Figure 5-2A). Similar trend was observed keeping a S(IV) concentration constant to 1 mM and varying the Fe(III) from 0.05 to 0.2 mM (Figure 5-2B). Increasing the Fe(III) concentration may enhance the generation of  $\text{SO}_3^{\bullet-}$  via intermolecular electron transfer, however at high concentration of Fe(III) formation of colloidal  $\text{Fe(OH)}_3$  particles, which are responsible for inhibition of AN degradation, may occur even at pH 4 [21]. Considering the factors above, we deem 0.1/1.0 (mM/mM) as the optimum Fe(III)/S(IV) molar ratio for this system.

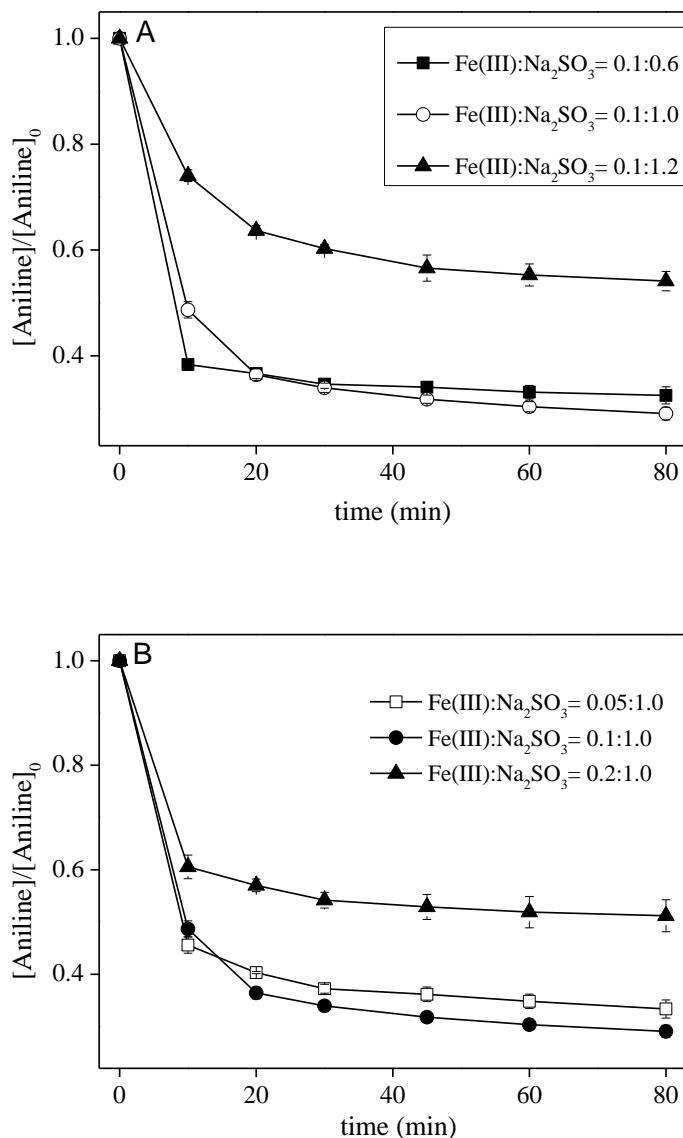


**Figure 5-2.** Degradation of AN (10  $\mu\text{M}$ ) using different Fe(III) /S(IV) ratios at pH = 4.0 under aerated solution. Condition:  $[\text{AN}]_0 = 10\mu\text{M}$ ,  $\text{pH}_{\text{ini}} = 4.0$ .

Modification of pH strongly affect AN removal using 0.1 mM of Fe(III) and 1 mM of S(IV) as reported in Figure 5-3. At pH 7.0, AN removal is less than 10 % after 80 min while, decreasing the pH the degradation efficiency increased, reaching 70% when the initial pH of solution is 4.0. This effect can be attributed to the stability of Fe(III)-S(IV) complex as reported in different works [14, 26]. Although it is rather difficult to summarize the overall influence of pH on Fe(III)-S(IV) induced oxidation (a change in pH can impact the speciation of S(IV) ( $\text{pK}_a \text{H}_2\text{SO}_3/\text{HSO}_3^- = 1.8$ ) and stability of Fe(III)), it is interesting to note that at pH 4.0 only  $\text{HSO}_3^-$  are present in solution. Under these conditions high formation of  $\text{FeSO}_3^+$  complexes are expected in agreement with previously reported studies on cobalt reactivity

[27].

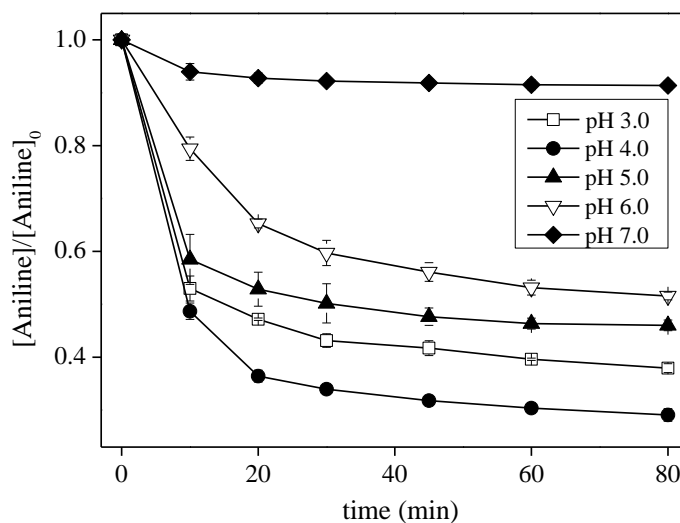


**Figure. 5-3.** Degradation of AN using 0.1 mM of Fe(III) and 1 mM of S(IV) at different pH values under aerated solution. Condition:  $[AN]_0 = 10\mu\text{M}$ ,  $[\text{Fe(III)}]_0 = 0.1\text{mM}$ ,  $[\text{S(IV)}]_0 = 1.0\text{mM}$ .

### 5.3.2 Determination of the reactivity constants with $\text{SO}_4^{\bullet-}$ and $\text{SO}_5^{\bullet-}$

The second-order rate constants between AN and  $\text{SO}_4^{\bullet-}$  ( $k_{AN,\text{SO}_4^{\bullet-}}$ ) or  $\text{SO}_5^{\bullet-}$  ( $k_{AN,\text{SO}_5^{\bullet-}}$ ) are determined by using chemical competition kinetic with radical scavengers as listed in Table 5-1. Bimolecular reactivity constant with  $\text{SO}_4^{\bullet-}$  is determined in a conventional Fe(II)-PS system in which  $\text{SO}_4^{\bullet-}$  and  $\text{OH}^{\bullet}$  generated at initial pH 3. Isopropanol is used to scavenge  $\text{HO}^{\bullet}$  while Benzotriazole (BTA) is employed as chemical competitor for the reaction with  $\text{SO}_4^{\bullet-}$  (eqs 5-1 and eqs 5-2).



Considering a first-order decay of chemical species and applying the competition kinetic method, the relation between the decay of two species gives (Eq 5-1):

$$\ln\left(\frac{[AN]_0}{[AN]_t}\right) = \frac{k_{AN,\text{SO}_4^{\bullet-}}}{k_{BTA,\text{SO}_4^{\bullet-}}} \times \ln\left(\frac{[BTA]_0}{[BTA]_t}\right) \quad (\text{Eq 5-1})$$

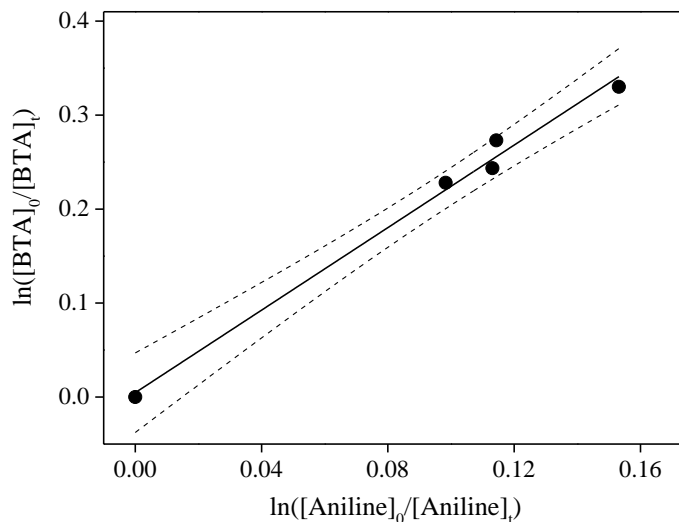
Where  $[AN]_0$ ,  $[BTA]_0$  and  $[AN]_t$ ,  $[BTA]_t$  are initial concentrations of AN and BTA and at time  $t$  respectively. The slope of the linear fit of experimental data as  $\ln\left(\frac{[BTA]_0}{[BTA]_t}\right)$  vs

$\ln\left(\frac{[AN]_0}{[AN]_t}\right)$  gives the ratio of two second order rate constants  $\frac{k_{AN,SO_4^{\bullet-}}}{k_{BTA,SO_4^{\bullet-}}}$ . In Figure 5-4 the linear fit gives a slope of  $2.20 \pm 0.13$  which corresponds to  $k_{AN,SO_4^{\bullet-}} = (7.7 \pm 0.5) \times 10^9 \text{ M}^{-1}\text{s}^{-1}$ .

**Table 1.**

Summaries of second-order rate constant  $k$  of the reactions of chemical scavengers with oxysulfur radicals.

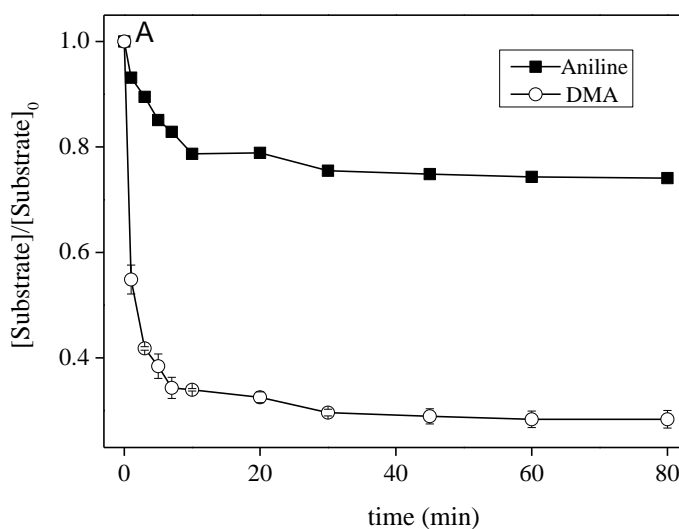
| Reaction   | Rate constant, $k$ ( $\text{M}^{-1}\text{s}^{-1}$ ) | Reference |
|--|---|-----------|
| EtOH + $\text{SO}_4^{\bullet-}$                              | $7.7 \times 10^7$                                   | [34, 35]  |
| EtOH + $\text{SO}_3^{\bullet-}$                              | $< 2 \times 10^3$                                   | [36]      |
| EtOH + $\text{SO}_5^{\bullet-}$                              | $< 1 \times 10^3$                                   | [36]      |
| EtOH + $\text{HO}^{\bullet}$                                 | $1.9 \times 10^9$                                   | [37]      |
| Benzotriazole + $\text{SO}_4^{\bullet-}$                     | $3.5 \times 10^9$                                   | [38]      |
| $(\text{C}_6\text{H}_5)_2\text{NH} + \text{SO}_3^{\bullet-}$ | $< 1.0 \times 10^7$ (pH 3-7)                        | [39]      |
| $(\text{C}_6\text{H}_5)_2\text{NH} + \text{SO}_5^{\bullet-}$ | $5 \times 10^7$ (pH 3)                              | [39]      |
| $\text{C}_6\text{H}_5\text{NH}_2 + \text{SO}_3^{\bullet-}$   | $< 1.0 \times 10^6$ (pH 13)                         | [39]      |
| $\text{C}_6\text{H}_5\text{NH}_2 + \text{SO}_5^{\bullet-}$   | $\sim 3 \times 10^6$ (pH 13)                        | [39]      |
| $\text{C}_6\text{H}_5\text{NH}_2 + \text{SO}_4^{\bullet-}$   | $5.8 \pm 0.6 \times 10^6$                           | this work |
| $\text{C}_6\text{H}_5\text{NH}_2 + \text{SO}_4^{\bullet-}$   | $7.7 \pm 0.5 \times 10^9$                           | this work |
| tert-butyl alcohol + $\text{HO}^{\bullet}$                   | $7.6 \times 10^8$                                   | [17]      |
| tert-butyl alcohol + $\text{SO}_4^{\bullet-}$                | $9.1 \times 10^5$                                   | [17]      |



**Figure. 5-4.** Linear fit of  $\ln([AN]_0/[AN]_t)$  vs  $\ln([BTA]_0/[BTA]_t)$  in the system  $Fe(II)-S_2O_8^{2-}$  in the dark at pH 3.0. Dashed lines denote the 95% confidence of the linear fit. Initial concentrations are:

$$[AN]_0 = [BTA] = 10\mu M, [Isopropanol] = 2.0mM, [Fe(II)]_0 = 0.5mM, [K_2S_2O_8] = 5.0mM$$

For the determination of the second order rate constant between AN and  $SO_5^{\bullet-}$  ( $k_{AN,SO_5^{\bullet-}}$ ), N,N-dimethylaniline (DMA) is selected to be the competition reagent for AN to react with  $SO_5^{\bullet-}$  in Fe(III)-S(IV) system. Ethanol (EtOH), which has a negligible reactivity with  $SO_5^{\bullet-}$  ( $< 1 \times 10^3 M^{-1} s^{-1}$ ), is used to selectively scavenge other radicals such as  $HO^{\bullet}$  and  $SO_4^{\bullet-}$  ( $k_{EtOH,HO^{\bullet}} = 1.9 \times 10^9 M^{-1} s^{-1}$  and  $k_{EtOH,SO_4^{\bullet-}} = 7.7 \times 10^7 M^{-1} s^{-1}$ ). A concentration of 0.5 M of EtOH is used in solution during experiments. The same approach adopted for sulfate radical is used in this system and  $k_{AN,SO_5^{\bullet-}}$  is found to be equal to  $(5.8 \pm 0.6) \times 10^6 M^{-1} s^{-1}$ .



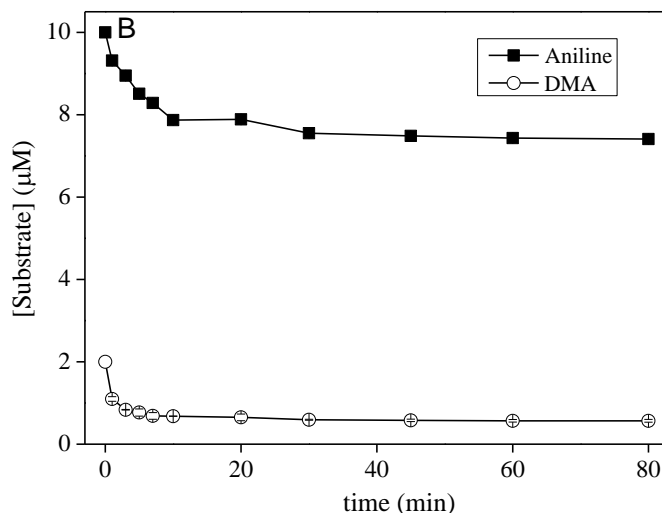


**Figure. 5-5.** The initial rate of DMA and  $\text{SO}_5^{\bullet-}$  ( $k_1$ ) and aniline and  $\text{SO}_5^{\bullet-}$  ( $k_2$ ). Conditions:  $[\text{aniline}]_0 = 10\mu\text{M}$ ,  $[\text{DMA}] = 2\mu\text{M}$ ,  $[\text{EtOH}] = 0.5\text{M}$ ,  $[\text{Fe(III)}]_0 = 0.1\text{mM}$ ,  $[\text{S(IV)}]_0 = 1.0\text{mM}$ ,  $\text{pH}_{\text{ini}} = 4.0$ .

### 5.3.3 Role of $\text{SO}_4^{\bullet-}$ and $\text{SO}_5^{\bullet-}$

Although the formation of  $\text{SO}_4^{\bullet-}$  and  $\text{SO}_5^{\bullet-}$  in this system is demonstrated, their relative contribution on the oxidation of AN has been investigated. Under adopted experimental conditions, hydroxyl radical cannot be generated in the system at enough concentration for the oxidation of organic contaminants mainly due to high concentration of S(IV) and acidic environment [24, 28]. The fact that no significant inhibition of AN degradation is observed using different TBA concentrations (Figure. 5-6) suggests that  $\text{HO}^{\bullet}$  radicals are not generated in our system. In order to validate this hypothesis, the initial degradation rate of AN ( $R_{\text{AN}}^d$ ) is calculated under specific concentration of scavengers, when the concentration of TBA is 100 times higher than those of AN, the corresponding contribution of  $\text{HO}^{\bullet}$  was less than 3% (the result was shown in Table 5-2). To dissociate the contribution of  $\text{SO}_4^{\bullet-}$  and  $\text{SO}_5^{\bullet-}$ , different scavengers are added into the reaction system. Scavenging of  $\text{SO}_3^{\bullet-}$  by EtOH even at very high concentration (0.5 M) can be neglected due to the very high reactivity between  $\text{SO}_3^{\bullet-}$  and dissolved oxygen ( $k_{\text{O}_2, \text{SO}_3^{\bullet-}} = 2.3 \times 10^9 \text{ M}^{-1} \text{ s}^{-1}$  [29]). However, EtOH can be used to differentiate  $\text{SO}_4^{\bullet-}$  and  $\text{SO}_5^{\bullet-}$  due to large difference (more than  $10^4$ -fold) between  $k_{\text{EtOH}, \text{SO}_4^{\bullet-}}$  and  $k_{\text{EtOH}, \text{SO}_5^{\bullet-}}$ .

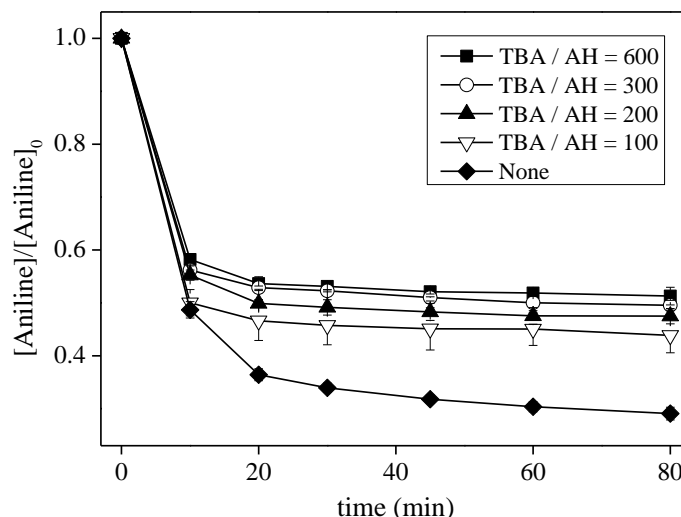


**Figure. 5-6.** Inhibition of the oxidation of aniline by TBA in Fe(III)-S(IV) system. Conditions:

$[\text{aniline}]_0 = 10\mu\text{M}$ ,  $[\text{Fe(III)}]_0 = 0.1\text{mM}$ ,  $[\text{S(IV)}]_0 = 1.0\text{ mM}$ ,  $\text{pH}_{\text{ini}} = 4.0$ .

**Table 2**

Initial degradation rate of AN ( $R_{AN}^d$ ) in the Fe(III)-S(IV) system in the presence of various radical scavengers

| Parameter   | No scavengers     | $[\text{TBA}]_0/[\text{AN}]_0 = 100$ | $[\text{EtOH}]_0/[\text{AN}]_0 = 5000$                  | $[\text{DPA}]_0/[\text{AN}]_0 = 100$ |
|---|-------------------|--------------------------------------|---|--------------------------------------|
| $R_{AN}^d$<br>( $\mu\text{M} \cdot \text{min}^{-1}$ ) | $0.513 \pm 0.015$ | $0.500 \pm 0.025$                    | $0.316 \pm 0.005$                                       | $0.008 \pm 0.004$                    |
| contribution of radicals                              |                   |                                      | $(1 - R_{DPA}/R) \times 100 = 98.4 \pm 0.8 \%$          |                                      |
| contribution of $\text{HO}^\bullet$                   |                   |                                      | $(1 - R_{TBA}/R) \times 100 = 2.5 \pm 4.9 \%$           |                                      |
| contribution of $\text{SO}_4^{\bullet-}$              |                   |                                      | $(1 - R_{EtOH}/R) \times 100 - 2.5\% = 35.9 \pm 1.0 \%$ |                                      |
| contribution of $\text{SO}_5^{\bullet-}$              |                   |                                      | $98.4\% - 38.4\% = 60.0\%$                              |                                      |

In order to set the appropriate EtOH concentration to scavenge only  $\text{SO}_4^{\bullet-}$  without interferences with  $\text{SO}_5^{\bullet-}$  reactivity with AN, experiments using different concentrations of EtOH (in the range of 5 to  $500 \times 10^2 [\text{AN}]$ ) are performed (Figure 5-7A). The AN degradation presents slight decrease with the increase of EtOH, showing that at high EtOH/AN ratios an effect on the  $\text{SO}_5^{\bullet-}$  reactivity is expected. For the reaction between  $\text{SO}_4^{\bullet-}$  and EtOH or AN, a

competition kinetics method is used to determine the inhibition efficiency ( $\rho$ ). In the absence and presence of inhibitor (EtOH), we can assume that the initial  $\text{SO}_4^{\bullet-}$  radical yield is the same in both solution, and the standard competition kinetic equations (Eq.2-3) can be used to estimate the inhibition efficiency of EtOH on AN oxidation. In these equations,  $k'_{\text{EtOH}=0}$  and  $k'_{\text{EtOH}}$  represent pseudo-first-order rate constants of aniline reacting with  $\text{SO}_4^{\bullet-}$  in absence and presence of various EtOH concentrations respectively.

$$\frac{k'_{\text{EtOH}=0}}{k'_{\text{EtOH}}} - 1 = \frac{k_{\text{SO}_4^{\bullet-}, \text{EtOH}}}{k_{\text{SO}_4^{\bullet-}, \text{AN}}} \times \frac{[\text{EtOH}]_0}{[\text{AN}]_0} \quad (\text{Eq 5-2})$$

which, after rearrangement gives:

$$\frac{k'_{\text{EtOH}}}{k'_{\text{EtOH}=0}} = \frac{1}{\frac{k_{\text{SO}_4^{\bullet-}, \text{EtOH}}}{k_{\text{SO}_4^{\bullet-}, \text{AN}}} \times \frac{[\text{EtOH}]_0}{[\text{AN}]_0} + 1} \quad (\text{Eq 5-3})$$

the inhibition efficiency of [EtOH] ( $\rho$ ) on Aniline oxidation by  $\text{SO}_4^{\bullet-}$  can be determined as:

$$\rho(\%) = 1 - \frac{k'_{\text{EtOH}}}{k'_{\text{EtOH}=0}} \times 100 \quad (\text{Eq 5-4})$$

$$\rho(\%) = \left( 1 - \frac{1}{\frac{k_{\text{SO}_4^{\bullet-}, \text{EtOH}}}{k_{\text{SO}_4^{\bullet-}, \text{AN}}} \times \frac{[\text{EtOH}]_0}{[\text{AN}]_0} + 1} \right) \quad (\text{Eq 5-5})$$

Equation 5-5 can be plotted as  $y = 1 - \frac{1}{ax+1} \times 100$  with  $a = \frac{k_{\text{SO}_4^{\bullet-}, \text{EtOH}}}{k_{\text{SO}_4^{\bullet-}, \text{AN}}} = 7.7 \times 10^7 / 7.7 \times 10^9 =$

0.01.

In Figure 5-7B the inhibition efficiency is reported as function of ratio  $[\text{EtOH}]_0/[\text{AN}]_0$  and the inhibition efficiency can reach  $\sim 98\%$ , which reasonably shows that complete inhibition of  $\text{SO}_4^{\bullet-}$  is achieved. However, the model fit overestimates the inhibition efficiency. This effect is attributed to the fact that the presence of  $\text{SO}_5^{\bullet-}$  is not considered in the equations.

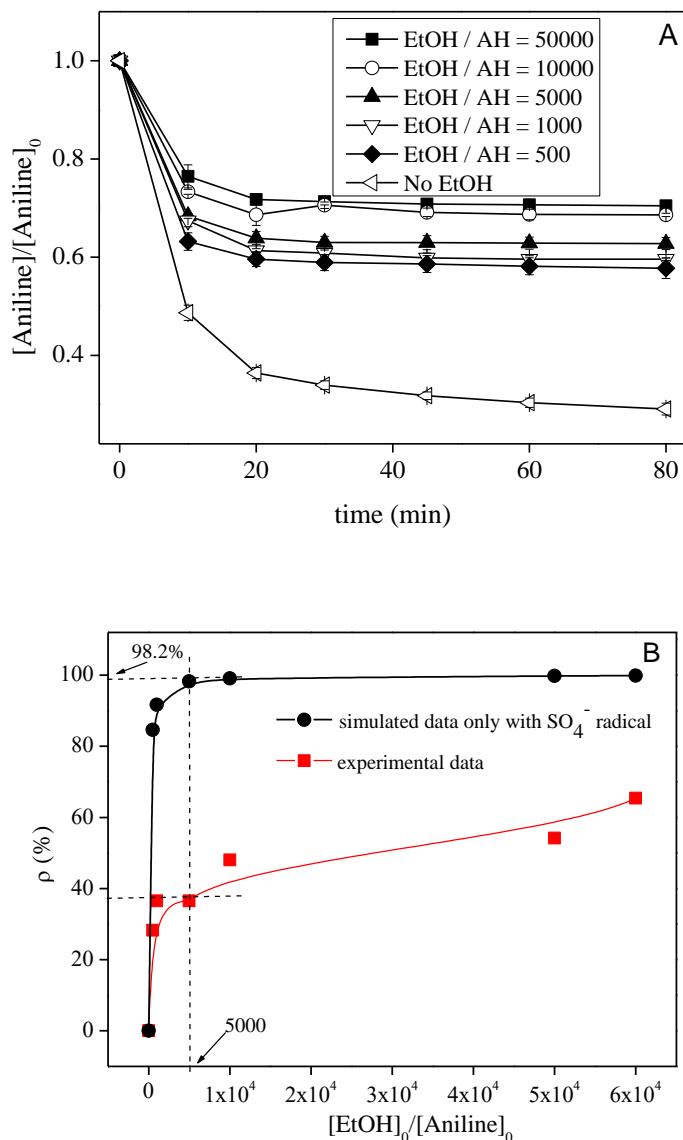


**Figure. 5-7.** (A) Degradation of AN during time using different  $[\text{EtOH}]_0/[\text{AN}]_0$  ratios. (B) Inhibition efficiency ( $\rho$ ) as function of with different  $[\text{EtOH}]_0/[\text{AN}]_0$  ratios. Conditions are:  $[\text{AN}]_0 = 10 \mu\text{M}$ ,  $[\text{Fe(III)}]_0 = 0.1 \text{ mM}$ ,  $[\text{S(IV)}]_0 = 1.0 \text{ mM}$ ,  $\text{pH} = 4.0$ .

DPA and EtOH are also used in order to discriminate the contribution of  $\text{SO}_4^{\bullet-}$  and  $\text{SO}_5^{\bullet-}$  to the AN degradation in the Fe(III)-S(IV) system. In the presence of 50  $\mu\text{M}$  of DPA that is able to quantitatively trap both  $\text{SO}_4^{\bullet-}$  and  $\text{SO}_5^{\bullet-}$ , almost no degradation of AN is observed in solution as reported in Figure. 5-8 indicating that  $\text{SO}_4^{\bullet-}$  and  $\text{SO}_5^{\bullet-}$  are the most important species generated in solution. Using 50 mM of EtOH which is able to scavenge  $\text{SO}_4^{\bullet-}$  and not significantly  $\text{SO}_5^{\bullet-}$ , AN degradation is inhibited of about 50 %.

The contribution of these two radicals can be then determined and, as shown in Table 2, the inhibition efficiency accounted by for  $\text{SO}_4^{\bullet-}$  is only  $(35.9 \pm 1.0)$  % and it is possible to

determine that contribution of  $SO_5^{\bullet-}$  to aniline degradation is ~60%.

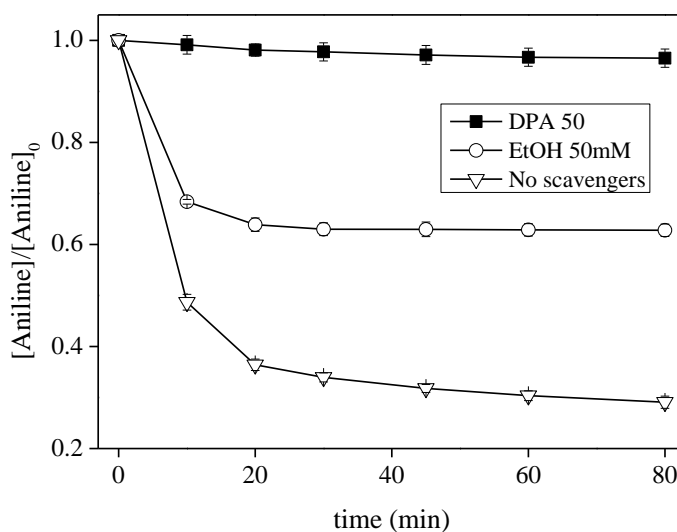


**Figure. 5-8.** AN degradation in the system Fe(III)-S(IV) in absence (no scavengers) and presence of different radical scavengers. Conditions are  $[AN]_0 = 10 \mu\text{M}$ ,  $[\text{Fe(III)}]_0 = 0.1 \text{ mM}$ ,  $[\text{S(IV)}]_0 = 1.0 \text{ mM}$ ,  $\text{pH} = 4.0$ .

From study above, when the concentration of EtOH was  $5000[AN]_0$ , the  $SO_4^{\bullet-}$  could be inhibited exactly without any  $SO_5^{\bullet-}$  quenched simultaneously. For the sake of accurate differentiating the contributions of various radicals,  $SO_4^{\bullet-}$  and  $SO_5^{\bullet-}$ , to AN oxidation, the experiments with variations of the AN initial concentrations (from  $10\mu\text{M}$  to  $100\mu\text{M}$ ) were conducted in the presence/ absence of EtOH (when with EtOH added, the concentration was  $5000[AN]_0$ ) in the solution, and the data was shown in Figure 5-9A and 5-9B. According to the competition kinetics method, the initial rate of Aniline/EtOH with radicals  $SO_4^{\bullet-}$  and  $SO_5^{\bullet-}$  can be expressed as Eq 5-6 to 5-7), respectively.

$$r_{0,AN,SO_5^-} = k_{AN,SO_5^-}[AN]_0[SO_5^-]_{ss} \quad (\text{Eq.5-6})$$

$$r_{0,EtOH,SO_4^-} = k_{EtOH,SO_4^-}[EtOH]_0[SO_4^-]_{ss} \quad (\text{Eq.5-7})$$

$$r_{0,EtOH,SO_5^-} = k_{EtOH,SO_5^-}[EtOH]_0[SO_5^-]_{ss} \quad (\text{Eq.5-8})$$

Furthermore, we define inhibited efficiency ( $\rho$ ) of initial rate of aniline by excessive EtOH as:

$$\rho_{SO_4} = \left(1 - \frac{r_{0,EtOH}}{r_0}\right) \times 100\% \quad (\text{Eq.5-9})$$

where  $r_{0,EtOH}$  and  $r_0$  represent the initial rate of aniline in the presence and absence of excessive EtOH, respectively.

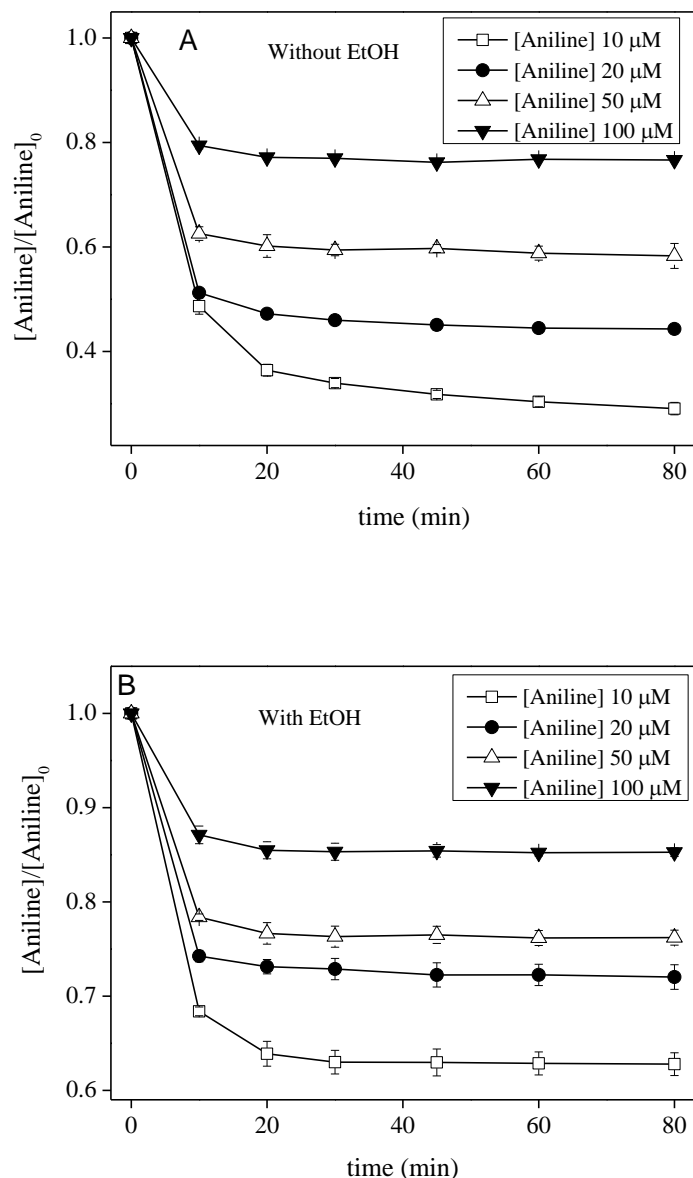


**Figure. 5-9.** The effect of initial aniline concentration during oxidation in Fe(III)-S(IV) system  
 A: without or B: with EtOH. Conditions:  $[\text{Fe(III)}]_0 = 0.1\text{mM}$ ,  $[\text{S(IV)}]_0 = 1.0\text{mM}$ ,  $\text{pH}_{\text{ini}} = 4.0$ .  $[\text{EtOH}]_0 = 50\text{mM}$

Basing on the initial rate fitted at the first reactions stage (0-10min), the curves of inhibited efficiency ( $\rho$ ) could be calculated out as follows: when the concentration of aniline were 10, 20, 50, 100 $\mu\text{M}$ , the inhibited efficiency ( $\rho$ ) were 38.36%, 46.9%, 42.25%, 37.12%, respectively. Thus, it can be said that the average  $\rho$  41.3% could be the precise concentration of  $\text{SO}_4^-$  in this Fe(III)-sulfite system, this result did not show a big difference to  $(35.9 \pm 1.0)\%$  which obtained in the radical scavengers experiments above. The residual part contribution of 58.7% should belongs to  $\text{SO}_5^{\cdot-}$ .

### 5.3.4 Dissolved oxygen implication

To shed light onto the effect of oxygen on aniline oxidation, different experiments are performed at different oxygen concentrations in solution by continuous bubbling pure O<sub>2</sub>, air and N<sub>2</sub> during the whole experiment. As depicted in Figure 5-10, when the experiments are conducted in the presence of air or pure O<sub>2</sub> ([O<sub>2</sub>] > 20 mg L<sup>-1</sup> in the solution), a plateau corresponding to 70% of AN degradation is found after 20-30 min. However, the efficiency decreases to 10% in nitrogen purged solutions. This result implies that oxygen plays an important role in transformation of aniline in the Fe(III)-S(IV) system mainly through the generation of SO<sub>4</sub><sup>•-</sup> and SO<sub>5</sub><sup>•-</sup> after reaction with SO<sub>3</sub><sup>•-</sup> in solution. On the other hand, there are not remarkable differences among the degradation effects between bubbling of pure O<sub>2</sub> or air after 80 min of reaction, which illustrates that the oxygen bubbling is less effective on PARA degradation only accelerate oxysulfur radical cycle, as shown in reaction 7-10 in Table 5-3.

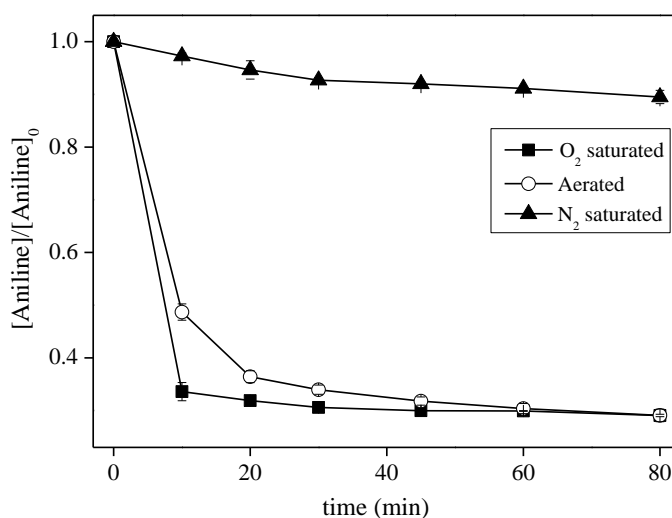


**Figure. 5-10.** Concentration changes of aniline ( $C/C_0$ ) during oxidation in Fe(III)-S(IV) system with or without oxygen. Conditions are  $[AN]_0 = 10 \mu\text{M}$ ,  $[\text{Fe(III)}]_0 = 0.1 \text{ mM}$ ,  $[\text{S(IV)}]_0 = 1.0 \text{ mM}$ ,  $\text{pH} = 4.0$ .

Experiments also are conducted to investigate the consumption of S(IV), the Fe(II) generation which can clearly reveal the Fe(III)/Fe(II) cycle, oxygen concentration and pH variation during the whole reaction under oxic (pure O<sub>2</sub> and air bubbling) or anoxic conditions (N<sub>2</sub> bubbling).

**Table 5-3**

Main reactions and rate ( $k$  in  $s^{-1}$  or  $M^{-1} s^{-1}$ ) and equilibrium constant ( $K$  in  $M$ ) involved in kinetic simulation in Fe(III)-S(IV) system at initial pH 4.

| No. | Reaction  | Kinetic constant $k$               |
|-----|---|------------------------------------|
| 1   | $Fe^{3+} + HSO_3^- \leftrightarrow FeSO_3^+ + H^+$                        | $\log k = 2.45$                    |
| 2   | $FeSO_3^+ \leftrightarrow Fe^{2+} + SO_3^{\bullet-}$                      | $0.19 s^{-1}$                      |
| 3   | $Fe^{2+} + HSO_3^- \rightarrow FeHSO_3^+$                                 | $10^4 M^{-1}$                      |
| 4   | $FeSO_3^+ + \frac{1}{4} O_2 \rightarrow FeSO_3^+ + \frac{1}{2} H_2O$      | $1.69 \times 10^3 M^{-1} s^{-1}$   |
| 5   | $SO_3^{\bullet-} + O_2 \rightarrow SO_5^{\bullet-}$                       | $2.5 \times 10^9 M^{-1} s^{-1}$    |
| 6   | $SO_5^{\bullet-} + HSO_3^- \rightarrow SO_3^{\bullet-} + HSO_5^-$         | $\leq 3 \times 10^5 M^{-1} s^{-1}$ |
| 7   | $SO_5^{\bullet-} + HSO_3^- \rightarrow SO_4^{\bullet-} + H^+ + SO_4^{2-}$ | $1.2 \times 10^4 M^{-1} s^{-1}$    |
| 8   | $SO_4^{\bullet-} + HSO_3^- \rightarrow SO_3^{\bullet-} + H^+ + SO_4^{2-}$ | $7.5 \times 10^8 M^{-1} s^{-1}$    |
| 9   | $SO_5^{\bullet-} + SO_5^{\bullet-} \rightarrow 2 SO_4^{\bullet-} + O_2$   | $2.2 \times 10^8 M^{-1} s^{-1}$    |
| 10  | $Fe^{2+} + SO_5^{\bullet-} \rightarrow Fe^{3+} + HSO_5^-$                 | $2 \times 10^8 M^{-1} s^{-1}$      |

Referring to the consumption of S(IV) which is shown in Figure 5-11A sulfite ions are oxidized to S(VI) very quickly especially in oxygen saturated solution. The reason for decline of S(IV) amount under anoxic conditions is due to the formation of  $SO_3^{\bullet-}$  (equilibria 1 and 2 in Table 5-3). Under oxic conditions, rapid increase in S(IV) oxidation within several minutes may be explained by rapid formation of  $FeSO_3^+$  [14, 30]. In figure 5-11B, it is possible to follow the formation of Fe(II) in solution during AN oxidation. Only in absence of oxygen ( $N_2$  purged solutions) Fe(II) concentration rapidly increases up to 36.6  $\mu M$  after 5 min corresponding to the complete consumption of S(IV) (see figure. 5-11A). In aerated and  $O_2$  saturated solutions, slight formation of Fe(II) can be determine after first 2 min followed by its disappearance due to the fast oxidation into Fe(III). Despite no significant variations of pH when  $N_2$  is bubbled in the solution, when air or oxygen is used, the aniline could be oxidized quickly in a period of short time.

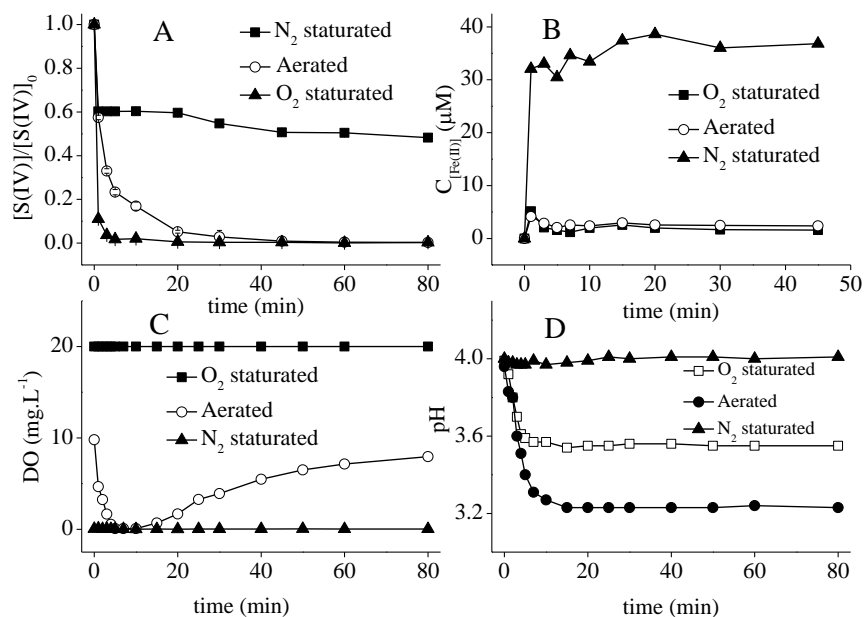
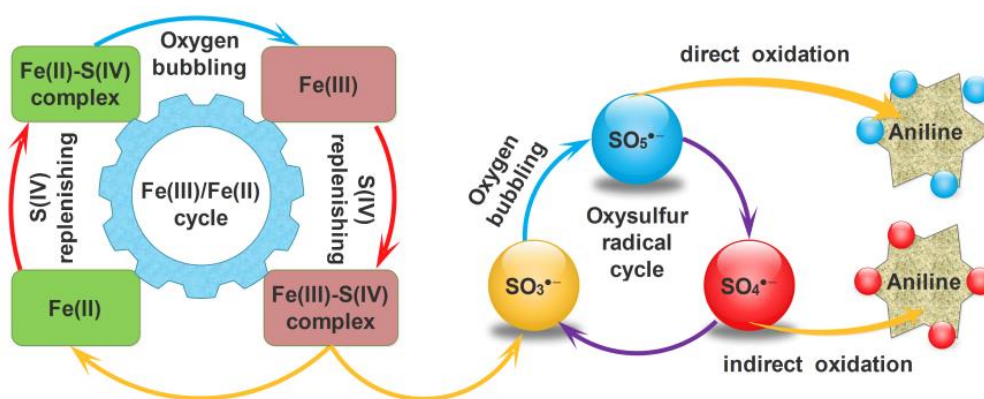


**Figure. 5-11.** Variation of S(IV) (A), Fe(II) (B), [O<sub>2</sub>] (C), and pH (D) during oxidation of AN in Fe(III)-S(IV) system. Conditions are: [AN]<sub>0</sub> = 10 μM, [Fe(III)]<sub>0</sub> = 0.1 mM, [S(IV)]<sub>0</sub> = 1.0 mM, pH = 4.0.

Figure. 5-11C shows that oxygen concentration sharply declined in the first 10 min before to slightly reach again stable concentration of 8 mg L<sup>-1</sup>. This trend can be explained considering the fast reactivity with SO<sub>3</sub><sup>•-</sup> leading to the formation of SO<sub>5</sub><sup>•-</sup> (see Table 5-3), which would increase the efficiency of oxidation. In the latter stage of the reaction, sulfite consumption and spontaneous re-oxygenation may explain the slow increase in oxygen content. The pH also changes in the presence of oxygen (Figure 5-11D). H<sup>+</sup> is mainly generated through reaction between SO<sub>4</sub><sup>•-</sup> and HSO<sub>3</sub><sup>-</sup> (Accordingly to reaction 9-10 in Table 5-3). In saturated oxygen solutions, the reason of higher pH drop was due to the oxysulfur radical cycle acceleration and then enhancement of Fe(III)-S(IV) cycle. On the basis of all the results above, the mechanism of integrated process of this Fe(III)-sulfite system can be shown in Scheme 5-1.



**Scheme. 5-1.** Major reactions of aniline in the Fe(III)–S(IV) system in the presence or absence of oxygen. The cycles of Fe(III)/Fe(II) and oxysulfur radicals ( $\text{SO}_3^{\cdot-}$ ,  $\text{SO}_5^{\cdot-}$ , and  $\text{SO}_4^{\cdot-}$ ) are connected with the disassociation reaction of Fe(III)-S(IV) complex. Oxygen may promote these two cycles simultaneously under the proper conditions.

### 5.3.5 Catalytically cycle investigation

Sequential experiment are conducted with fixed concentration of Fe(III) ( $0.1 \text{ mmol.L}^{-1}$ ) and multiple addition of  $\text{SO}_3^{2-}$ , at pH 4.0 in order to check the effect of  $\text{SO}_3^{2-}$  on catalytical degradation of high AN concentrated solutions. In this experiment, the concentration of aniline is  $100 \text{ }\mu\text{M}$ , and  $1.0 \text{ mM S(IV)}$  is added to the solution at the beginning and then  $1.0 \text{ mM S(IV)}$  are spiked every 20 min, The results are displayed in Figure. 5-12 indicating that multiple additions of sulfite can nearly completely degrade the AN after 140 min of reaction (>90% degradation efficiency). However, it is important to mentioned that the high concentration of S(IV) cannot improve the degradation of AN. In fact, when  $7 \text{ mM S(IV)}$  (corresponding to 7 times  $1 \text{ mM}$ ) were added to the solution in one step, the reaction is strongly inhibited. In fact, an increase in S(IV) dosage is not always able to enhance organic contaminants oxidation. On the contrary, excessively high S(IV) concentrations retards the subsequent reaction as it is observed in Figure 2A and in different references [17, 31]. This results is in agreement with previously reported works on high  $[\text{M(n)}]/[\text{S(IV)}]$  and low  $[\text{S(IV)}]/[\text{O}_2]$  ratios (M(n): heavy-metal ion) [32, 33]. Otherwise, the system tends to predominantly undergo reduction. However, as the source of generating oxysulfur radicals, an appropriate concentration of S(IV) can increase the oxidation reaction.

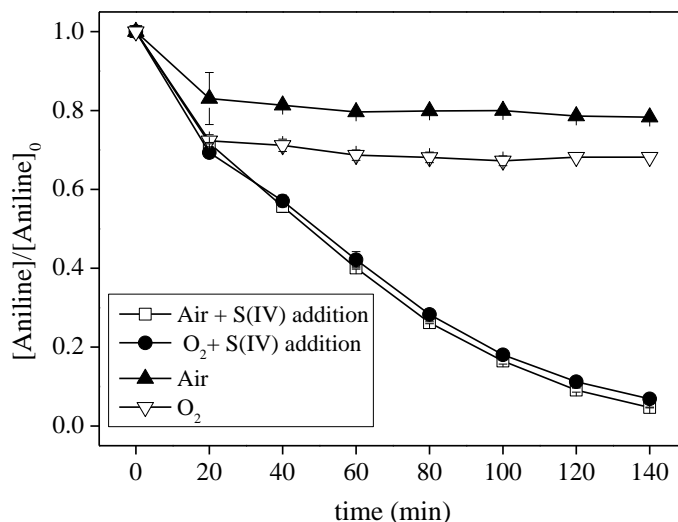


**Figure. 5-12.** AN 100  $\mu\text{M}$  degradation during oxidation in Fe(III)-S(IV) with sequential addition of S(IV) each 20 min under oxygen and air bubbling at pH 4. Conditions are  $[\text{Fe(III)}]_0 = 0.1 \text{ mM}$ ,  $[\text{S(IV)}]_0 = 1.0 \text{ mM}$ .

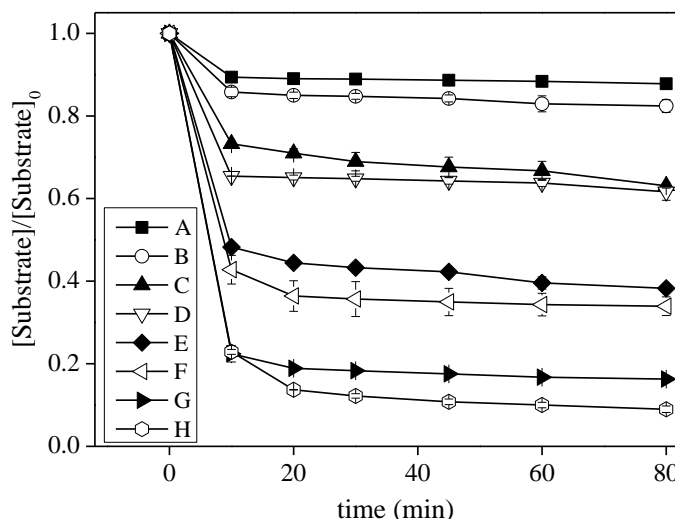


**Figure. 5-13.** The degradation efficiency of various kinds of organic pollutants used in Fe(III)-S(IV) system. Conditions:  $[\text{substrate}]_0 = 10 \mu\text{M}$ ,  $[\text{Fe(III)}]_0 = 0.1 \text{ mM}$ ,  $[\text{S(IV)}]_0 = 1.0 \text{ mM}$ ,  $\text{pH}_{\text{ini}} = 4.0$ . In the figure, A: o-Nitroaniline, B: p-Nitroaniline, C: p-aminophenol, D: Sulfonamides, E: Phenol, F: NN-dimethylaniline, G: p-Chloroaniline, H: Paracetamol.

To further verify the application of this Fe(III)-S(IV) system, the experiments of degrading various aromatic amines, such as o-Nitroaniline, p-Nitroaniline, Sulfonamides and their substituted analogs within 80 min also were conducted at specific Fe(III)/S(IV) molar ratios (0.1: 1 mM) at initial substrates concentration of  $10 \mu\text{M}$  and at pH 4.0. After 80 min reaction, all the pollutants selected in this study underwent different degree of degradation which can

be seen from Figure 5-13. As identified above, the application of this system was reasonably proved.

## 5.4 Conclusions

This work shows that the high efficiency in AN decontamination has been achieved in this Fe(III)-S(IV) system under specific conditions. Consequently, oxysulfur radicals including  $\text{SO}_4^{\bullet-}$  and  $\text{SO}_5^{\bullet-}$  are the dominant oxidants which are mainly responsible for aniline degradation. Furthermore, in aniline oxidization,  $\text{SO}_5^{\bullet-}$  also played a relatively important role. Its contribution takes a considerable part (~ 60%) of all radical species. Additionally, the rate constant  $k_{AN,SO_4^{\bullet-}}$  and  $k_{AN,SO_5^{\bullet-}}$  are estimated to be  $(7.7 \pm 0.5) \times 10^9 \text{ M}^{-1}\text{s}^{-1}$  and  $(5.8 \pm 0.6) \times 10^6 \text{ M}^{-1} \text{ s}^{-1}$ , respectively. When the experiments conducted with different level of oxygen in solution, it shows that dissolved oxygen plays a significant role in radicals generating. This work, not only provides a feasible candidate for use in the efficient oxidation of aromatic amines, but also highlights a novel concept that the role of  $\text{SO}_5^{\bullet-}$  cannot be neglected in the future studies.

## References

- [1] Ahmad M, Teel A L, Watts R J. Mechanism of Persulfate Activation by Phenols [J]. Environmental Science & Technology, 2013, 47(11): 5864-5871.
- [2] Anipsitakis G P, Dionysiou D D. Degradation of organic contaminants in water with sulfate radicals generated by the conjunction of peroxymonosulfate with cobalt [J]. Environmental Science & Technology, 2017, 37(20): 4790-4797.
- [3] Anipsitakis G P, Tufano T P, Dionysiou D D. Chemical and microbial decontamination of pool water using activated potassium peroxymonosulfate [J]. Water Research, 2008, 42(12): 2899-2910.
- [4] Ghauch A, Tuqan A M, Kibbi N. Naproxen abatement by thermally activated persulfate in aqueous systems [J]. Chemical Engineering Journal, 2015, 279: 861-873.
- [5] Zeng T, Zhang X, Wang S, et al. Spatial confinement of a  $\text{Co}_3\text{O}_4$  catalyst in hollow metal-organic frameworks as a nanoreactor for improved degradation of organic pollutants [J]. Environmental Science & Technology, 2015, 49(4): 2350-2357.
- [6] Anipsitakis G P, Dionysiou D D, Gonzalez M A. Cobalt-mediated activation of

- peroxymonosulfate and sulfate radical attack on phenolic compounds. implications of chloride ions [J]. *Environmental Science & Technology*, 2006, 40(3): 1000-1007.
- [7] Feng Y, Wu D, Deng Y, et al. Sulfate radical-mediated degradation of sulfadiazine by CuFeO<sub>2</sub> rhombohedral crystal-catalyzed peroxymonosulfate: synergistic effects and mechanisms [J]. *Environmental Science & Technology*, 2016, 50(6): 3119-3127.
- [8] Guo H, Gao N, Yang Y, et al. Kinetics and Transformation Pathways on Oxidation of Fluoroquinolones with Thermally Activated Persulfate [J]. *Chemical Engineering Journal*, 2016, 292: 82-91.
- [9] Liang C, Su H W. Identification of sulfate and hydroxyl radicals in thermally activated persulfate [J]. *Industrial & Engineering Chemistry Research*, 2009, 48(11): 5558-5562.
- [10] Matzek L W, Carter K E. Activated persulfate for organic chemical degradation: A review [J]. *Chemosphere*, 2016, 151: 178-188.
- [11] Qi C, Liu X, Ma J, et al. Activation of peroxymonosulfate by base: Implications for the degradation of organic pollutants [J]. *Chemosphere*, 2016, 151: 280-288.
- [12] Zhang B T, Zhao L, Lin J M. Determination of folic acid by chemiluminescence based on peroxomonosulfate-cobalt(II) system [J]. *Talanta*, 2008, 74(5): 1154-1159.
- [13] Zhang T, Zhu H, Croué J P. Production of sulfate radical from peroxymonosulfate induced by a magnetically separable CuFe<sub>2</sub>O<sub>4</sub> spinel in water: efficiency, stability, and mechanism [J]. *Environmental Science & Technology*, 2013, 47(6): 2784-2791
- [14] Zhang Y, Zhou J, Li C, et al. Reaction Kinetics and Mechanism of Iron(II)-Induced Catalytic Oxidation of Sulfur(IV) during Wet Desulfurization [J]. *Industrial & Engineering Chemistry Research*, 2012, 51(3): 1158-1165.
- [15] Contreras E M. Stoichiometry of Sulfite Oxidation by Oxygen during the Determination of the Volumetric Mass Transfer Coefficient [J]. *Industrial & Engineering Chemistry Research*, 2008, 47(23): 9709-9714.
- [16] Hu P, Long M. Cobalt-catalyzed sulfate radical-based advanced oxidation: A review on heterogeneous catalysts and applications [J]. *Applied Catalysis B Environmental*, 2016, 181: 103-117.
- [17] Long C, Peng X, Liu J, et al. Decolorization of Orange II in Aqueous Solution by an Fe(II)/sulfite System: Replacement of Persulfate [J]. *Industrial & Engineering Chemistry Research*, 2016,

- 51(42): 13632-13638.
- [18] Shi W, Cheng Q, Zhang P, et al. Catalytic decolorization of methyl orange by the rectorite-sulfite system [J]. *Catalysis Communications*, 2014, 56(56): 32-35.
- [19] Zhou D, Chen L, Zhang C, et al. A novel photochemical system of ferrous sulfite complex: kinetics and mechanisms of rapid decolorization of Acid Orange 7 in aqueous solutions [J]. *Water Research*, 2014, 57(5): 87-95.
- [20] Yuan Y, Yang S, Zhou D, et al. A simple Cr(VI)–S(IV)–O<sub>2</sub> system for rapid and simultaneous reduction of Cr(VI) and oxidative degradation of organic pollutants [J]. *Journal of Hazardous Materials*, 2016, 307: 294-301.
- [21] Xu J, Ding W, Wu F, et al. Rapid catalytic oxidation of arsenite to arsenate in an iron(III)/sulfite system under visible light [J]. *Applied Catalysis B Environmental*, 2016, 186: 56-61.
- [22] Jiang B, Liu Y, Zheng J, et al. Synergetic Transformations of Multiple Pollutants Driven by Cr(VI)-Sulfite Reactions [J]. *Environmental Science & Technology*, 2014, 49(20): 12363-12371..
- [23] Huie R E, Neta P. One-electron redox reactions in aqueous solutions of sulfite with hydroquinone and other hydroxyphenols [J]. *Journal of Physical Chemistry*, 1985, 89(18): 3918-3921.
- [24] Brandt C, Fabian I, Eldik R V. Kinetics and mechanism of the Iron(III)-catalyzed autoxidation of sulfur(IV) oxides in aqueous solution. evidence for the redox cycling of iron in the presence of oxygen and modeling of the overall reaction mechanism [J]. *Inorganic Chemistry*, 1994, 33(4): 687-701.
- [25] Tamura H, Goto K, Yotsuyanagi T, et al. Tamura H, Goto K, Yotsuynagi T, Nagayama M. Spectrophotometric determination of iron(II) with 1,10-phenanthroline in the presence of large amounts of iron(III) [J]. *Talanta* 21: 314-318.
- [26] Lee Y J, Rochelle G T. Oxidative degradation of organic acid conjugated with sulfite oxidation in flue gas desulfurization: products, kinetics, and mechanism [J]. *Environmental Science & Technology*, 1987, 21(3): 266-272.
- [27] Yuan Y, Zhao D, Li J, et al. Rapid oxidation of paracetamol by cobalt(II) catalyzed sulfite at alkaline pH [J]. *Catalysis Today*, 2017.
- [28] Zhou D, Yuan Y, Yang S, et al. Roles of oxysulfur radicals in the oxidation of acid orange 7 in the Fe(III)-sulfite system [J]. *Sulfur Reports*, 2015, 36(4): 373-384.
- [29] Restelli G, Angeletti G. *Physico-Chemical Behaviour of Atmospheric Pollutants: Air Pollution*

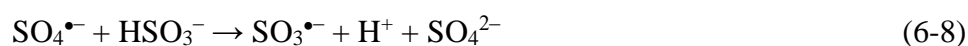
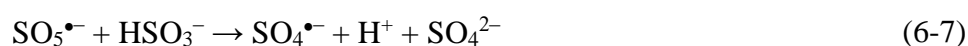
- Research Reports [M]. 1990.
- [30] Grgić I, Poznič M, Bizjak M. S(IV) Autoxidation in atmospheric liquid water: the role of Fe(II) and the effect of oxalate [J]. *Journal of Atmospheric Chemistry*, 1999, 33(1): 89-102.
- [31] Zhang L, Chen L, Xiao M, et al. Enhanced decolorization of orange II solutions by the Fe(II)–sulfite system under xenon lamp irradiation [J]. *Industrial & Engineering Chemistry Research*, 2013, 52(30): 10089-10094.
- [32] Carvalho L B, Alipazaga M V, Crivelente W C T, Coichev N. The autoxidation of Co(II)/2-Amino-2-Hydroxymethyl-1,3-Propanediol in the presence of Mn(II) and S(IV) [J]. *Bioinorganic Reaction Mechanisms*, 2004, 5(2): 101-108.
- [33] Kuo D T F, Kirk D W, Jia C Q. The chemistry of aqueous S(IV)-Fe-O<sub>2</sub> system: state of the art [J]. *Journal of Sulfur Chemistry*, 2006, 27(27): 461-530.
- [34] Dogliotti L, Hayon E. Flash photolysis of per[oxydi]sulfate ions in aqueous solutions. The sulfate and ozonide radical anions [J]. *Journal of Physical Chemistry*, 1967, 71(8). 2511-2516.
- [35] Clifton C L, Huie R E. Rate constants for hydrogen abstraction reactions of the sulfate radical, SO<sub>4</sub><sup>-</sup>. Alcohols [J]. *International Journal of Chemical Kinetics*, 1989, 21(8): 677–687.
- [36] Hayon E, Treinin A, Wilf J. Electronic spectra, photochemistry, and autoxidation mechanism of the sulfite-bisulfite-pyrosulfite systems. SO<sub>2</sub><sup>-</sup>, SO<sub>3</sub><sup>-</sup>, SO<sub>4</sub><sup>-</sup>, and SO<sub>5</sub><sup>-</sup> radicals [J]. *Journal of the American Chemical Society*, 1972, 94(1): 47-57.
- [37] Buxton G V, Greenstock C L, Helman W P, et al. Critical review of rate constants for reactions of hydrated electrons chemical kinetic data base for combustion chemistry. Part 3: propane [J]. *Journal of Physical & Chemical Reference Data*, 1988, 17(2): 513-886.
- [38] Naik D B, Moorthy P N. Studies on the transient species formed in the pulse radiolysis of benzotriazole [J]. *Radiation Physics & Chemistry*, 1995, 46(46): 353-357.
- [39] Neta P, Huie R E. One-electron redox reactions involving sulfite ions and aromatic amines [J]. *Journal of Physical Chemistry*, 1985, 89(9): 1783-1787.

## **Chapter 6 Enhanced degradation of paracetamol by the Fe(III)-sulfite system under UV irradiation**

## 6.1 Introduction

We already reported the system utilizing Fe(III)-sulfite for degradation of aniline and some other kinds organic compounds in acidic environment in Chapter 5, the main reactions involved in this system are described by reactions 6-1 to 6-10 [1-6]. Although rapid degradation of aniline is achieved, the optimum initial pH for the reaction is about 4.0, and the degradation efficiency is less than 10% at the initial pH 7.0. So An important point of interest is how to enhance the efficiency of the Fe(III)-sulfite system at near-neutral pH. We addressed this problem by exploiting the photochemical activity of ferric iron complexes under UV-vis irradiation [7-8]. The most well-known Fenton system (Fe(II)/H<sub>2</sub>O<sub>2</sub>), when exposed to UV-vis is strongly enhanced.

Moreover, the photochemical reduction of ferric species leads to a cycle between Fe(III) and Fe(II) species, and minimizes the precipitation of ferric hydroxide by a large percentage [9-10].



In this study, a detailed discussion on the degradation of paracetamol (PARA), which is chosen to be the organic substrate, in the Fe(III)-sulfite system at near-neutral pH by UV-vis irradiation is reported, and the difference between pH 4.0 and 7.0 with or without UV-vis is also checked to identified and optimized the mechanism for different systems. The effects of initial pH, the Fe(III)/S(IV) molar ratio, oxygen content, buffer are investigated to determine

the optimum conditions of the novel photochemical system, and the radical scavengers experiments are conducted to determine the predominant oxidant in such systems.

## 6.2 Material and methods

### 6.2.1 Chemicals.

Iron(III) perchlorate hydrate ( $\text{Fe}(\text{ClO}_4)_3 \times \text{H}_2\text{O}$ ), potassium dichromate ( $\text{K}_2\text{Cr}_2\text{O}_7$ ), Cobalt(II) sulfate ( $\text{CoSO}_4 \cdot 7\text{H}_2\text{O}$ ), Copper(II) sulfate ( $\text{CuSO}_4 \cdot 5\text{H}_2\text{O}$ ), paracetamol (PARA), 5,5-Dimethyl-1-pyrroline N-oxide (DMPO), Sulfite Sodium ( $\text{Na}_2\text{SO}_3$ ) are obtained from Sigma, France. Tert-butyl alcohol (TBA) and ethanol (EtOH) are used as scavengers to quench the relevant radicals, PIPES (piperazine-N,N'-bis(2-ethanesulfonic acid)) is used to be the buffer to keep the pH value of the solution at 6.7-7.0. NaOH and  $\text{HClO}_4$  purchased from Sigma-Aldrich, France, are used to adjust the pH of the solution. Ferrozine (3-(2-Pyridyl)-5,6-diphenyl-1,2,4-triazine-p,p'-disulfonic acid monosodium salt hydrate) and ascorbic acid purchased from Sigma-Aldrich, France, are used to determine the concentration of Fe(II) and Fe(III). Methanol is HPLC grade and purchased from Fluka. All chemicals were used without further purification. Ultrapure water with 18.2 M $\Omega$  cm resistivity used in this work is obtained through a water purification system.

### 6.2.2 Experimental setup

Batch experiments are conducted in a 200 mL open cylindrical reactor held at a constant temperature of 20°C by circulating thermostatically controlled water through an outer jacketed in the dark or under irradiation with a xenon lamp ( $\lambda_{\text{max}} = 365 \text{ nm}$ ), and the emission spectrum is shown in Figure 6-1. Predetermined amounts of PARA and Fe(III) are diluted in a 100 mL flask and transferred to a reactor after complete mixing, and the pH is adjusted by adding NaOH or  $\text{HClO}_4$  concentrated solutions to slightly lower than the desired value. Then  $\text{Na}_2\text{SO}_3$  solution (which pH was already adjusted according to the reactions) is added to this reaction solution to reach the desired pH value, and then the lamp is switched on. At specified time intervals, a certain amount of the solution sample is collected for analysis. Solutions are continuously bubbled with pure  $\text{O}_2$  (99.99%) to keep an aerobic environment. In  $\text{N}_2$  purging experiments, the top of the cylinder reactor was sealed with a rubber stopper. Purging of

solutions with high-purity N<sub>2</sub> (99.99%) is performed with bubbling for 30 min before reactions and is continued during reactions to ensure that oxygen is excluded.

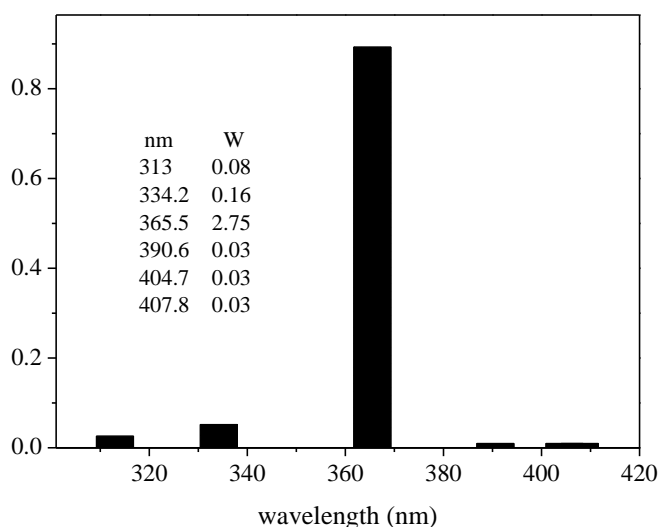


**Figure. 6-1.** Emission spectrum of Xenon lamp

Fe(II) and Fe(III) concentrations are determined by complexation with Ferrozine [11]. Firstly, Fe(II) is determined measuring the absorption at 562 nm of the solution obtained by mixing 1 mL of sample, 4 mL of water and 500 $\mu$ L of Ferrozine 20mM. As shown in eqs 6-1, the molar absorption coefficient of the complex at 562 nm is 27900 M<sup>-1</sup>cm<sup>-1</sup>.

$$\text{Fe(II)} = \frac{A_{\text{sample}} - A_{\text{blank}}}{\epsilon_{562} \times l} \times \frac{V_{\text{tot}}}{V_{\text{sample}}} \quad \text{eqs 6-1}$$

To determine Fe(III) concentration it is necessary to reduce it to Fe(II) : 0.5 M of ascorbic acid stock solution is used for the reduction. 1 mL sample and 4 mL water were mixed with 600  $\mu$ L of the ascorbic acid, and after 20 min 500  $\mu$ L of Ferrozine are added to the solution. Fe(III) is determined by the eqs 6-2. No buffer is used because the complex between Ferrozine and Fe(II) is stable between pH 4 and 7.

$$\text{Fe(III)} = \frac{A_{\text{sample}} - A_{\text{blank}}}{\epsilon_{562} \times l} \times \frac{V_{\text{tot}}}{V_{\text{sample}}} - \text{Fe(II)} \quad \text{eqs 6-2}$$

Where  $A_{\text{sample}}$  and  $A_{\text{blank}}$  are the sample and blank adsorption, respectively,  $\epsilon_{562}$  is the molar extinction coefficient,  $l$  is the optic path length,  $V_{\text{tot}}$  is the total volume and  $V_{\text{sample}}$  is the sample volume (1 mL).

### 6.2.3 Analytical methods

The concentration of PARA is determined using a high-performance liquid chromatography

(HPLC) Shimadzu LC-10A system equipped with UV-vis detector (SPD-10AV; Shimadzu) and an ODS-C18 column (25 cm × 4.6 mm, 5 μm; Shimadzu, Kyoto, Japan). The separation is carried out using methanol:water (25:75 v/v) as isocratic mobile phase at a flow rate of 1.0 mL min<sup>-1</sup>. The detector is set at 241 nm maximum of absorption of PARA in aqueous solution.

The calibration of Fe(II) is shown in Figure 6-2A, and for Fe(III) is shown in Figure 6-2B.

$$[\text{Fe(II)}] (\mu\text{M}) = 35.84 \times \text{Abs}_{562\text{nm}} - 0.15 \quad (R^2 = 1)$$

$$[\text{Fe(III)}] (\mu\text{M}) = 35.84 \times \text{Abs}_{562\text{nm}} - 1.05 \quad (R^2 = 1)$$

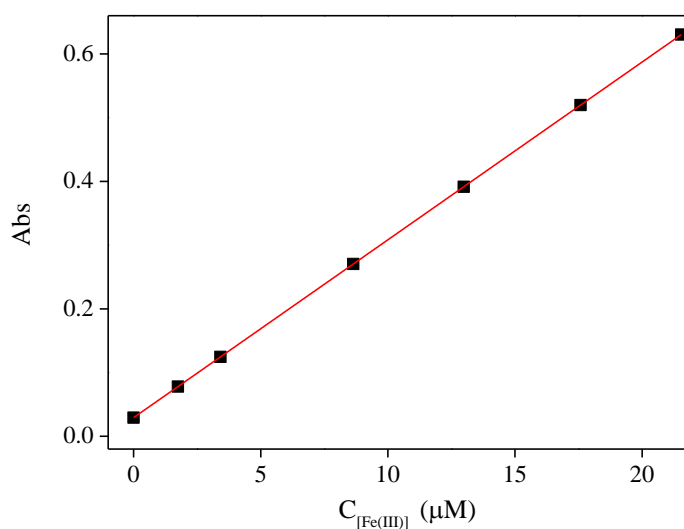
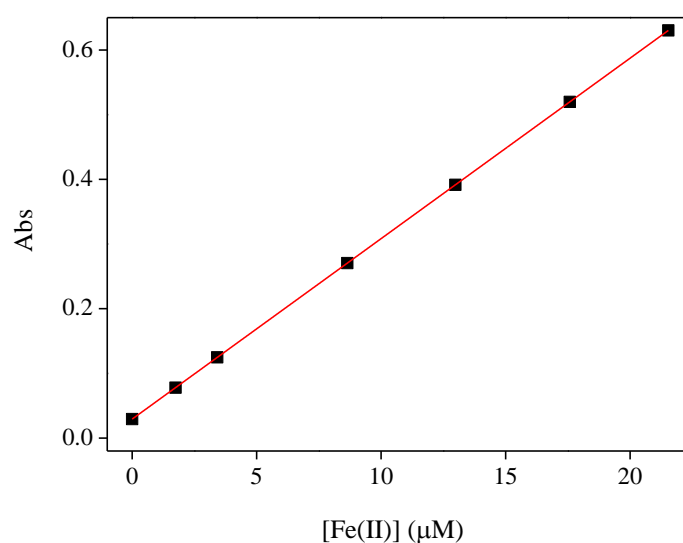


**Figure. 6-2.** Calibration curves of (A) Fe(II); (B) Fe(III) at 562 nm

## 6.3 Results and discussion

### 6.3.1 Control experiments

To evaluate the performance of the Fe(III)-S(IV)-O<sub>2</sub>-h $\nu$  system, PARA is selected to be the model pollutant, and its degradation in aqueous solution at near-neutral pH is investigated. Figure 6-3 compares the extents of PARA degradation under the different conditions. UV, UV-S(IV), UV-Fe(III), Fe(III)+S(IV) at pH 7.0 could not substantively lead to PARA degradation. As no photochemical degradation of PARA is observed in the absence of sulfite ions indicates that the reaction between Fe(III) ions and oxygen under irradiation to produce reactive oxygen species do not contribute to the degradation of PARA at near-neutral pH. Hence, the enhancement by irradiation has no effect on the photochemical reaction of free Fe(III) ions at near-neutral pH. Only UV-Fe(III)-S(IV) at pH 7.0 is capable to degrade PARA. When the reaction is occurred under irradiation with 0.1 mM Fe(III) and 1.0 mM S(IV) in the solution, more than 60% of PARA are decomposed within 40 min in Fe(III)-S(IV)-O<sub>2</sub>-h $\nu$  system.

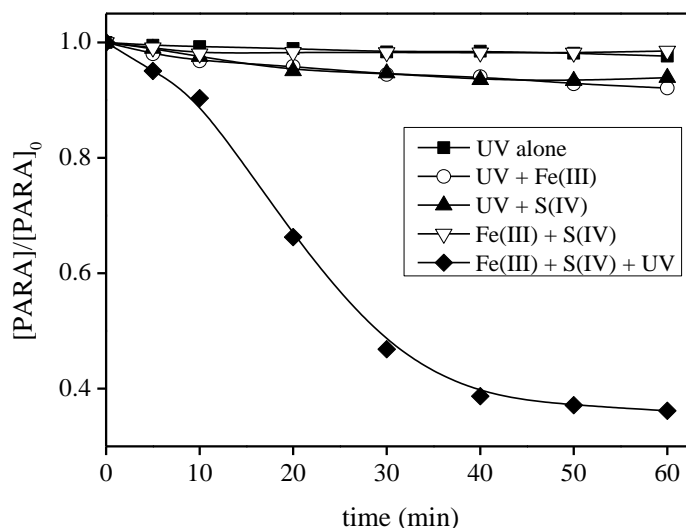


**Figure 6-3.** Degradation of PARA in the control experiments under various conditions in aerated solution. Condition:  $[\text{PARA}]_0 = 10 \mu\text{M}$ ,  $[\text{Fe(III)}]_0 = 0.1 \text{ mM}$ ,  $[\text{S(IV)}]_0 = 1.0 \text{ mM}$ ,  $\text{pH}_{\text{init}} = 7.0$ .

This phenomenon suggests that Fe(III)-S(IV) complex,  $\text{FeSO}_3^+$  could be formed first [6,7 12-13], then the  $\text{FeSO}_3^+$  complex might have undergone LMCT (ligand-to-metal charge transfer) [14] and  $\text{SO}_3^{\bullet-}$  could be generated as described in Zhang et al. report [7]. On the

other hand, when the change of pH is checked during the reaction, the result shown in Figure 6-4 indicates that when there is irradiation, pH will decrease to a great extent during the reaction. At the first stage of the reaction, pH decreases slightly, then after 10-20 min reaction, the pH decreases sharply. When comparing the trend of PARA degradation, it is found that the speed of degradation of PARA has the same trend with the pH decreasing. From the result above, it can be seen that irradiation can enhance the reaction at near-neutral pH in this Fe(III)-S(IV)-O<sub>2</sub>-h $\nu$  system due to the stronger decrease of pH until an acidic environment (pH = 3.5).

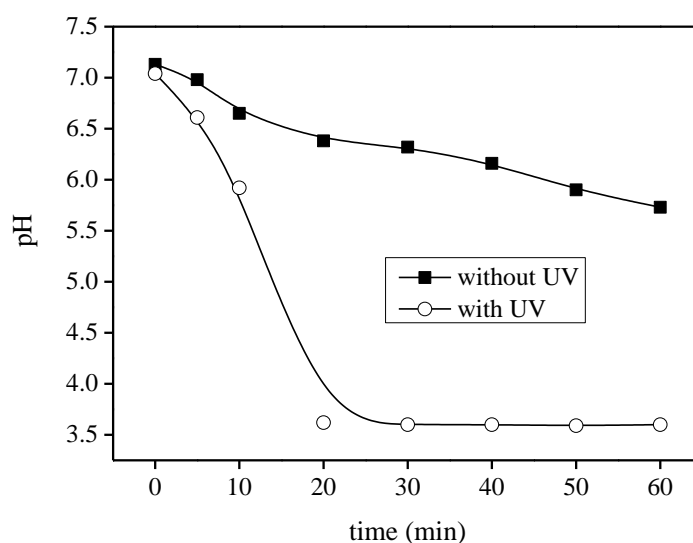


**Figure. 6-4.** Change of pH during the reaction under aerated solution. Condition: [PARA]<sub>0</sub> = 10  $\mu$ M, [Fe(III)]<sub>0</sub> = 0.1 mM, [S(IV)]<sub>0</sub> = 1.0 mM, pH<sub>init</sub> = 7.0.

### 6.3.2 Effect of pH on PARA degradation

To determine the effect of pH on PARA degradation, samples are analyzed at initial pH values of 4.0 to 9.0 with or without irradiation. Figure 6-5A shows that when there is no irradiation the efficiency of PARA degradation decreases with the increase of initial pH values. When the initial pH is at 6.0, the degradation efficiency of PARA is near just 39% after 60 min of reaction. And when the pH value of the solution is equal or higher to 7.0, there is nearly no PARA degradation. Corresponding experiments with irradiation are analyzed to verify the effect of illumination on PARA degradation in the same pH range between 4.0 to 9.0. As shown in Figure 6-5B, under irradiation even the efficiency of PARA degradation still decreases with the increase in pH values. However, the reaction can happen at pH 7.0, after 60

minutes of reaction, the degradation efficiency reached around 69%, and at pH 8.0 or even higher pH, there is still a little extent of PARA degradation. When we compare the efficiency of PARA degradation with or without irradiation, the reaction rate is very fast and could achieve completely the degradation at pH 4.0 with and in a lower extent without light. This result is consistent with earlier reports by our group of greatly enhanced rates of contaminants degradation for Fe(III)-S(IV) system [6,15-16]. The optimum initial pH of the Fe(III)-S(IV) system is pH 4.0. When the initial pH of the solution increases to 5.0, the initial reaction rate of PARA degradation under irradiation is much faster than without irradiation, but after 60 min of reaction, both of them could reach nearly the same degradation efficiency. This is due to the pH decrease which enhanced the reaction. However, when pH is higher than 6.0, the difference of PARA degradation with or without irradiation become much bigger. For example, at pH = 6.0, the degradation efficiencies are around 39% and 83% without and with irradiation, respectively. This result illustrates that the irradiation greatly enhanced the reaction. The reason can be explained by the pH decreasing to acidic values due to the irradiation. This phenomenon could reveal that photodegradation of organic compounds should be considered as one of the important pathway near-neutral pH environment.

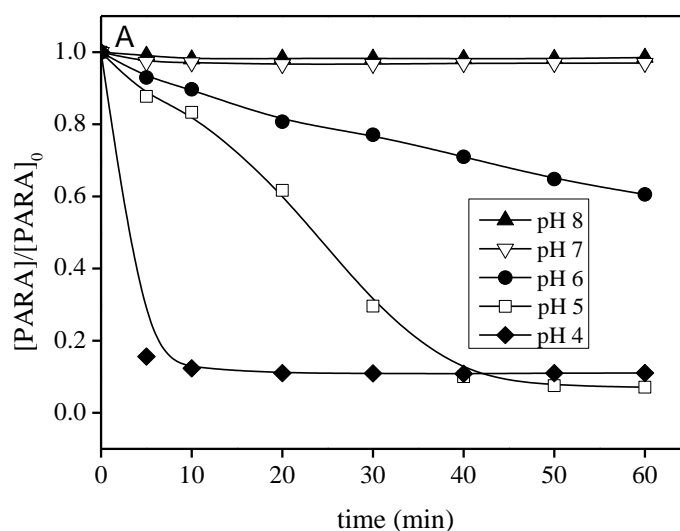


**Figure. 6-5A.** Effect of pH on PARA degradation without UV irradiation under aerated solution .

Condition:  $[\text{PARA}]_0 = 10 \mu\text{M}$ ,  $[\text{Fe(III)}]_0 = 0.1 \text{ mM}$ ,  $[\text{S(IV)}]_0 = 1.0 \text{ mM}$ .

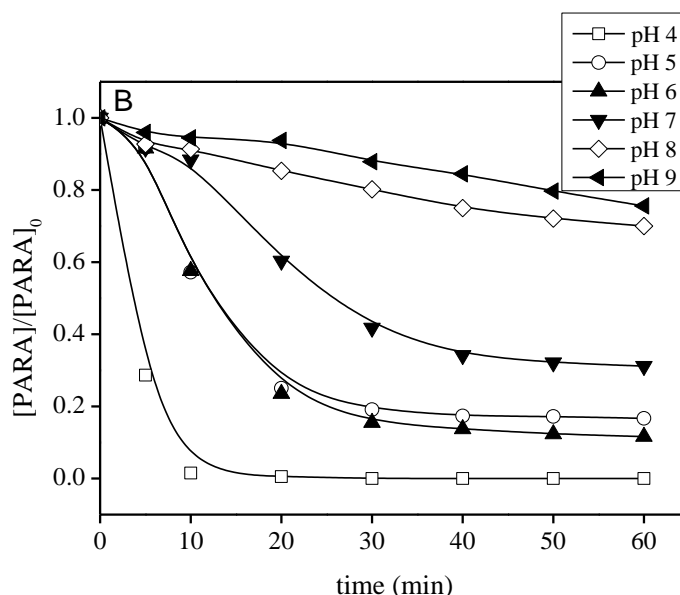


**Figure. 6-5B.** Effect of pH on PARA degradation with UV irradiation under aerated solution.

Condition:  $[\text{PARA}]_0 = 10 \mu\text{M}$ ,  $[\text{Fe(III)}]_0 = 0.1 \text{ mM}$ ,  $[\text{S(IV)}]_0 = 1.0 \text{ mM}$ .

### 6.3.3 Effect of the Fe(III)/S(IV) concentration on PARA degradation

The efficiency of PARA degradation at various Fe(III) or S(IV) concentration at initial PARA concentration of  $10 \mu\text{M}$  and at initial  $\text{pH} = 7.0$  is determined. Results in Figure 6-6A and 6B clearly show that the Fe(III) and S(IV) concentration greatly influenced the efficiency of PARA degradation. The efficiency of PARA degradation increases with the increase in S(IV) dosage under the same conditions (Figure 6-6A). When the concentrations of added S(IV) are 0.5, 1.0, 2.0, 3.0 and 4.0 mM with fixed 0.1 mM initial concentration of Fe(III), the efficiencies of PARA degradation after 60 min are 28.3%, 68.9%, 75.7%, 87.6% and 91.1% respectively. However, from our previous work [6, 17], at higher sulfite ions concentrations there is no more enhancement of organic compounds degradation due to the reactivity competition of  $\text{SO}_4^{\bullet-}/\text{SO}_5^{\bullet-}$  between contaminant and  $\text{SO}_3^{2-}$  (eqs 6-8). In our case, there is no observed inhibition with excess sulfite ions, indicating that photochemical reactions, with the consumption of sulfite, become more significant than the inhibition reactions by excess sulfite. Considering its potential for causing serious pollution, potential application, and feasibility of use in industrial processes or engineered systems, 1.0 mM is used as the S(IV) dosage when other individual effects are investigated.

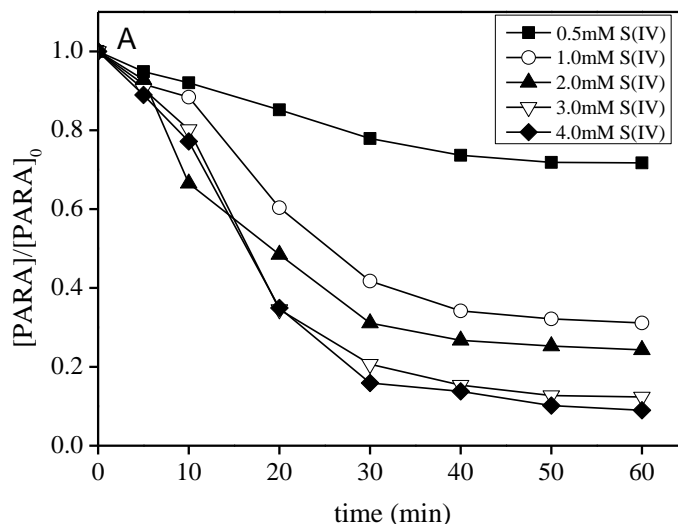


**Figure. 6-6A.** Effect of S(IV) concentration on PARA degradation with UV irradiation under aerated solution. Condition:  $[\text{PARA}]_0 = 10\mu\text{M}$ ,  $[\text{Fe(III)}]_0 = 0.1\text{ mM}$ ,  $\text{pH}_{\text{init}} = 7.0$ .

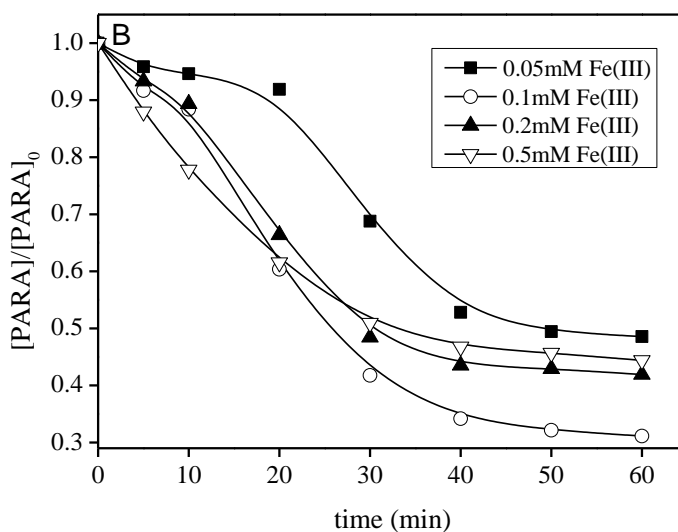


**Figure. 6-6B.** Effect of Fe(III) concentration on PARA degradation with UV irradiation under aerated solution. Condition:  $[\text{PARA}]_0 = 10\mu\text{M}$ ,  $[\text{S(IV)}]_0 = 1.0\text{ mM}$ ,  $\text{pH}_{\text{init}} = 7.0$ .

Batch experiments under irradiation with fixed initial concentration of S(IV) (1.0 mM) are conducted to investigate the effect of initial concentration of Fe(III) in the range of 0.05 to 0.5 mM. Figure 6-6B reveals that the increase of the Fe(III) concentration do not significantly improves the PARA disappearance., On the contrary, when Fe(III) concentration is higher

than 0.1 mM, there is an inhibition of PARA degradation. This negative effect is due to the high amount of  $\text{Fe}^{2+}$  generated in the iron cycle and its reaction with sulfate radicals. So these results show that to remove PARA from the aqueous solutions, a small amount of Fe(III) is quite sufficient to obtain good degradation efficiency. So, 0.1 mM of Fe(III) is added to the solution when other individual effects are investigated. One of the reasons explaining the slightly effect of Fe(III) concentration may be the fast recycle of Fe(II) and Fe(III) in the presence of a stoichiometry excess of S(IV) concentrations in aerated solution (eqs 6-1 to 6-2). Moreover, when the concentration of Fe(III) is monitored during the reaction, it is found that its concentration was nearly stable (Figure 6-7). Such results suggest that in the presence of enough sulfite in solution, the iron recycle could be achieved very fast leading to the generation of  $\text{SO}_3^{\bullet-}$  at the same time.

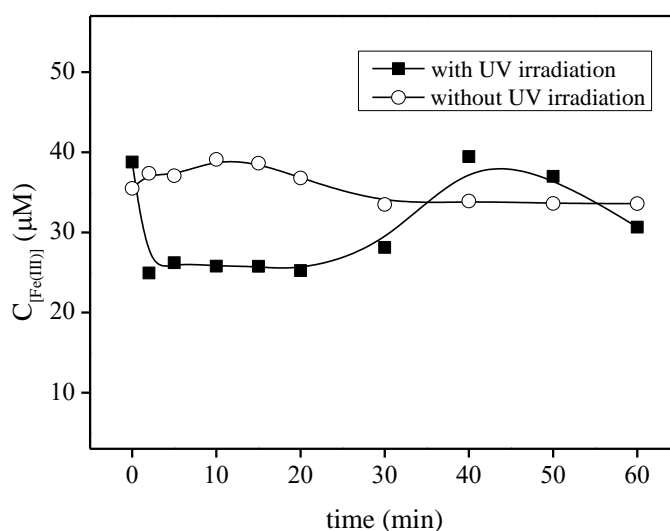


**Figure. 6-7.** Fe(III) concentration during the reaction under aerated solution. Condition:  $[\text{PARA}]_0 = 10 \mu\text{M}$ ,  $[\text{S(IV)}]_0 = 1.0 \text{ mM}$ ,  $[\text{Fe(III)}]_0 = 0.1 \text{ mM}$ ,  $\text{pH}_{\text{init}} = 7.0$ .

### 6.3.4 Effect of oxygen and buffer.

The effect of oxygen on PARA degradation is studied using 0.1 mM Fe(III) and 1.0 mM S(IV), 10  $\mu\text{M}$  PARA at both pH 4.0 and 7.0 with UV irradiation. As shown in Figure 6-8, in the deaerated solution, there is nearly no degradation at pH 7.0 and only 16% loss of PARA at pH 4.0 after 60 min of irradiation is observed. This percentage of PARA degradation is much

smaller than the 64% loss at pH 7.0 and complete degradation at pH 4.0 obtained in the aerated solution. This result indicated that oxygen is a very important parameter that affects the photodegradation of PARA in those Fe(III)-S(IV)-O<sub>2</sub>-h $\nu$  system at different pH. So oxygen takes part in the photochemical process in such a system. As oxygen plays its role by leading to the generation of SO<sub>4</sub><sup>•-</sup> and SO<sub>5</sub><sup>•-</sup> after reaction with SO<sub>3</sub><sup>•-</sup> in solution, so the phenomenon that there is still some PARA disappearance at pH 4.0 without oxygen can be explained by the fact that there is some hydroxyl radical (HO<sup>•</sup>) generated at pH 4.0 under irradiation [18-20].

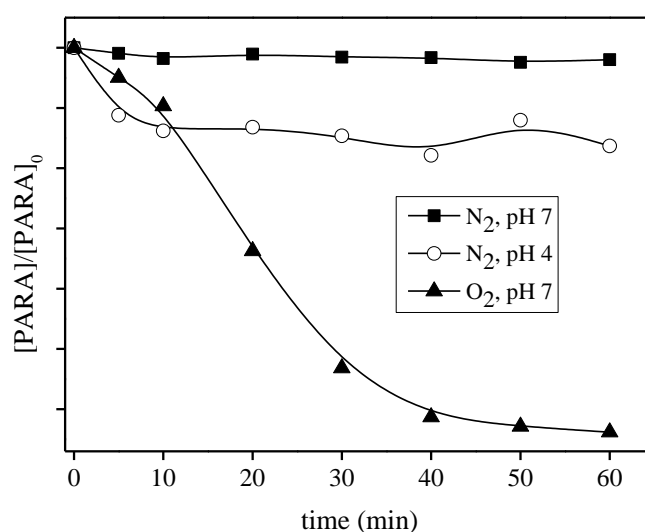


**Figure. 6-8.** Effect of oxygen on PARA degradation with UV irradiation. Condition:  $[PARA]_0 = 10 \mu\text{M}$ ,  $[S(IV)]_0 = 1.0 \text{ mM}$ ,  $[Fe(III)]_0 = 0.1 \text{ mM}$ .

When employed PIPES to be the buffer to keep pH constant at pH 6.7 to 7.0, the result shown in Figure 6-9 indicates that there is nearly no PARA degradation during the whole reaction. This result is in agreement with the section of pH effect, as the reaction depends heavily on the pH and irradiation can enhanced pH decrease until the reaction happen. However, when using the buffer to keep the pH stable, the system cannot have the appropriate conditions to perform the reaction.

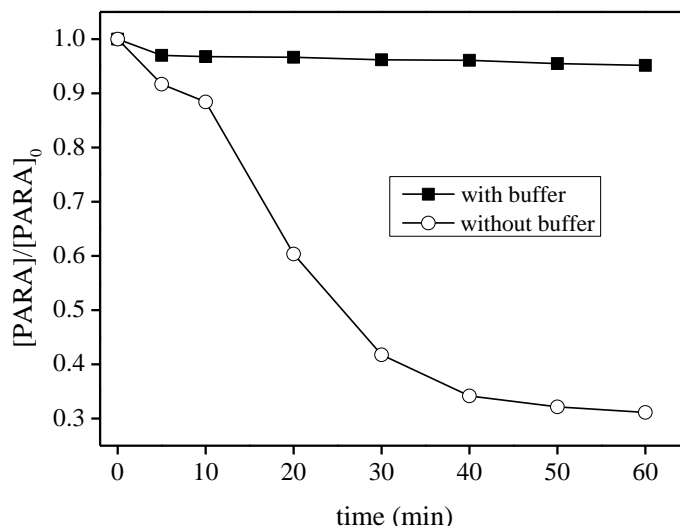


**Figure. 6-9.** Effect of buffer on PARA degradation with UV irradiation under aerated solution.

Condition:  $[\text{PARA}]_0 = 10 \mu\text{M}$ ,  $[\text{S(IV)}]_0 = 1.0 \text{ mM}$ ,  $[\text{Fe(III)}]_0 = 0.1 \text{ mM}$ ,  $\text{pH}_{\text{init}} = 7.0$

### 6.3.5 Effect of radical scavengers.

To evaluate the reaction mechanism of this system, The radical scavenger experiments are conducted at pH 7.0 with UV, pH 4.0 with UV, and pH 4.0 without UV with fixed concentration of 0.1 mM Fe(III) and 1.0 mM S(IV), 10  $\mu\text{M}$  PARA, using TBA and EtOH to identify the primary effective radicals. As the reaction rate constant of EtOH with  $\text{HO}^\bullet$  is about  $1.9 \times 10^9 \text{ M}^{-1} \text{ s}^{-1}$ , which is about 50-fold greater than with  $\text{SO}_4^{\bullet-}$ , which is around  $7.7 \times 10^7 \text{ M}^{-1} \text{ s}^{-1}$  and on the other hand, as  $k_{\text{TBA}, \text{HO}^\bullet} = 6.0 \times 10^8 \text{ M}^{-1} \text{ s}^{-1}$  [21] which is nearly three orders of magnitude higher than  $k_{\text{TBA}, \text{SO}_4^{\bullet-}} = 8.5 \times 10^5 \text{ M}^{-1}$ , hence on the basis of these properties, by using TBA and EtOH, different inhibitory effects can be observed on the PARA degradation.

When the experiment is conducted at pH 4.0 with irradiation, the results are shown in Figure 6-10A. 2.0 mM TBA added to the solution results in partial inhibition, and 50 mM EtOH almost completely inhibits PARA degradation. These results illustrate that PARA degradation at pH 4.0 under UV irradiation is due to  $\text{HO}^\bullet$  and  $\text{SO}_4^{\bullet-}$ . The generation of  $\text{HO}^\bullet$  could be divided into two pathways, one of them is due the reaction between  $\text{SO}_4^{\bullet-}$  and  $\text{H}_2\text{O}$  (eqs6-11) [22], and another pathway belongs to the photolysis of  $\text{FeOH}^{2+}$  in acidic environment (eqs

6-12 to 6-13) [12]. And the formation of  $\text{SO}_4^{\bullet-}$  come from decomposing  $\text{FeSO}_3^+$  complexes and the oxidation of  $\text{SO}_3^{\bullet-}$  radicals.



For the experiment performs at pH 4.0 in dark and keep other conditions the same, the result shows in Figure 6-10B illustrates that when TBA is added to the reaction solution, no significant inhibition of PARA degradation was observed suggests that  $\text{HO}^{\bullet}$  are not generated in this system.

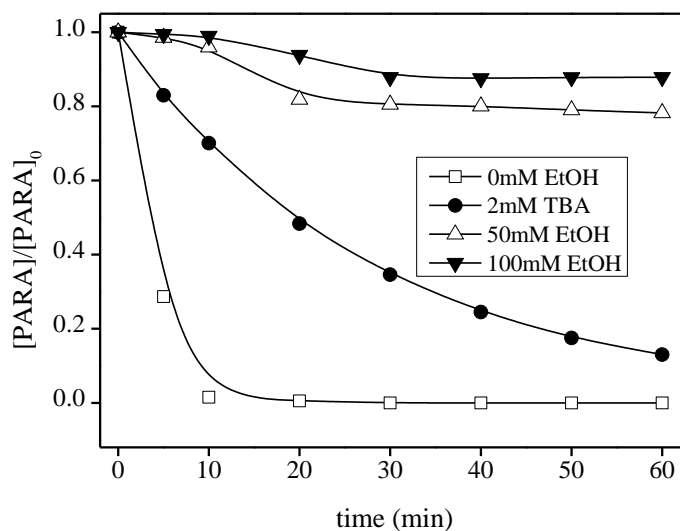


**Figure. 6-10A.** Effect of radical scavengers on PARA degradation with UV irradiation under aerated solution. Condition:  $[\text{PARA}]_0 = 10 \mu\text{M}$ ,  $[\text{S(IV)}]_0 = 1.0 \text{ mM}$ ,  $[\text{Fe(III)}]_0 = 0.1 \text{ mM}$ ,  $\text{pH}_{\text{ini}} = 4.0$ .

This fact excludes the hypothesis of  $\text{HO}^{\bullet}$  formation caused by the reaction between  $\text{SO}_4^{\bullet-}$  and  $\text{H}_2\text{O}$ . And when high concentration of EtOH (50 mM) added to the solution, the PARA degradation is nearly inhibited completely. This phenomenon validates that  $\text{SO}_4^{\bullet-}$  is the only

species of oxidant that leads to PARA degradation under this condition.

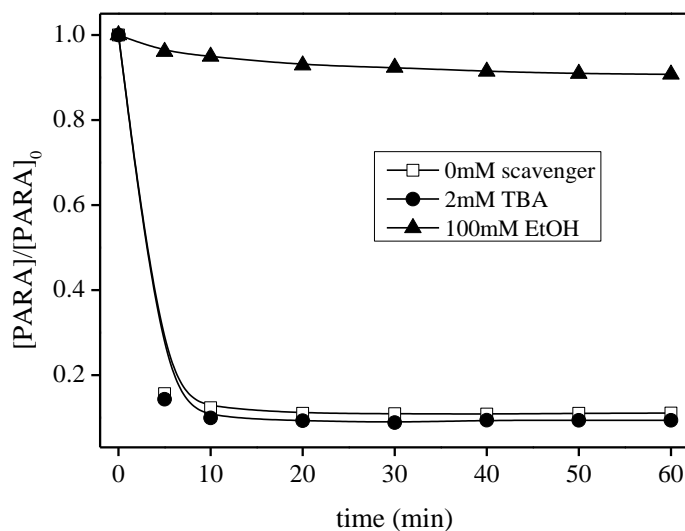


**Figure 6-10B.** Effect of radical scavengers on PARA degradation without UV irradiation under aerated solution. Condition:  $[\text{PARA}]_0 = 10 \mu\text{M}$ ,  $[\text{S(IV)}]_0 = 1.0 \text{ mM}$ ,  $[\text{Fe(III)}]_0 = 0.1 \text{ mM}$ ,  $\text{pH}_{\text{init}} = 4.0$ .

For the  $\text{Fe(III)-S(IV)-O}_2\text{-}h\nu$  system at pH 7.0, when EtOH is added to be the scavenger of  $\text{SO}_4^{\bullet-}$ , the results are shown in Figure 6-11A. Different concentration of EtOH has the same effect on PARA degradation, and the inhibition rate increases with the EtOH concentration increasing. When 50 mM EtOH are added in reaction solution, almost complete inhibition of PARA degradation is obtained. While in the presence of excess of TBA (Figure 6-11B), no inhibition of PARA degradation is observed, furthermore there is a slightly enhancement of PARA degradation in the presence of TBA. So in this case, it seems that there is no  $\text{HO}^\bullet$  generated in the system.

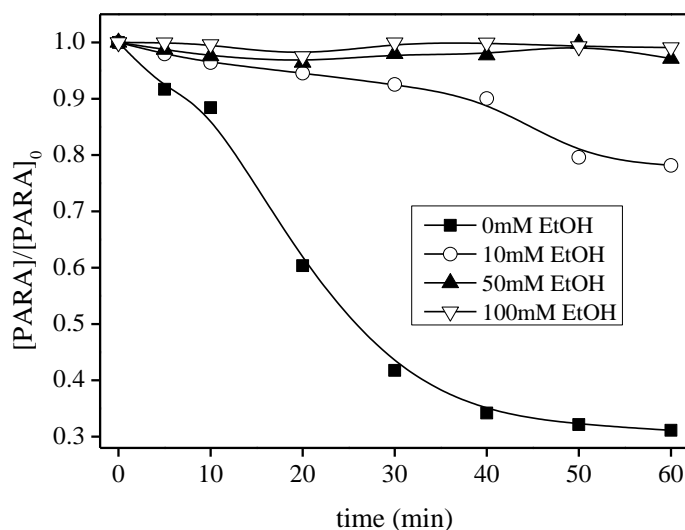


**Figure. 6-11A.** Effect of EtOH on PARA degradation with UV irradiation under aerated solution.

Condition:  $[\text{PARA}]_0 = 10 \mu\text{M}$ ,  $[\text{S(IV)}]_0 = 1.0 \text{ mM}$ ,  $[\text{Fe(III)}]_0 = 0.1 \text{ mM}$ ,  $\text{pH}_{\text{init}} = 7.0$ .

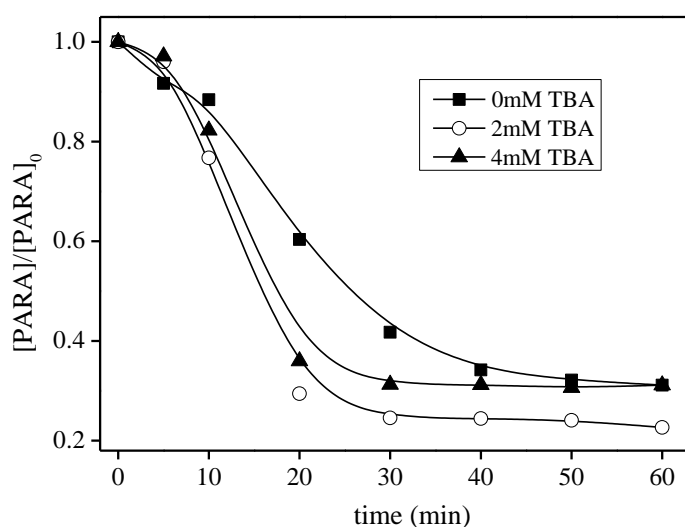


**Figure. 6-11B.** Effect of TBA on PARA degradation with UV irradiation under aerated solution.

Condition:  $[\text{PARA}]_0 = 10 \mu\text{M}$ ,  $[\text{S(IV)}]_0 = 1.0 \text{ mM}$ ,  $[\text{Fe(III)}]_0 = 0.1 \text{ mM}$ ,  $\text{pH}_{\text{init}} = 7.0$

To gain further evidence for the mechanism of  $\text{Fe(III)}\text{-S(IV)}\text{-O}_2\text{-}h\nu$  system, ESR spectra are recorded to identify radical intermediates formed during  $\text{Fe(III)}\text{-S(IV)}$  reactions using DMPO as a spin trap. And  $\text{SO}_4^{\bullet-}$  and  $\text{HO}^\bullet$  can be detected by measuring the signals of  $\text{DMPO-HO}^\bullet$  adducts and  $\text{DMPO-SO}_4^{\bullet-}$  adducts, respectively described in these references [23-24]. In control experiments ( $\text{Fe(III)}\text{-}h\nu$  system,  $\text{S(IV)}\text{-}h\nu$  system), there is no signal with the addition

of DMPO (results not shown). As a contrary, as shown in Figure 6-12 for the Fe(III) - S(IV) -  $h\nu$  system, the hyperfine coupling constants of measured spectra are consistent with those of DMPO/  $\text{SO}_3^{\bullet-}$  adducts, and no DMPO-OH adducts has been detected. The above phenomenon suggests that  $\text{HO}^\bullet$  is insignificant under this conditions, and  $\text{SO}_x^{\bullet-}$  (including  $\text{SO}_3^{\bullet-}$ ,  $\text{SO}_4^{\bullet-}$  and  $\text{SO}_5^{\bullet-}$ ) is the primary reactive oxidants responsible for PARA degradation. However, in the absence of DMPO and in the presence of oxygen,  $\text{SO}_3^{\bullet-}$  can be easily oxidized to  $\text{SO}_5^{\bullet-}$  (eq.6-5), thereby considerably mitigating the contribution of  $\text{SO}_3^{\bullet-}$  in our system. Combined with the results of radicals scavenger experiments, EtOH can inhibits completely the reaction, as EtOH has a negligible reactivity with  $\text{SO}_5^{\bullet-}$  ( $< 1 \times 10^3 \text{ M}^{-1} \text{ s}^{-1}$ ) [25], it could be concluded that in this Fe(III)-S(IV)- $\text{O}_2$ - $h\nu$  system,  $\text{SO}_4^{\bullet-}$  is the oxidants that mainly lead to the degradation of PARA.

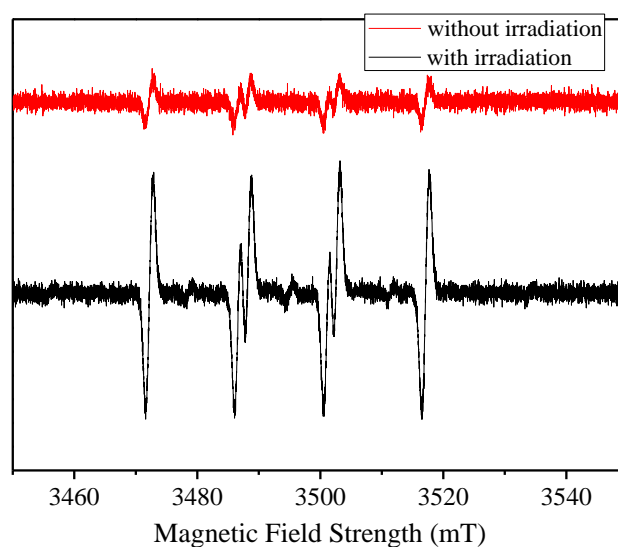
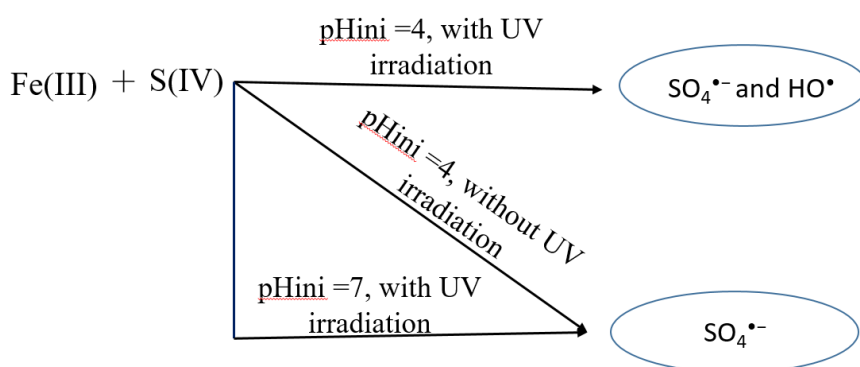


**Figure. 6-12.** ESR spectrum of reaction solution. Condition:  $[\text{S(IV)}]_0 = 1.0 \text{ mM}$ ,  $[\text{Fe(III)}]_0 = 0.1 \text{ mM}$ .  
 $[\text{DMPO}] = 1 \text{ g L}^{-1}$ .

Finally, a schematic diagram of the proposed pathways in this Fe(III)-S(IV)- $\text{O}_2$ - $h\nu$  system at pH 7.0 compared with Fe(III)-S(IV)- $\text{O}_2$ - system at pH 4.0 with or without UV irradiation for PARA degradation is shown in Scheme 1, where the species of oxidant generated such as  $\text{SO}_4^{\bullet-}$  and  $\text{HO}^\bullet$  are emphasized.



**Scheme. 6-1.** The proposed mechanism for Fe(III)–S(IV) system at different pH values.

### 6.3.6 Effect of transition metal ions-S(IV)-O<sub>2</sub>- system on PARA degradation

In order to investigate whether the other transition metal ions also has the same function as Fe(III), Cr(VI), Co(II), Cu(II) are chosen to react with sulfite under UV irradiation at near-neutral pH. From previous reports [22], Cr(VI) can work with S(IV) in dark under acidic environment, and pH 3.0 – 3.5 is the optimum condition for the reaction. In this case, using 365 nm UV to be the light source, the results in Figure 6-13 show that Cr(VI)-S(IV)-O<sub>2</sub>-system do not have ability to degrade PARA at initial pH 7.0 even with UV irradiation. The concentration of PARA start to decrease after 40 min reaction. Combined with the change of solution pH, the trend is totally the same than with Fe(III)-S(IV)-O<sub>2</sub>-h $\nu$  system, expect for the speed of decreasing pH that is much lower. From Figure 6-13, we can conclude that when the pH value of the reaction solution is decreased lower than 5.0, the reaction can start. In the case of the experiments are conducted without UV irradiation, after 60min reaction the pH decreases at a value lower than 5.0 and then PARA starts to degrade. From the result above, it can be concluded that this Cr(VI)-S(IV)-O<sub>2</sub>-h $\nu$  system also strongly depends on the pH, and irradiation enhances the PARA degradation via enhancing pH decrease.

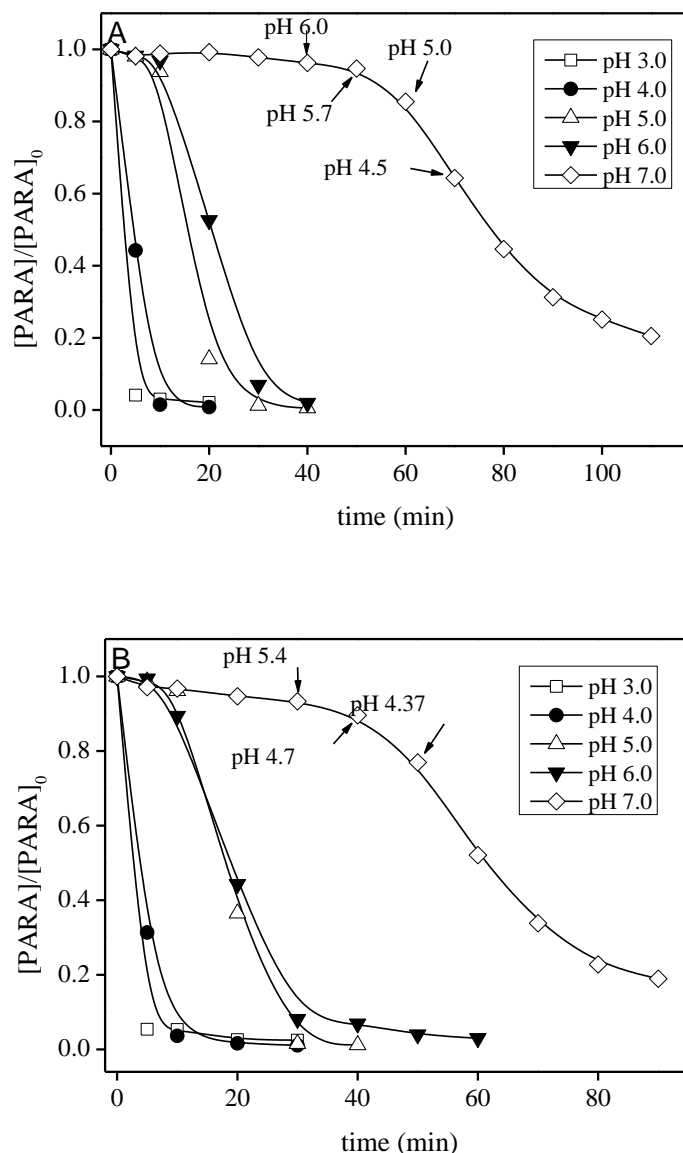


**Figure 6-13.** the difference of Cr(VI)-S(IV) system (A) without or (B) with UV irradiation at various pH values under aerated solution. Condition:  $[\text{PARA}]_0 = 10 \mu\text{M}$ ,  $[\text{S(IV)}]_0 = 1.0 \text{ mM}$ ,  $[\text{Cr(VI)}]_0 = 0.1 \text{ mM}$ .

As for Co(II)-S(IV)-O<sub>2</sub>-hν system, experiments are conducted at various pH values in suspensions initially containing 0.1 mM Co(II), 1.0 mM S(IV) and 10 μM PARA. However, from the results in Figure 6-14A and B, there is nearly no difference for PARA degradation with or without UV irradiation at pH 7.0 as well as at other pH values. As it is known [26-27], Co(II)-S(IV)-O<sub>2</sub> system works efficient under alkaline environment, pH decrease cannot facilitate the reaction at all, so it is confirm in our system Co(II)-S(IV)-O<sub>2</sub> with UV irradiation at near-neutral pH. The same phenomenon and same results are observed in Cu(II)-S(IV)-O<sub>2</sub>

system. As shown in Figure 6-15A and B Cu(II) and Co(II) have similar chemical properties, and the optimum pH value for their reaction with sulfite was above 8.0. As the use of UV irradiation enhance the PARA degradation is due to accelerate the pH decreasing, therefore UV irradiation doesn't work for those system which only occurred in alkaline environment.

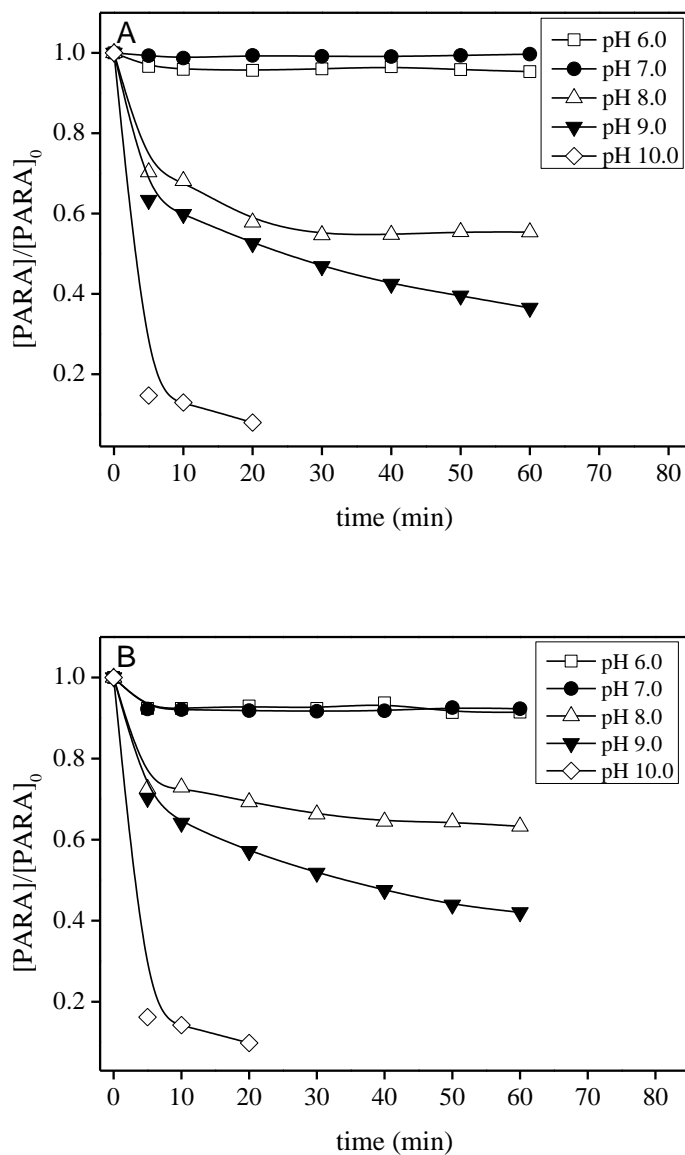


**Figure. 6-14.** the difference of Co(II)-S(IV) system (A) without or (B) with UV irradiation at various pH values under aerated solution. Condition:  $[PARA]_0 = 10 \mu\text{M}$ ,  $[S(IV)]_0 = 1.0 \text{ mM}$ ,  $[Co(II)]_0 = 0.1 \text{ mM}$ .

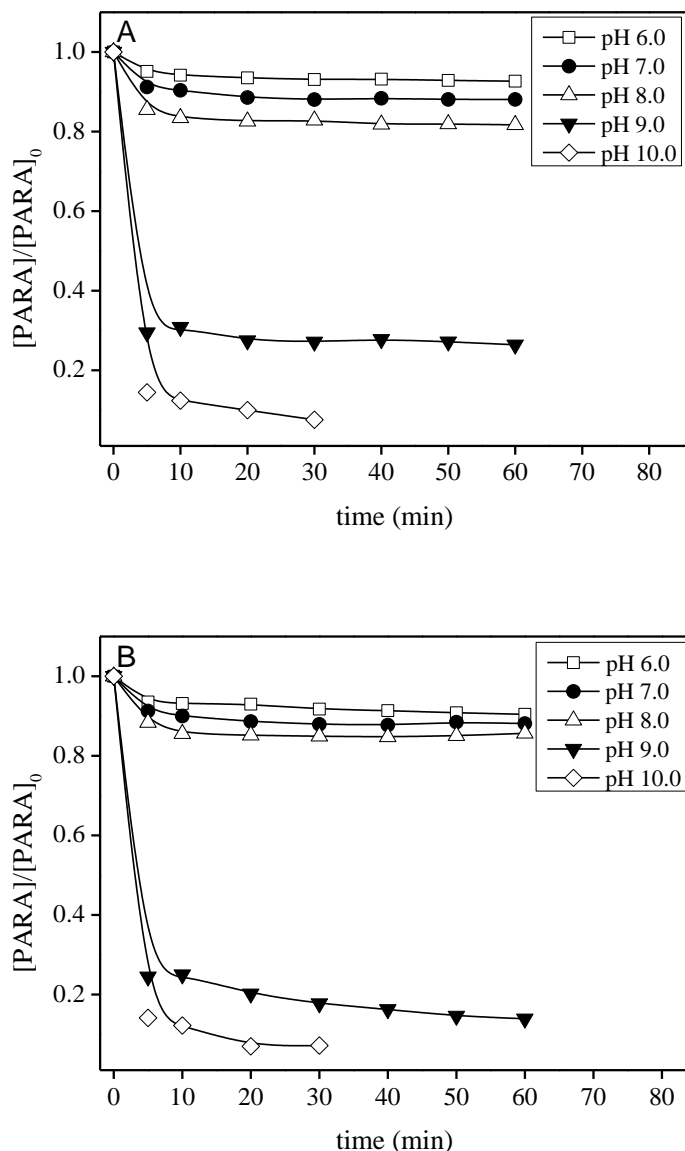


**Figure. 6-15.** the difference of Cu(II)-S(IV) system (A) without or (B) with UV irradiation at various pH values under aerated solution. Condition:  $[\text{PARA}]_0 = 10 \mu\text{M}$ ,  $[\text{S(IV)}]_0 = 1.0 \text{ mM}$ ,  $[\text{Cu(II)}]_0 = 0.1 \text{ mM}$ .

## 6.4 Conclusions

The photodegradation of PARA has been investigated in Fe(III)- S(IV)-O<sub>2</sub>- system in the absence and presence of UV irradiation. The results indicate that pH, Fe(III)/S(IV) concentration and oxygen content all have an important impact on the disappearance of PARA, and to achieve the highest efficiency of PARA degradation, the higher S(IV) concentration should be chosen. Irradiation enhance the PARA degradation via accelerating the pH

decreasing to acidic environment, as the optimal pH range for the degradation of PARA in Fe(III)- S(IV)-O<sub>2</sub>- system is about pH 4.0. After adding TBA to the suspension, there is almost no inhibition of PARA degradation, however when EtOH added to the solution, the PARA degradation is nearly completely inhibited. These results combined with the results of ESR experiments, indicate that the primary degradation pathway of PARA is a reaction with sulfate radical SO<sub>4</sub><sup>•-</sup>. As for other transition metal ions, only Cr(VI) can degrade PARA at initial pH of 7.0 under irradiation as Fe(III). Co(II) and Cu(II) which can react with sulfite in alkaline environment to degrade organic compounds cannot work with S(IV) at near-neutral pH with UV irradiation. In conclusion UV irradiation could be a plausible pathway for PARA degradation by Fe(III)- S(IV)-O<sub>2</sub>- system with initial pH around 7.0, these attributes make the Fe(III)-S(IV)-O<sub>2</sub>-hν system a more powerful system to deal with the wastewater at near-neutral pH.

## References

- [1] Brandt C, Fabian I, Eldik R V. Kinetics and Mechanism of the Iron(III)-catalyzed autoxidation of sulfur(IV) oxides in aqueous solution. evidence for the redox cycling of iron in the presence of oxygen and modeling of the overall reaction mechanism [J]. *Inorganic Chemistry*, 1994, 33(4): 47-51.
- [2] Buxton G V, Mcgowan S, Salmon G A, et al. A study of the spectra and reactivity of oxysulphur-radical anions involved in the chain oxidation of S(IV): A pulse and γ-radiolysis study [J]. *Atmospheric Environment*, 1996, 30(14): 2483–2493.
- [3] Das T N. Reactivity and role of SO<sub>5</sub><sup>•-</sup> radical in aqueous medium chain oxidation of sulfite to sulfate and atmospheric sulfuric acid generation [J]. *Journal of Physical Chemistry A*, 2017, 105(40): 9142-9155.
- [4] Warneck P, Ziajka J. Reaction mechanism of the Iron(III) - catalyzed autoxidation of bisulfite in aqueous solution: steady state description for benzene as radical scavenger [J]. *Berichte Der Bunsengesellschaft Für Physikalische Chemie*, 1995, 99(1): 59-65.
- [5] Zhang Y, Zhou J, Li C, et al. Reaction kinetics and mechanism of Iron(II)-induced catalytic oxidation of sulfur(IV) during wet desulfurization [J]. *Industrial & Engineering Chemistry Research*, 2012, 51(3): 1158–1165.

- [6] Chen, L.; Peng, X.; Liu, J.; Li, J.; Wu, F. Decolorization of Orange II in aqueous solution by an Fe(II)/sulfite system: Replacement of persulfate. *Ind. Eng. Chem. Res.* 2012, 51, 13632– 13638
- [7] Zhang L, Chen L, Xiao M, et al. Enhanced decolorization of Orange II solutions by the Fe(II)–sulfite system under xenon lamp irradiation [J]. *Industrial & Engineering Chemistry Research*, 2013, 52(30): 10089-10094.
- [8] Wu, F, Deng N S, Photochemistry of hydrolytic iron (III) species and photoinduced degradation of organic compounds. A minireview [J]. *Chemosphere*. 2000, 41: 1137-1147.
- [9] Zepp, R. G.; Faust, B. C.; Hoigne, J. Hydroxyl radical formation in aqueous reactions (pH 3-8) of iron(II) with hydrogen peroxide: The photo-Fenton reaction [J]. *Environmental Science & Technology*, 1992, 26, 313-319.
- [10] Zazouli M A, Yousefi Z, Eslami A, et al. Municipal solid waste landfill leachate treatment by fenton, photo-fenton and fenton-like processes: Effect of some variables [J]. *Iranian Journal of Environmental Health Science & Engineering*, 2012, 9(1): 3-10.
- [11] Salas E C, Berelson W M, Hammond D E, et al. The impact of bacterial strain on the products of dissimilatory iron reduction [J]. *Geochimica Et Cosmochimica Acta*, 2010, 74(2): 574-583.
- [12] Guo Y, Lou X, Fang C, et al. Novel photo-sulfite system: toward simultaneous transformations of inorganic and organic pollutants [J]. *Environmental Science & Technology*, 2013, 47(19): 11174-11181.
- [13] Kuo D T F, Kirk D W, Jia C Q. The chemistry of aqueous S(IV)-Fe-O<sub>2</sub> system: state of the art [J]. *Sulfur Reports*, 2006, 27(5): 461-530.
- [14] Xu J, Li J, Wu F, et al. Rapid photooxidation of As(III) through surface complexation with nascent colloidal ferric hydroxide [J]. *Environmental Science & Technology*, 2013, 48(1): 272-278.
- [15] Zhou D, Yuan Y, Yang S, et al. Roles of oxysulfur radicals in the oxidation of acid orange 7 in the Fe(III)-sulfite system [J]. *Sulfur Reports*, 2015, 36(4): 373-384.
- [16] Zhou D, Chen L, Zhang C, et al. A novel photochemical system of ferrous sulfite complex: kinetics and mechanisms of rapid decolorization of Acid Orange 7 in aqueous solutions [J]. *Water Research*, 2014, 57(5): 87-95.
- [17] Yuan Y, Yang S, Zhou D, et al. A simple Cr(VI)–S(IV)–O<sub>2</sub> system for rapid and simultaneous reduction of Cr(VI) and oxidative degradation of organic pollutants [J]. *Journal of Hazardous Materials*, 2016, 307: 294-301.

- [18] Bajt O, Mailhot G, Bolte M. Degradation of dibutyl phthalate by homogeneous photocatalysis with Fe(III) in aqueous solution [J]. *Applied Catalysis B Environmental*, 2001, 33(3): 239-248.
- [19] Benkelberg H J, Warneck P. Photodecomposition of Iron(III) hydroxo and sulfato complexes in aqueous solution: wavelength dependence of OH and  $\text{SO}_4^-$  Quantum Yields [J]. *J.phys.chem*, 1995, 99(14): 5214-5221.
- [20] Huang W, Brigante M, Wu F, et al. Development of a new homogenous photo-Fenton process using Fe(III)-EDDS complexes [J]. *Journal of Photochemistry & Photobiology A Chemistry*, 2012, 239: 17-23.
- [21] Buxton G V, Greenstock C L, Helman W P, et al. Critical review of rate constants for reactions of hydrated electron chemical kinetic data base for combustion chemistry. Part 3: Propane [J]. *Journal of Physical & Chemical Reference Data*, 1988, 17(2): 513-886.
- [22] Yuan Y, Yang S, Zhou D, et al. A simple Cr(VI)–S(IV)–O<sub>2</sub> system for rapid and simultaneous reduction of Cr(VI) and oxidative degradation of organic pollutants[J]. *Journal of Hazardous Materials*, 2016, 307:294-301.
- [23] Zou J, Ma J, Chen L, et al. Rapid acceleration of ferrous iron/peroxymonosulfate oxidation of organic pollutants by promoting Fe(III)/Fe(II) cycle with hydroxylamine [J]. *Environmental Science & Technology*, 2013, 47(20): 11685-11691.
- [24] Timmins, G. S.; Liu, K. J.; Bechara, E. J. H.; Kotake, Y.; Swartz, H. M. Trapping of free radicals with direct in vivo EPR detection: A comparison of 5,5-dimethyl-1-pyrroline-N-oxide and 5-diethoxyphosphoryl-5-methyl-1-pyrroline-N-oxide as spin traps for HO• and  $\text{SO}_4^{\cdot-}$ . *Free Radical Biol. Med.* 1999, 27 (3-4): 329-333
- [25] Hayon E, Treinin A, Wilf J. Electronic spectra, photochemistry, and autoxidation mechanism of the sulfite-bisulfite-pyrosulfite systems.  $\text{SO}_2^-$ ,  $\text{SO}_3^-$ ,  $\text{SO}_4^-$ , and  $\text{SO}_5^-$  radicals [J]. *Journal of the American Chemical Society*, 1972, 94(1): 47-57.
- [26] Liu Z, Yang S, Yuan Y, et al. A novel heterogeneous system for sulfate radical generation through sulfite activation on a  $\text{CoFe}_2\text{O}_4$  nanocatalyst surface [J]. *Journal of Hazardous Materials*, 2016, 324.
- [27] Yuan Y, Zhao D, Li J, et al. Rapid Oxidation of Paracetamol by Cobalt(II) Catalyzed Sulfite at Alkaline pH [J]. *Catalysis Today*, 2017.

## **Chapter 7 General conclusion and future perspective**

## 7.1 General conclusion

In this thesis, sulfite activation by transition metal ions Cr(VI), Co(II), Fe(III) to generate oxidant species such as oxysulfur radicals ( $\text{SO}_3^{\bullet-}$ ,  $\text{SO}_4^{\bullet-}$  and  $\text{SO}_5^{\bullet-}$ ) and hydroxyl radical ( $\text{HO}^{\bullet}$ ) was investigated. The results obtained during this thesis work concern the optimum conditions, the removal efficiency and the chemical mechanism investigation of all the systems.

- (1) The Cr(VI)-S(IV)-O<sub>2</sub> system is an efficient system for rapid and simultaneous reduction of Cr(VI) and oxidative degradation of organic pollutants in aqueous solution with dioxygen under acidic conditions. We have considered effects of pH, concentration of added Cr(VI) and S(IV), as well as the presence of O<sub>2</sub> or N<sub>2</sub> and various radical scavengers. Our results show that the reaction of Cr(VI) and degradation of organic pollutants depended heavily on the pH and initial concentrations of Cr(VI) and S(IV). In addition, oxysulfur radicals were the dominant oxidants for AO7 degradation. Thus, our Cr(VI)-S(IV)-O<sub>2</sub> system may be a new candidate for use in the efficient treatment of waste using waste chromium via simultaneous reduction of Cr(VI) and oxidation of organic contaminants.
- (2) High efficiency of the Co(II)-S(IV)-O<sub>2</sub> system using PARA as organic pollutant model in aqueous solution at alkaline pH was achieved. In this system, the degradation of paracetamol depends on initial concentrations of S(IV) and strongly on the pH. In fact, it is clear that dissolved oxygen plays a crucial role allowing the oxysulfur radical oxidation to initiate the reaction. The results of radical scavenger experiments demonstrate that  $\text{SO}_4^{\bullet-}$  and also  $\text{SO}_5^{\bullet-}$  (to a lesser extent) are involved during the paracetamol degradation. Furthermore, heterogeneous catalyst CoO also could react with sulfite to degrade paracetamol with high efficiency. In general, this research work provides a new promising strategy by using sulfite and transition metal Co(II) to degrade organic compounds in wastewater under alkaline environment. One of the perspectives of this work is to perform some experiments with other metals in order to assess their ability to promote the radical generation from sulfite under dark and light conditions.
- (3) High efficiency in AN decontamination has been achieved in this Fe(III)-S(IV)-O<sub>2</sub> system under specific conditions. Consequently, oxysulfur radicals including  $\text{SO}_4^{\bullet-}$  and  $\text{SO}_5^{\bullet-}$  are the dominant oxidants which are responsible for aniline degradation. Furthermore, in

aniline oxidation,  $\text{SO}_5^{\bullet-}$  also played a relatively important role, the contribution of which took the considerable part (~ 60%) of all species of radicals. Additionally, the rate constant  $k_{AN,SO_4^-}$  and  $k_{AN,SO_5^-}$  were estimated to be  $(7.7 \pm 0.5) \times 10^9 \text{ M}^{-1}\text{s}^{-1}$  and  $(5.8 \pm 0.6) \times 10^6 \text{ M}^{-1} \text{ s}^{-1}$ , respectively. The experiments conducted with different concentrations of oxygen in solution show that dissolved oxygen plays a significant role in radicals generating. This work not only provides a feasible candidate for use in the efficient oxidation of aromatic amines, also indicates a novel concept that the role of  $\text{SO}_5^{\bullet-}$  cannot be neglected in our future study.

- (4) The photodegradation of PARA has been investigated in Fe(III)-S(IV)- $\text{O}_2$  system in the absence and presence of UV irradiation. The results indicate that pH, Fe(III)/S(IV) concentration and oxygen content all have an important impact on the disappearance of PARA. Moreover, to achieve the highest efficiency of PARA degradation, the higher S(IV) concentration should be chosen. Irradiation enhances the PARA degradation via the pH decrease. In fact, the optimal pH range for the degradation of PARA in Fe(III)-S(IV)- $\text{O}_2$ -system as found to be around pH 4.0. After addition of TBA to the suspension, there was almost no inhibition of PARA degradation, however, when EtOH added to the solution, the PARA degradation was almost completely inhibited. Combined with the result of ESR experiments, we assess that the primary degradation pathway of PARA was the reaction with  $\text{SO}_4^{\bullet-}$ . As for other transition metal ions, only Cr(VI) can degrade PARA at initial pH of 7.0 under irradiation as Fe(III), Co(II) and Cu(II) which can react with sulfite in alkaline environment to degrade organic compounds cannot work with S(IV) at near-neutral pH with UV irradiation. In conclusion UV irradiation could be a plausible pathway for PARA degradation by Fe(III)-S(IV)- $\text{O}_2$  system with initial pH around 7.0. As consequence, the Fe(III)-S(IV)- $\text{O}_2$ - $h\nu$  system is a more powerful system to deal with the wastewater at near-neutral pH.

## 7.2 Perspectives

Using S(IV) to be the reductant,  $\text{O}_2$  to be the oxidant and transition metal ions to be the initiator, those transition metals-sulfite processes can open a new perspective of oxidative

reactions to degrade the organic pollutants. Discovering novel methods for activating S(IV) have been recently proliferated indicating these transition metals + sulfite processes as new tools for remediation of contaminated environments. However, it should be stated that those processes are neoteric processes which still have a lot to go through. Future studies should be developed as follows:

- (1) Finding out more kind of metal ions that can react with sulfite to form oxysulfur radicals, and find out the similarity for all those metal ions, the understanding of behavior of the metals is necessity for which further efforts and studies are required.
- (2) As TOC removal efficiency were very low in all those systems, so try to find out more method to make the metal ions/S(IV) systems works in alkaline environment, as it facilitate the generation of HO<sup>•</sup> which have the capacity to mineralize organic compounds. Furthermore, coupling of this transition metals + sulfite system with other AOPs for synergistic effect may also be an excellent strategy in the efficient degradation of organic compounds and achieve desired TOC removal efficiency.
- (3) All the solutions contained organic pollutants are synthetic wastewater which are prepared in the lab, in the future study, we can use those systems to degrade target pollutants in actual wastewater. Actually, their application in industrial scale requires many studies to stabilize their position. Howbeit, due to desirable performance of this transition metals + sulfite systems in degrading the pollutants, it is not an exaggeration to apply those processes in industrial scale in the near future.

## Publications

- 1, **Yuan Yanan**, Li Jinjun, Wu Feng. Solid surface photochemistry of montmorillonite: mechanisms for the arsenite oxidation under UV-A irradiation [J]. Environmental Science & Pollution Research, 2016, 23(2):1035.
- 2, **Yuan Yanan**, Yang Shaojie, Wu Feng. A simple Cr(VI)–S(IV)–O<sub>2</sub> system for rapid and simultaneous reduction of Cr(VI) and oxidative degradation of organic pollutants[J]. Journal of Hazardous Materials, 2016, 307:294
- 3, **Yanan Yuan**, Feng Wu, Marcello Brigante, et al. Rapid oxidation of paracetamol by cobalt(II) catalyzed sulfite at alkaline pH. Catalysis Today, 2017.
- 4, Yingtan Yu, **Yanan Yuan**, Feng Wu. Comment on “synergetic transformations of multiple pollutants driven by Cr(VI)-Sulfite Reactions”[J]. Environmental Science & Technology, 2015, 49(20):12363-71.
- 5, Danna Zhou, **Yanan Yuan**, Shaojie Yang. Roles of oxysulfur radicals in the oxidation of acid orange 7 in the Fe(III)–Sulfite system, J. Sulfur. Chem. 36 (2015) 373-384
- 6, Zizheng Liu, Shaojie Yang, **Yanan Yuan**, et al. A novel heterogeneous system for sulfate radical generation through sulfite activation on a CoFe<sub>2</sub>O<sub>4</sub> nanocatalyst surface [J]. Journal of Hazardous Materials, 2016, 324.